AN ENERGY-EFFICIENT P2P PROTOCOL FOR VALIDATING MEASUREMENTS IN WIRELESS SENSOR NETWORKS

BY

VARUN BADRINATH KRISHNA

THESIS

Submitted in partial fulfillment of the requirements
for the degree of Master of Science in Electrical and Computer Engineering
in the Graduate College of the
University of Illinois at Urbana-Champaign, 2016

Urbana, Illinois

Adviser:

Professor William H. Sanders

ABSTRACT

Wireless sensor networks (WSNs) should collect accurate measurements to reliably capture the state of the environment that they monitor. However, measurement data collected from one or more sensors may drift or become erroneous due to hardware failures or sensor degradation. In WSNs with remote deployments, detecting those measurement errors through a centralized reporting approach can result in a large number of message transmissions, which in turn dramatically decreases the battery life of sensors in the network. In this thesis, we address this issue through three main contributions. First, we propose a protocol in which sensors detect errors in a peer-to-peer (P2P) fashion, and that extends the life of the WSN by minimizing the number of messages transmitted. Second, we propose an effective anomaly detection approach that has low memory and processing requirements, allowing for easy deployment on low-cost sensor hardware. Third, we develop a trace-driven, discrete-event simulator that allows us to evaluate the developed protocol and approach. In doing so, we use three datasets from real WSN deployments, which include indoor air temperature, sea surface water temperature and seismic wave amplitude sensors. Our results show that our P2P protocol can accurately detect errors and simultaneously extend the effective WSN lifetime dramatically compared to the centralized protocol.

To Bill Sanders, Marianne Winslett and David Yau.

ACKNOWLEDGMENTS

I would first like to acknowledge Michael Rausch and Benjamin Ujcich for their contributions to this work. They contributed to the abstract, introduction and related work sections of this thesis. They also helped with improving the quality of the writing. Most importantly, the brainstorming sessions with them produced some of the main ideas in this thesis.

I would like to thank the following people:

- Prof. William Sanders, Dr. Kiryung Lee and Prof. Indranil Gupta for their technical guidance on the project that led to this thesis. Several aspects of the thesis, including writing and organization were improved based on their feedback.
- Prof. Marianne Winslett, Prof. David Yau and Dr. Bimlesh Wadhwa, who recommended me for graduate school.
- Prof. Sanders, Prof. Winslett and Prof. Ravishankar Iyer for their continued support of my endeavors.
- Jenny Applequist, James Hutchinson, Aarti Shah, Dr. Wander Wadman, Brett Feddersen, and Sangeetha A. J. for their help with proof-reading and improving the writing quality of the thesis.
- My colleagues in the PERFORM Group (Ahmed Fawaz, Atul Bohara, Ben Ujcich, Carmen Cheh, Ken Keefe, Michael Rausch, Mohammad Noureddine, Ronald Wright, and Uttam Thakore) for their support.
- My colleagues in the Information Trust Institute (Prof. David Nicol, Amy Irle, Tim Yardley, Jeremy Jones, Tonia Siuts, Amy Clay, Cheri Soliday, Al Valdes) for their support.

- My former colleagues in the Advanced Digital Sciences Center (Prof. Douglas Jones, Dr. Rui Tan, Dr. Deokwoo Jung, Dr. Binbin Chen, Nguyen Hoang Hai, William Temple, and Ngo Quang Minh Khiem), from whom I have learned a lot.

- The authors of the papers that I have cited in this thesis. They have provided an invaluable knowledgebase.

- My friends and family for their support.

We use three datasets in this study and thank the providers. First, the GeoNet Project in New Zealand for the seismic waveform data [1] (and, in particular, Kevin Fenaughty for his assistance). Second, the TAO Project Office of NOAA/PMEL for the sea water surface temperature data. Finally, the Intel Berkeley Research Lab [2] for the indoor air temperature data.

Finally, I would like to thank the University of Illinois at Urbana-Champaign for providing me with a highly conducive environment for research, access to great people and resources, travel opportunities, and social opportunities.

TABLE OF CONTENTS

LIST OF FIGURES viii

LIST OF ABBREVIATIONS xi

CHAPTER 1 INTRODUCTION 1

CHAPTER 2 PRELIMINARIES 4
2.1 System Model 4
2.2 Failure Model 5
2.3 Protocol Requirement 5
2.4 Evaluation Metrics 6

CHAPTER 3 POTENTIAL APPLICATIONS 8
3.1 Indoor Air Temperature of an Office (Berkeley) 8
3.2 Sea Surface Temperatures (TAO) 8
3.3 Seismic Wave Measurement Data (NZ) 12

CHAPTER 4 P2P ERROR DETECTION PROTOCOL 16
4.1 Protocol Description 16
4.2 Required Properties of the Anomaly Detection Approach and Similarity Metric 20
4.3 Memory Requirement 21
4.4 Handling Changes in the Network 21
4.5 Proof of Energy-Optimality 22
4.6 Main Strength and Limitation 25

CHAPTER 5 VALIDATION OF SENSOR MEASUREMENTS 27
5.1 Summary of Approach 27
5.2 Anomaly Detection Approach Assumptions 28
5.3 Isocontours of the Bivariate Normal Distribution 29
5.4 Anomaly Detection Procedure 34
5.5 Similarity Metric 38
5.6 Demonstrating Required Properties of Approach 39
5.7 Illustration of Approach on Datasets 42

CHAPTER 6 PROTOCOL EVALUATION 48
6.1 Sensor Network Protocol Simulator 48
6.2 Protocol Implementation 51
6.3 Detection Accuracy Results 70
6.4 Reachability Results 70

CHAPTER 7 RELATED WORK 77

CHAPTER 8 CONCLUSION 80

APPENDIX A UNSUITABLE ANOMALY DETECTION APPROACHES 81
A.1 OLS Linear Regression 81
A.2 TLS Linear Regression 83
A.3 Correlation and Dot Products 85

APPENDIX B SENSOR ID AND NAME MAPPING 86
B.1 Berkeley Dataset 86
B.2 TAO Dataset 86
B.3 NZ Dataset 86

REFERENCES 89

LIST OF FIGURES

3.1 Sample of temperature data from Intel Berkeley Research. The white spots are anomalous measurements. 9
3.2 Sample of sea surface temperature data from the Tropical Atmosphere Ocean Project by the Pacific Environmental Laboratory. The white spot in Sensor 2 is an anomaly. 9
3.3 TAO Dataset: linear relationships and closeness in measurements values as a function of physical distance. 10
3.4 Sample of the seismic waveform data in the GeoNet National Seismograph Network in New Zealand. Note that the seismic amplitude has no unit specified since the data is uncalibrated. 12
3.5 NZ Dataset: Anomalies observed in the measurements taken by Sensors 7 and 10. 14
3.6 NZ Dataset: Earthquake observed in the measurements taken by three sensors. It is manifested as a spike in the waveform. 15

4.1 P2P protocol at each sensor 17
4.2 P2P protocol for Stage 1 (complete_stage1) at each sensor 18
4.3 P2P protocol for Stage 2 (complete_stage2) at each sensor 19
4.4 P2P Protocol for Stage 3 at sink 20
4.5 WSN showing the routing path of the optimal message in our protocol that reports the erroneous measurement (solid red arrow), unnecessary messages that report anomalous measurements (dashed red arrows), and messages containing measurements (dotted blue arrows). Sensor $S^{(1)}$ is faulty. 22

5.1 Single anomalous measurement (in red) in the NZ dataset is detected by constructing an isocontour (blue shaded elliptical region) as a detection boundary. Normal measurements are inside the isocontour and are jointly Gaussian. 28
5.2 Anomalies (red crosses) in the NZ dataset due to earthquake observed in normalized measurement space (left) and the space spanned by the two principal components (right). 32
5.3 Anomalies (yellow stars) due to the earthquake presented in the seismic waveform in the NZ Dataset (200 sec view). 43

5.4 Anomalies (red crosses) in the three datasets are egregious. They would be detected even if the isocontour were drawn 75, 500 and 3600 standard deviations from the mean in the Berkeley, TAO and NZ datasets, respectively. 44
5.5 Map of physical location of select seismic wave sensors in the NZ dataset. The four sensors grouped in the largest circle are located around a volcano. . 46

6.1 Components of the custom-built discrete event simulator. 49
6.2 Centralized validation protocol (Berkeley: Actual Layout): Battery life illustration for static routing with routing paths shown for 4 arbitrary sensors. Sink is the star in the center. Crossed-out sensors are unreachable. . 57
6.3 P2P validation protocol (Berkeley: Actual Layout): Battery life illustration for static routing with routing paths shown for 4 arbitrary sensors. Sink is the star in the center. Crossed-out sensors are unreachable. 58
6.4 Centralized validation protocol (Berkeley: Actual Layout): Battery life illustration for MBCR routing with routing paths shown for 4 arbitrary sensors. Sink is the star in the center. Crossed-out sensors are unreachable. . 59
6.5 P2P validation protocol (Berkeley: Actual Layout): Battery life illustration for MBCR routing with routing paths shown for 4 arbitrary sensors. Sink is the star in the center. Crossed-out sensors are unreachable. 60
6.6 Centralized validation protocol (Berkeley: Grid Layout): Battery life illustration for static routing with routing paths shown for 4 arbitrary sensors. Sink is near the center. Crossed-out sensors are unreachable. 61
6.7 P2P validation protocol (Berkeley: Grid Layout): Battery life illustration for static routing with routing paths shown for 4 arbitrary sensors. Sink is near the center. Crossed-out sensors are unreachable. 62
6.8 Centralized validation protocol (Berkeley: Grid Layout): Battery life illustration for MBCR routing with routing paths shown for 4 arbitrary sensors. Sink is near the center. Crossed-out sensors are unreachable. 63
6.9 P2P validation protocol (Berkeley: Grid Layout): Battery life illustration for MBCR routing with routing paths shown for 4 arbitrary sensors. Sink is near the center. Crossed-out sensors are unreachable. 64
6.10 Centralized validation protocol (NZ: Actual Layout): Battery life illustration for static routing with routing paths shown for 2 arbitrary sensors. Sink is the star in the ring topology. Crossed-out sensors are unreachable. . . 66
6.11 P2P validation protocol (NZ: Actual Layout): Battery life illustration for static routing with routing paths shown for 2 arbitrary sensors. Sink is the star in the ring topology 67
6.12 Centralized validation protocol (NZ: Actual Layout): Battery life illustration for MBCR routing with routing paths shown for 2 arbitrary sensors. Sink is the star in the ring topology 68
6.13 P2P validation protocol (NZ: Actual Layout): Battery life illustration for MBCR routing with routing paths shown for 2 arbitrary sensors. Sink is the star in the ring topology 69

6.14 Results for Intel Berkeley Dataset (Actual Layout). The inverse functions of Longevity and Reachability, which are the number of sensors dead and unreachable, respectively, are plotted. 72
6.15 Results for Intel Berkeley Dataset (Grid Layout). The inverse functions of Longevity and Reachability, which are the number of sensors dead and unreachable, respectively, are plotted. 73
6.16 Results for TAO Dataset. The inverse functions of Longevity and Reachability, which are the number of sensors dead and unreachable, respectively, are plotted. 75
6.17 Results for NZ Dataset. The inverse functions of Longevity and Reachability, which are the number of sensors dead and unreachable, respectively, are plotted. 76

A.1 NZ dataset: OLS regression used in anomaly detection. 82
A.2 NZ dataset: Failure of OLS regression used in anomaly detection. 83
A.3 NZ dataset: TLS regression used in anomaly detection. 84

LIST OF ABBREVIATIONS

2-D	Two Dimensional
AR	Auto-Regressive
ARIMA	Auto-Regressive Integrated Moving Average
CPU	Central Processing Unit
EPIC	Explicitly Parallel Instruction Computing
MBCR	Minimum Battery Cost Routing
NOAA	US National Oceanic and Atmospheric Administration
NZ	New Zealand
P2P	Peer-to-peer
PCA	Principal Component Analysis
PDF	Probability Density Function
PMEL	Pacific Marine Environmental Laboratory
SST	Sea Surface Temperatures
TAO	Tropical Atmosphere Ocean Project
TPM	Trusted Platform Module
US	United States
WSN	Wireless Sensor Network

CHAPTER 1

INTRODUCTION

Wireless sensor networks (WSNs) are being increasingly deployed in a number of different areas, most recently in scenarios involving the Internet of Things (IoT devices). In remote monitoring applications, sensors measure temperature and humidity of forest environments [3], animal habitats [4], crops [5], etc., and measure vibrations in volcanoes [6] and in civil structures [7], such as bridges [8]. It is essential that those WSNs are designed in a way that minimizes energy consumption of sensors, since the sensors are typically battery-powered. Therefore, extensive research has been performed in designing protocols that extend the lifetime of sensor networks [9].

Measurements from sensors in a WSN may become faulty or drift with time from their true values because of natural degradation of hardware, hardware failures, or manufacturing defects [10]. This can lead to poor measurement quality, which can in turn undermine the monitoring benefits of installing the sensors. There is a need to develop an automated error detection protocol, but the challenge is to minimize its overhead and impact on battery life of individual sensors as well as the connectivity of the network.

Sensor measurement errors manifest themselves as anomalies, and these anomalies need to be reported to the *sink* (i.e., base station of the sensor network) in a timely fashion, so that the faulty sensors can be investigated. In a naive centralized protocol for validating measurements [10] [11], every sensor periodically reports its measurements to the sink (e.g., via a spanning tree or a DAG topology). The sink then runs a centralized anomaly detection algorithm on these collected measurements, to detect anomalies. While this scheme is attractive in its simplicity, it has two major drawbacks. First, sensors farthest from the sink (by number of hops) may have to route their sensor data through many other sensors to reach the sink. As message transmission consumes significantly more energy than other sen-

sor functions [12], the number of message transmissions should be minimized when possible to extend the sensor network's life. Second, over a long timeframe, sensors closest to the sink will have more data routed through them on behalf of other sensors farther from the sink. As a result, those sensors closest to the sink will exhaust their battery power and die before sensors farthest from the sink. This disconnects the network earlier, and results in far away sensors needing to transmit at higher amplitudes to reach the sink, further depleting their batteries. Unreachable sensors are effectively "dead" from the sink's point of view.

In this thesis we adopt a peer-to-peer (P2P) approach for error detection. Such an approach drains the power of sensors in the network more equitably. As a result, sensors closest to the sink can last longer in the P2P approach than in the centralized approach. That allows sensors farther from the sink to communicate with the sink for a longer time than possible in the centralized approach. While the usefulness of such a distributed protocol was acknowledged in [6] (in the context of seismic activity monitoring in volcanoes), the authors did not propose an energy-efficient solution.

To the best of our knowledge, ours is the first measurement error detection protocol for WSNs that minimizes the energy cost of transmitting the additional messages required to report measurement errors. The protocol is distributed, and is designed to be widely applicable in the context of battery-constrained sensor monitoring, for environments including (but not limited to) indoor spaces, forests, agricultural soil, oceans, volcanoes, distant planets, etc.

Although the P2P protocol reduces the number of message transmissions needed to capture a sensor that is in error, it shifts the onus of anomaly detection from the sink onto the sensors themselves. Therefore, the CPU consumption on sensors increases, and this has an impact on sensor battery life. However, we show that increasing computation costs while decreasing communication costs leads to a net benefit in extending the life of the WSN because communication drains sensor battery faster than computation.

We make three main contributions in designing an energy-efficient protocol to validate sensor measurements. First, we design a P2P error detection protocol that is optimal in that it minimizes message transmissions, thereby extending sensor battery life. Second, we provide a theoretically supported error detection mechanism that has properties required by

the protocol in order to minimize message transmissions. Finally, we evaluate our protocol using a custom-built simulator that uses data traces from two real WSN deployments, as well as real topologies. Our results show that the P2P approach dramatically extends network lifetime.

The thesis is organized as follows. The assumptions within which the protocol is energy-optimal are stated in Chapter 2. The datasets we use to motivate and evaluate our approach are described in Chapter 3. The protocol is described and analyzed in Chapter 4. A validation mechanism to support the protocol is presented in Chapter 5. The results of the evaluation of our protocol on the datasets are presented in Chapter 6. Related work is discussed in Chapter 7, and we conclude in Chapter 8.

CHAPTER 2

PRELIMINARIES

In this chapter, we describe our assumptions for the model within which our error detection protocol is energy-optimal with regard to minimizing message transmissions.

2.1 System Model

A WSN comprises a multitude of sensors that use wireless radio communications to transmit, receive, and forward measurements to a base station or sink. Depending on the application, the measurements may be of temperature or humidity of environments, seismic vibrations, etc. Our protocol was designed to be broadly applicable to a range of WSN applications, and is thus agnostic to the application or physical quantities being measured by the sensors in the network. We do, however, require that every sensor have at least two other neighboring sensors that can be used for voting on whether that sensor's measurements are anomalous. The WSN may comprise heterogeneous and multimodal sensors that measure different physical quantities, such as temperature and pressure.

In this thesis, we design the error detection approach for a WSN model in which each sensor has a finite, exhaustible, and non-renewable power supply. That is the case for sensors that rely solely on batteries and do not have access to external power sources (e.g., solar power, or the power grid). Each sensor communicates wirelessly. There are many different wireless communication technologies that a sensor could employ; laser, infrared, and radio frequency (RF) are the most common. We chose to focus on an RF-based system with omnidirectional antennae, which implies that all communication is broadcast to sensors within wireless range.

Upon system deployment, there are a multitude of sensors alive in the WSN. The sensors sample and report measurements at discrete time intervals Δt, whose value is set by the

network administrator depending on the application (e.g., $\Delta t = 15$ s). Between consecutive reports, sensors can go into a low-powered state to reduce battery consumption (see [13]).

2.2 Failure Model

In our model, a sensor is faulty if it reports measurements that statistically deviate significantly from past measurements, given the same environmental conditions. We refer to measurements that are not erroneous as "proper." We assume sensors will not intentionally act in a malicious manner, and that Byzantine faults do not occur.

We do not assume a fail-stop model. In the event of a transient error, the network administrator may allow the sensor to continue reporting measurements to the sink. In the event of a persistent error, the sensor may be forced by the network administrator to fall back to a "routing-only mode," in which it serves as a routing node in a multi-hop network, but does not generate measurement packets itself.

We say that sensors in our model are *alive* until their batteries are depleted, in which case they are *dead*. Our P2P protocol operates at the application level of the networking stack, and can run on top of lower-level routing protocols such as SPMS [14] and MBCR [15], or gossip style failure detection protocols such as [16] to detect node failures that occur before battery depletion. Our protocol may be able to run along with the methods in [17], for robustness to message drops or ordering issues, but that is not the focus of this thesis.

2.3 Protocol Requirement

The WSN network administrator requires erroneous measurements to be reported immediately after detection. Since the detection is performed at the sink in the centralized protocol, the sensors must *synchronously* report measurements periodically (at every discrete time interval) to the sink for real-time error detection. In the P2P approach, however, sensors exchange readings among themselves synchronously for error detection, but messages are reported to the sink *asynchronously*, only when an error is detected. In addition, the sensors

in the P2P approach could report their measurements to the sink in large batches if the network administrator needs to keep a record of all measurements at the sink. Such batching prolongs the overall lifetime of the network [18].

The error may be due to a fault or a legitimate rare event in the environment being monitored (such as an earthquake). We believe both events are of interest to the network administrator, and show in Section 5.7 that they can be easily differentiated using appropriate detection thresholds. The Hidden Markov Model-driven approach presented in [19] may also be applicable in making that differentiation.

2.4 Evaluation Metrics

Sensors with finite, nonrenewable energy sources will inevitably expend all of their energy and cease to report measurements, so it is important to design protocols that extend the lifetime of the WSN. At start-up, all sensors are alive with full battery power, and as time progresses their battery power gets depleted. The rate at which that depletion happens depends mostly on how much radio and CPU are used by the sensor.

We quantify the lifetime of the entire WSN by defining two metrics from different perspectives:

Longevity quantifies the WSN's lifetime from each sensor's perspective. We define $longevity(\lambda)$ as the time it takes for λ sensors to die because of battery depletion.

Reachability quantifies the WSN's lifetime from the sink's perspective. We define $reachability(\omega)$ as the time it takes before ω sensors lose end-to-end connectivity with the sink (or become unreachable).

Together, longevity and reachability quantify the *survivability* of the WSN. We say that the validation protocol is *energy-efficient* if it extends the survivability of the WSN.

In examining the shortcomings of the centralized validation approach, one can see that the survivability of the WSN is constrained by the time it takes for sensors closest to the sink to expend their energy, and the repercussions that has on the reachability of sensors farthest from the sink. Similarly, survivability is constrained in the P2P validation approach, where CPU consumption increases on the sensors, affecting longevity. Because of that trade-off, it

is not immediately clear that the P2P approach is more beneficial.

CHAPTER 3

POTENTIAL APPLICATIONS

In this chapter, we use three independent datasets to motivate the applications of our distributed validation protocol. The datasets illustrate the kinds of anomalies seen in measurements taken from sensors measuring air temperature of buildings, water temperature of seas and seismic waves on the Earth's surface.

We use these datasets to evaluate our approach, and refer to them in the thesis by the shorthand given in the parenthesis.

3.1 Indoor Air Temperature of an Office (Berkeley)

This is a dataset of temperature measurements from 54 Mica2Dot sensors with weather boards deployed at the Intel Berkeley Research Lab [2], in the US. The dataset in its entirety is plotted as a heatmap in Fig. 3.1. The temperatures are nearly all below 30 °C, which is normal for an indoor environment. However, it can be clearly seen that sensor 14 (in the 14^{th} row) has reported temperatures of over 120 °C between 2 and 9 March 2004. The sensor readings proceed to deteriorate and ultimately all become anomalous. These anomalies were present in the dataset despite averaging of measurements in one-hour periods, and are clearly indicative of errors, which are most likely due to battery drain.

3.2 Sea Surface Temperatures (TAO)

This dataset was obtained from the Tropical Atmosphere Ocean Project (TAO) by the Pacific Marine Environmental Laboratory (PMEL), and supported by the US National Oceanic and Atmospheric Administration. We extract-time aligned data from 8 moorings located in the

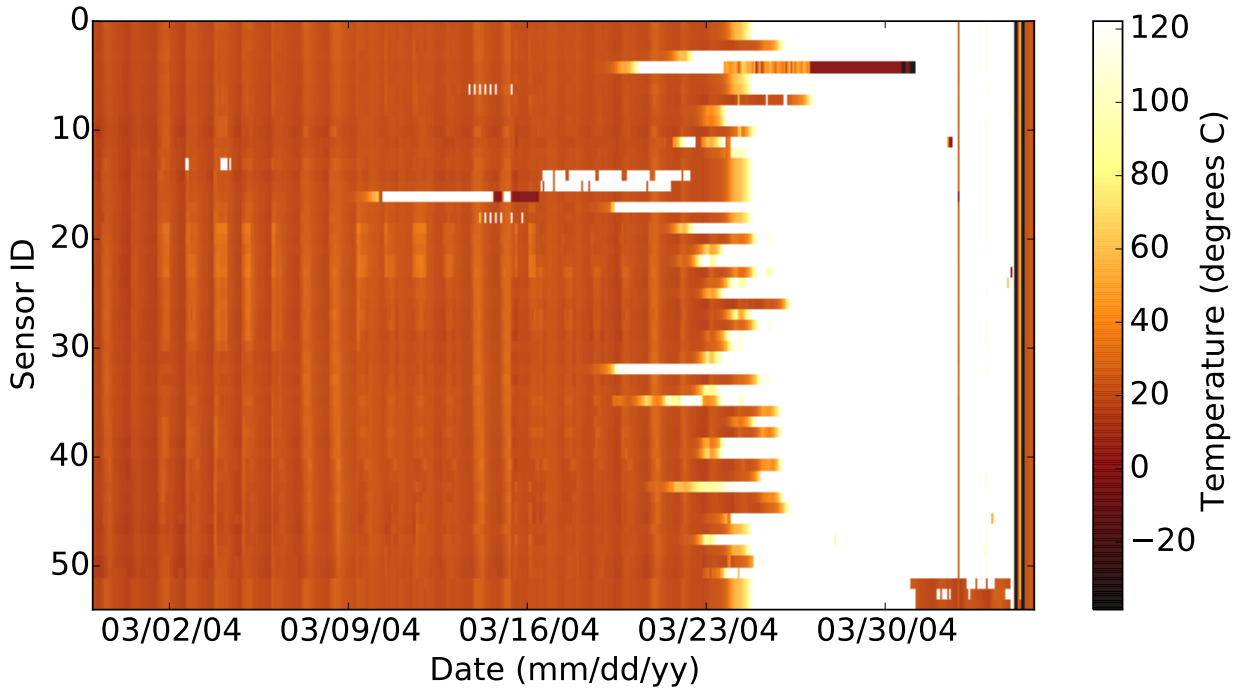

Figure 3.1: Sample of temperature data from Intel Berkeley Research. The white spots are anomalous measurements.

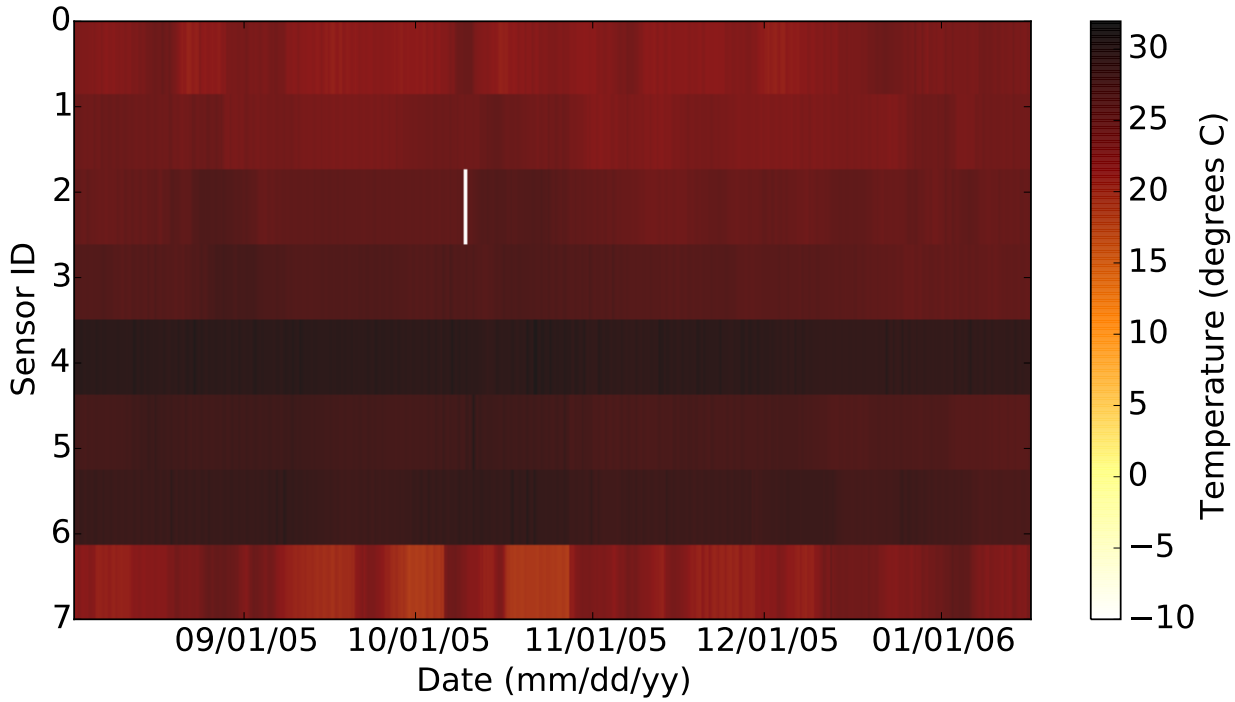

Figure 3.2: Sample of sea surface temperature data from the Tropical Atmosphere Ocean Project by the Pacific Environmental Laboratory. The white spot in Sensor 2 is an anomaly.

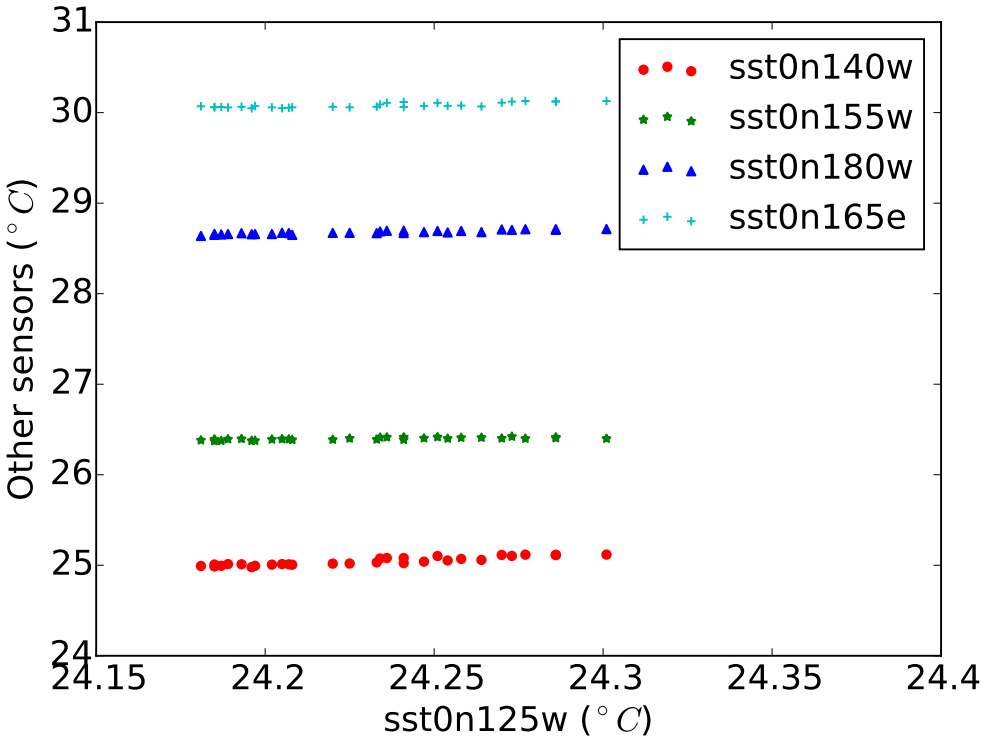

Figure 3.3: TAO Dataset: linear relationships and closeness in measurements values as a function of physical distance.

Pacific Ocean on the equator (0°N) at 95°W, 110°W, 125°W, 140°W, 155°W, 170°W, and 165°E. Several sensors are located on the moorings, as described in [20], and we analyze the sea water temperature data measured by the thermistors at 1 to 1.5 m below the surface.

The data for all 8 sensors was available between 2 Aug 2005 and 16 Jan 2006, and is illustrated in Fig. 3.2. The anomaly in the dataset is the obvious white mark for Sensor 2. The reason for the anomaly was not described by the providers of the dataset, and we assume that the sensor malfunctioned in those time periods. Note that water temperatures can go below 0 °C, but that only happens near the North and South poles, and the temperature never goes below −2 °C. Therefore, the anomalies in this particular dataset could be detected by trivial thresholds set with that prior knowledge.

Figure 3.3 shows how linearly related the ocean temperatures seem to be over a five hour period. There are 30 measurements in the plot and it can be seen that the magnitudes of the temperatures bear some relationship to the physical distance between the sensors. Sensor $sst0n125w$ measures temperatures in the range of 24 °C. Among the sensors plotted, Sensor

$sst0n140w$ is the nearest to $sst0n125w$ in distance (it is 15 degrees west of $sst0n125w$, as measured by longitudinal geodesic distance). It can be seen that the measurements taken by $sst0n140w$ are nearest in magnitude to $sst0n125w$. The next sensor west of $sst0n140w$ on the equator is $sst0n155w$, and its magnitude is the next closest to $sst0n125w$. That trend continues on till $sst0n165e$, which is farthest (both in geodesic distance and measurement magnitude) to $sst0n125w$.

The highest resolution data obtained from the sensors was a 10 minute average reading. That data was stored internally in the mooring, and acquired from the memory later when recovering the mooring. Daily averages were transmitted to satellites for what the PMEL refers to as real-time monitoring. We do not know why the more fine-grained information is not transmitted, but we assume it is because of the sensors are battery-powered and the energy cost of transmission is high.

Since the data is monitored once a day, the more fine-grained weather changes cannot be monitored. If anomalous readings were to be recorded, they would not be discovered until the end of the 24 hour cycle (assuming they significantly alter the daily mean). For example, if changes in sea temperature were important to monitor to identify potential cyclones, the necessary granularity would be missing in this data. The TAO project was set up to study the El Nino Southern Oscillations, which can lead to severe cyclones.

In order to capture and report the fine-grained changes in measurements, our energy-efficient P2P validation protocol can be applied in a way that minimizes the transmission cost for the sensors. The protocol can be used to monitor and report anomalies in more fine-grained temporal resolution so that the appropriate actions can be taken (raise an alarm for a storm, or disregard the reading as unreliable). The non-anomalous readings could continue to be recorded once a day, or on recovering the mooring, and are not as important to transmit since they do not contain information that needs to be acted upon immediately. In addition, more spatially fine-grained data can be obtained by installing more moorings in the area, forming a more dense sensor network.

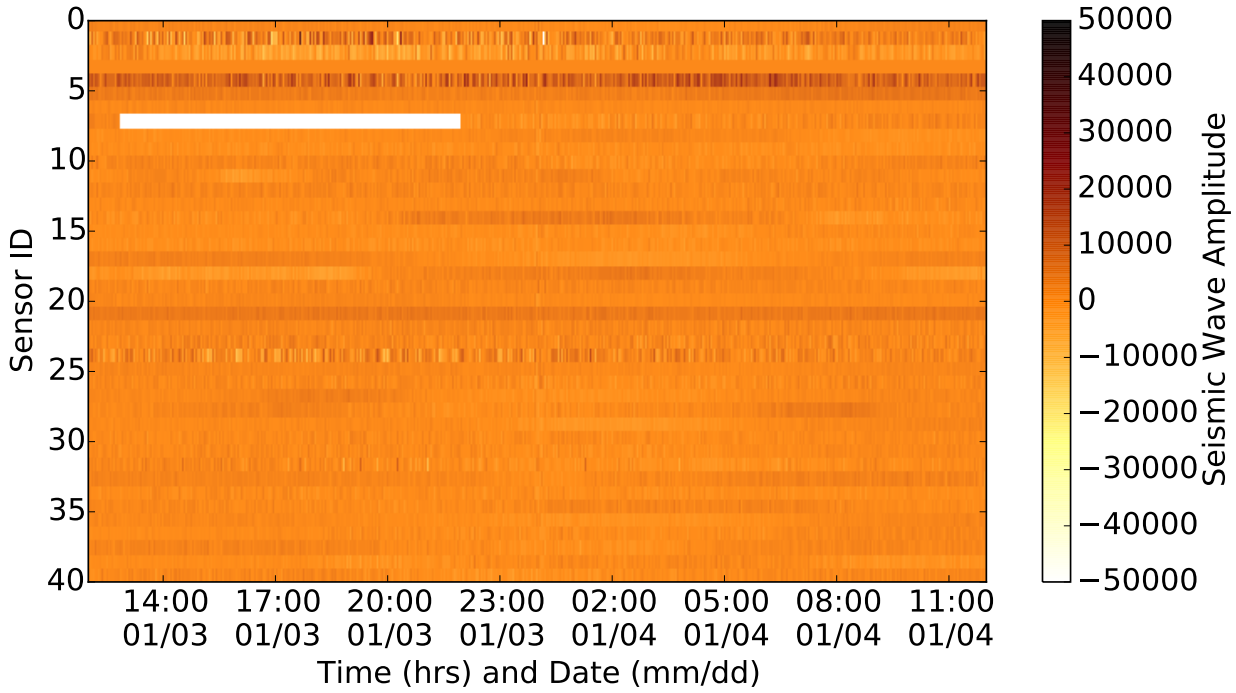

Figure 3.4: Sample of the seismic waveform data in the GeoNet National Seismograph Network in New Zealand. Note that the seismic amplitude has no unit specified since the data is uncalibrated.

3.3 Seismic Wave Measurement Data (NZ)

This dataset was obtained from the GeoNet National Seismograph Network in New Zealand [1]. Broadband seismic data was obtained from stations evenly distributed throughout the country.

This dataset is the most interesting of the three that we study in this thesis. That is because the anomalies in this dataset not only correspond to sensor failures, but also are caused by extreme events (an earthquake).

The seismic waveform data we extracted is from 41 stations in the seismograph network, for the 24hr period between 12:00hrs on 3 January and 12:00hrs on 4 January 2016. The sampling rate is 100 samples per second. We take the average of each second and detect anomalies in those averages. As a result, we do not perform anomaly detection at the same rate at which the data is sampled, but at a much lower rate. The lower rate at which we perform anomaly detection is sufficiently high to capture anomalies, and sufficiently

low to ensure that anomalies are reported in a timely manner. The lower rate also helps dramatically minimize computation and network usage related costs. The averaged data is shown as a heat map in Fig. 3.4.

The seismic amplitude has no unit specified since the data is uncalibrated. The providers of the data informed us that calibrating the data is a complex procedure, and we avoided the need for that procedure by normalizing the data in our models so that the normalized values are inherently unitless.

The large white gap for Sensor 7 was due to a failure. That anomaly is illustrated along with another anomaly with Sensor 10 in time series plots in Fig 3.5.

There were other, less noticeable, white spots (most noticeable in Sensor 1, at high zoom) at 00:08 hrs on 4 January, and they coincided with a strong earthquake that had occurred at the same time (with a magnitude of 5.0 on the Richter scale). Based on separate earthquake data provided by GeoNet, we found the ground truth on the earthquake recorded at 00:08 hrs on 4 January. The details of the earthquake are available at `http://www.geonet.org.nz/quakes/region/newzealand/2016p008122`.

The impact of the earthquake on the seismic waveforms for three seismic stations (closest to the earthquake epicenter) is illustrated in Fig 3.6. The spike due to the earthquake is noticeable in the measurements taken by all the stations in the seismograph network, but to varying degrees. For example, the spike due to the earthquake is less prominent for Sensors 7 and 10, but is still visible in Fig 3.5.

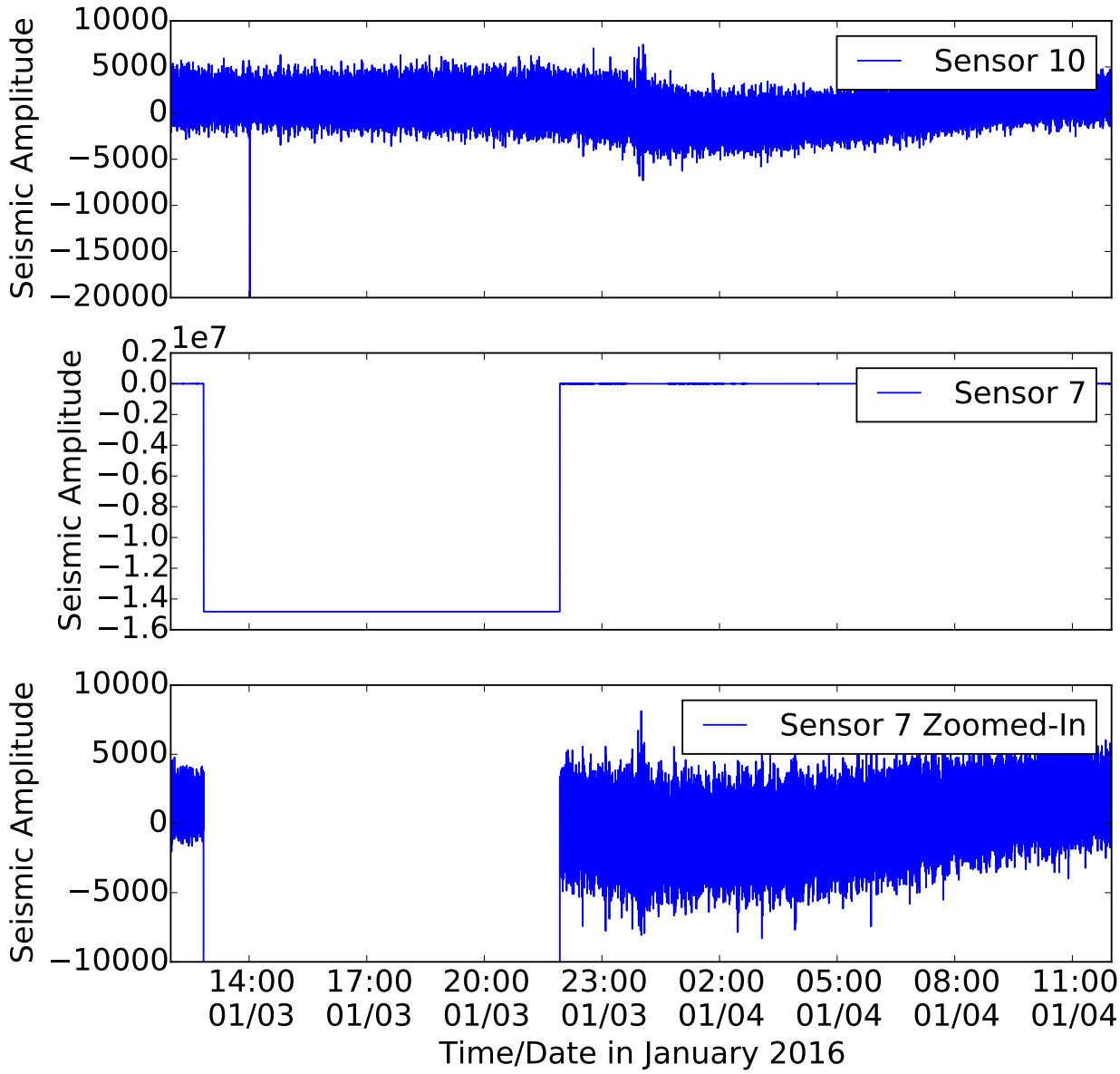

Figure 3.5: NZ Dataset: Anomalies observed in the measurements taken by Sensors 7 and 10.

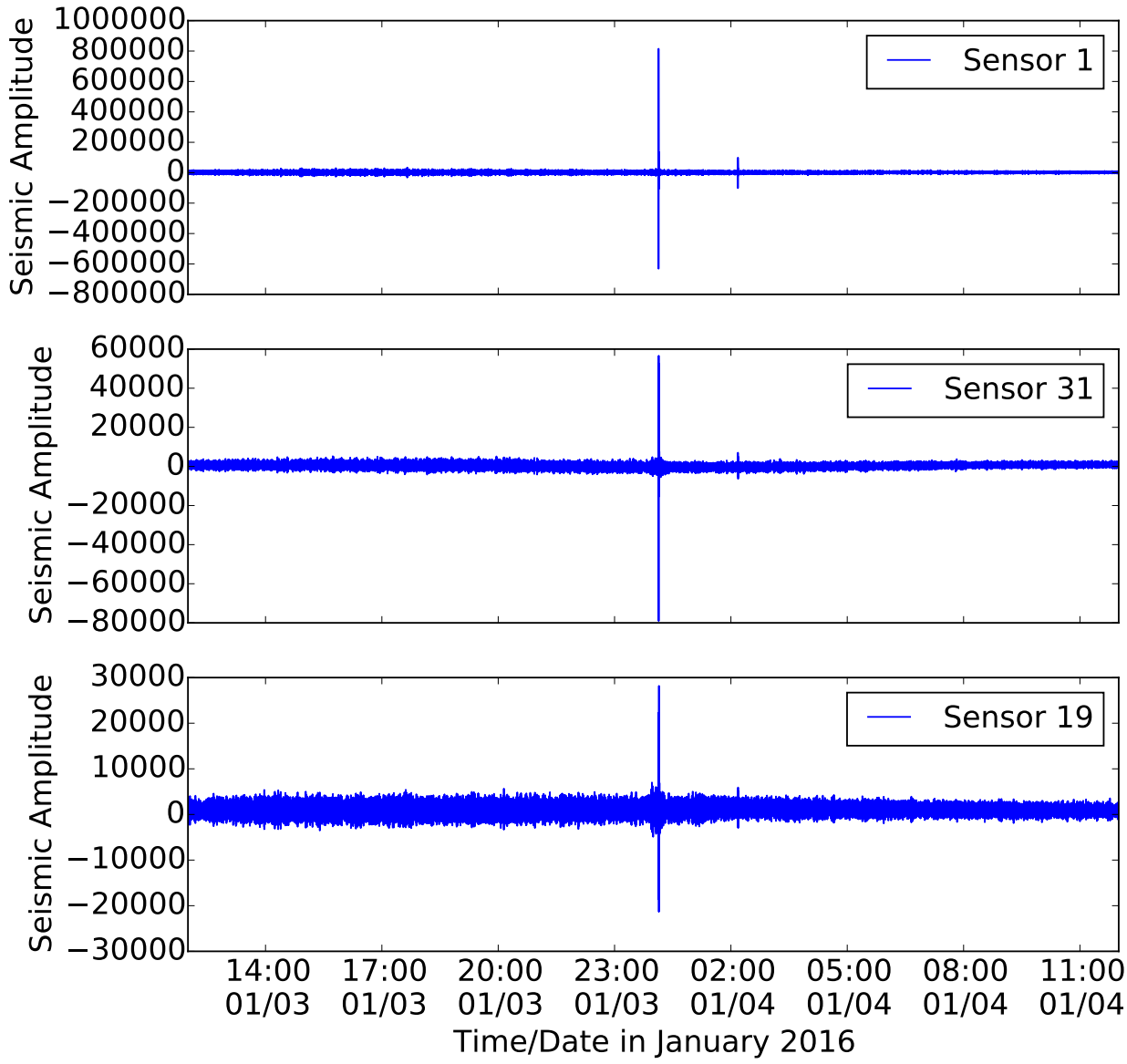

Figure 3.6: NZ Dataset: Earthquake observed in the measurements taken by three sensors. It is manifested as a spike in the waveform.

CHAPTER 4

P2P ERROR DETECTION PROTOCOL

We propose a P2P sensor measurement error detection protocol as an alternative to the centralized protocol described in Chapter 1, which we use as a comparison baseline. In this section, we describe that protocol and show that it minimizes the number of message transmissions within the assumptions stated in Chapter 2. In that sense, it is energy-optimal.

4.1 Protocol Description

The protocol comprises three stages: reference sensor identification, telemetry/detection, and response. In the first stage, each sensor identifies neighboring sensors whose measurements are most similar to its own, and marks those sensors as *reference sensors*. The *reference sensors* are used in the second stage of the protocol, which combines telemetry with error detection and fault reporting. In the third stage, the sink identifies the faulty sensor from fault reports, and responds to the reports.

The main algorithm running on each sensor, which encompasses all three stages, is described in Fig. 4.1. Note that Stage 2 cannot be started until Stage 1 is completed. Also, note that Stage 3 happens at the sink, and is only reflected in the sensor behavior in lines 17–18 of the algorithm in Fig. 4.1. Stage 3 happens after a fault has been reported in Stage 2, and if a sensor has been commanded to operate in a forwarding-only mode, the sensor remains in that mode, effectively exiting from Stage 2.

Each sensor in the WSN operates independently and its stage does not need to be in sync with other sensors' stages. For example, sensor $S^{(1)}$ might have just joined the WSN and be in Stage 1, while sensor $S^{(2)}$ is in Stage 3.

In this Stages 1 and 2, each sensor broadcasts its measurements to its immediate neighbors

using its omnidirectional antenna at all discrete time steps given by the sampling_interval.

Figure 4.1: P2P protocol at each sensor

```
 1: stage1_complete ← False
 2: candidates ← empty_1D_array(size_M)
 3: reference_sensors ← empty_1D_array(size_R)
 4: candidate_measurements ← empty_2D_array(size_M,size_T)
 5: in_forwarding_only_mode ← False
 6: while True do
 7:    neighbor_messages ← get_messages_from_buffer()
 8:    for message in neighbor_messages do
 9:       if message.id = sink.id and message.command = forwarding_only then
10:          in_forwarding_only_mode ← True
11:       else if message.destination_id = sink_id then
12:          forward_message(message)
13:       else if message.command = routing_details then
14:          update_routing_details(message)
15:       end if
16:    end for
17:    if in_forwarding_only_mode then
18:       continue
19:    end if
20:    if not stage1_complete then
21:       complete_stage1(neighbor_messages)
22:       stage1_complete ← True
23:    else
24:       complete_stage2(neighbor_messages)
25:    end if
26:    sleep(sampling_interval)
27: end while
```

4.1.1 Stage 1

Stage 1 is illustrated at a high level in Fig. 4.2 and inherits the global variables defined in Fig. 4.1. Let sensor $S^{(1)}$ be within range of N sensors. In Stage 1, $S^{(1)}$ randomly selects up to M *candidate sensors* from those N sensors, as shown in line 1 of Fig. 4.2. $S^{(1)}$ then stores T measurements that have been broadcast by each of those M sensors, as shown in in line 5 of Fig. 4.2. The store function overwrites the oldest measurement in memory if T values are already stored. Thus, the memory requirement for the sensors is $O(MT)$, where M and

T are fixed.

After $S^{(1)}$ has received T measurements for a candidate sensor, it determine its similarity with that candidate sensor using the function *get_similarity_with_self*() (line 7 of Fig. 4.2). That function uses a similarity metric, for which we present a detailed example in Chapter 5. $S^{(1)}$ then chooses the top R most similar sensors to be its *reference sensors* ($R \leq M \leq N$), as shown in line 8 of Fig. 4.2). Stage 1 is completed once the reference sensors have been determined.

The parameters M, R, and T can be set by the WSN administrator during installation as needed (for example, $M = 10$, $R = 5$, and $T = 30$). N is a feature of the physical sensor layout, and is not as flexible as the other parameters. Note that $S^{(2)}$ may be a reference sensor for $S^{(1)}$, but the reverse relationship may not hold, as there may be R sensors within $S^{(2)}$'s range that are more similar to $S^{(2)}$ than $S^{(1)}$ is to $S^{(2)}$.

Figure 4.2: P2P protocol for Stage 1 (complete_stage1) at each sensor

```
 1: broadcast_current_reading_to_neighbors()
 2: candidates ← randomly_select_M_sensors(neighbor_messages)
 3: for i = 1 to M do
 4:    m ← get_measurement_from_messages(candidates[i],neighbor_messages)
 5:    candidate_measurements[i].store(m)
 6:    if count(candidate_measurements[i]) = T then
 7:       similarity ← get_similarity_with_self(candidate_measurements[i])
 8:       reference_sensors.insert_at_sorted_position(candidates[i],similarity)
 9:    end if
10: end for
```

Note that we have an extension to the P2P protocol, in which Stage 1 is repeated periodically to accommodate changes in the network (discussed in Section 4.4). Thus, the neighbors are not preconfigured in each sensor, but determined from the messages received from broadcasts (as shown in line 1 of Fig. 4.2).

4.1.2 Stage 2

Stage 2 is described at a high level in Fig. 4.3. In Stage 2, at every time period, $S^{(1)}$ examines the new measurement received from each of its R reference sensors. $S^{(1)}$ uses the T past

measurements to model the behavior of each of its reference sensors, using an approach detailed in Chapter 5. If a sensor measurement from one of the reference sensors is found to be anomalous as per that model (line 5 of Fig. 4.3), $S^{(1)}$ marks its own measurement as *anomalous*. If $S^{(1)}$'s measurement is found to be anomalous with respect to the majority of its R reference sensors' measurements, $S^{(1)}$ declares its own measurement as *erroneous*. $S^{(1)}$ then immediately reports itself to the sink as faulty along with the erroneous measurement. If $S^{(1)}$ has only two reference sensors, it reports the fault only if its measurement is anomalous with respect to the measurements of both those reference sensors. The majority vote increases the confidence in a fault report, and is a measure against false positives. A scenario is possible in practice, although unlikely, wherein the majority of reference sensors are faulty, and the sensor incorrectly marks itself as being faulty, following the majority. To enable investigation in that scenario, when a sensor reports itself as faulty, it includes in that message a list of all reference sensors that it used to find itself faulty (suspecting_sensors). That allows a network administrator to investigate those suspecting_sensors (line 10 of Fig. 4.3).

Figure 4.3: P2P protocol for Stage 2 (complete_stage2) at each sensor

```
 1: broadcast_current_reading_to_neighbors()
 2: suspecting_sensors ← empty_queue()
 3: for reference_sensor in reference_sensors do
 4:     r ← get_measurement_from_messages(reference_sensor,neighbor_messages)
 5:     if is_anomalous(r,candidate_measurements) then
 6:         suspecting_sensors.enqueue(reference_sensor)
 7:     end if
 8: end for
 9: if count(suspecting_sensors) > count(reference_sensors)/2 then
10:     report_fault_to_sink(current_measurement,suspecting_sensors)
11: end if
```

4.1.3 Stage 3

Stage 3 happens at the sink after a sensor has asynchronously reported a fault in Stage 2. In this stage, the sink responds to the fault report by taking one of three decisions: 1) commanding that sensor to serve purely as a forwarding node in a multi-hop network, 2)

ignoring the error, assuming it will be transient, or 3) treating the error as an indication of an event of interest (e.g., earthquake or cyclone), and taking appropriate steps to alert stakeholders (administrators, government agencies, the public, etc.). We illustrate the first response in Fig. 4.4. The other two responses may not be automated, so we do not illustrate them.

When a sensor receives the forwdaring_only message from the sink (line 9 of Fig. 4.1), it remains in forwarding mode and does not run Stages 1 or 2 (line 17–18 of Fig. 4.1).

Figure 4.4: P2P Protocol for Stage 3 at sink

```
1: sensor_messages ← get_messages_from_buffer()
2: for message in sensor_messages do
3:    if message.command = report_fault then
4:       update_sensor_fault_stats(message)
5:       if is_persistent_fault(message) then
6:          send_sensor_command(message.sender_id,forwarding_only)
7:       end if
8:    end if
9: end for
```

4.2 Required Properties of the Anomaly Detection Approach and Similarity Metric

The similarity metric, which is used to find reference sensors in $get\_similarity\_with\_self()$ (line 7 of Fig. 4.2), and the anomaly detection approach (used in $is\_anomalous()$ in line 5 of Fig. 4.3) are key to ensuring that the P2P protocol minimizes error report transmissions.

Consider three sensors, $S^{(1)}$, $S^{(2)}$, and $S^{(3)}$, each of which is a reference sensor for the other two. Let their readings at time t be $S_t^{(1)}$, $S_t^{(2)}$, and $S_t^{(3)}$, respectively. In order to minimize error report transmissions, the P2P protocol may use *any* anomaly detection approach and similarity metric that have the following two properties:

Property 1 *(Symmetry)*: The probability that $S^{(2)}$ finds $S_t^{(1)}$ to be anomalous is equal to the probability that $S^{(1)}$ will simultaneously find $S_t^{(2)}$ to be anomalous.

Property 2 *(Greater similarity implies greater sensitivity to anomalies)*: Assume that

the similarity between $S^{(1)}$ and $S^{(2)}$ is greater than the similarity between $S^{(1)}$ and $S^{(3)}$. Then, the probability that $S^{(2)}$ will mark $S_t^{(1)}$ as anomalous is greater than the probability that $S^{(3)}$ will mark $S_t^{(1)}$ as anomalous, because $S^{(2)}$ was more similar to $S^{(1)}$.

We prove energy-optimality assuming the above properties in Section 4.5, and present an anomaly detection approach and similarity metric that have both properties in Chapter 5.

4.3 Memory Requirement

In all stages, each sensor stores T measurements broadcast by each of the M candidate sensors. At each time period, a new measurement is stored and oldest of the T measurements is discarded, so that the memory requirement is bounded to MT floating point measurements. As a result, the memory requirement is $O(MT) = O(1)$, since M and T are fixed for a given WSN. A typical experiment may have $R = 3$, $M = 10$, $T = 300$, and $N = 200$. Thus, the memory requirement is well within low-cost sensor hardware capabilities.

4.4 Handling Changes in the Network

The WSN may change over time because of churn (in mobile settings) or changes in the environment being monitored (resulting in a need for an updated model of sensor measurement behavior). To account for those changes, the latest T measurements are refreshed after a new set of M measurements (from the M candidate sensors) are received at every time interval. Stage 1 of the protocol may be repeated, and a new set of R reference sensors may be selected if the similarity rankings of the candidate sensors changed.

Instead of randomly selecting a new set of M candidates, Stage 1 as given in Fig.4.3 can be modified as follows. The Q least similar sensors are occasionally removed from the candidate sensor list and replaced with Q other randomly chosen sensors from the $N - M$ neighbors, where $Q \leq M - R$. This allows those Q other sensors to be given a chance to be chosen as reference sensors. All that is implemented in place of line 1 of Fig.4.3. The remaining lines of Fig.4.3 remain the same.

In order to accurately realize the energy-efficient protocol, it is necessary for the reference sensors to represent the most similar sensors within a given sensor's range.

4.5 Proof of Energy-Optimality

Many strategies for energy-optimized communication have been proposed that highlight the importance of minimizing the number and length of messages to extend the lifetime of the network (as surveyed in [9]). The advantage of our protocol is that a single message sent by the erroneous sensor (solid red arrows in Fig. 4.5) is sufficient to correctly report an error. Therefore, our approach is energy-optimal in that it minimizes the number of messages required to report the error to the sink.

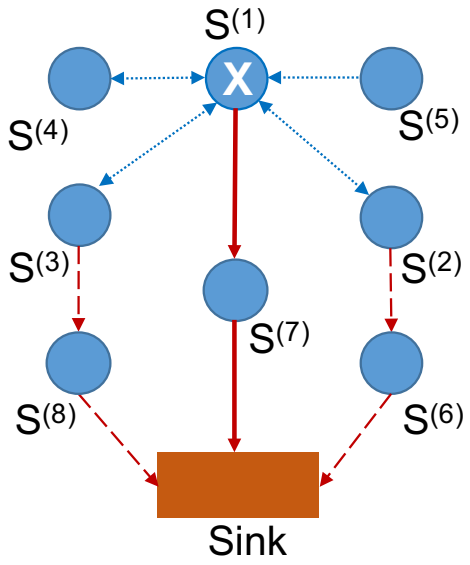

Figure 4.5: WSN showing the routing path of the optimal message in our protocol that reports the erroneous measurement (solid red arrow), unnecessary messages that report anomalous measurements (dashed red arrows), and messages containing measurements (dotted blue arrows). Sensor $S^{(1)}$ is faulty.

Figure 4.5 illustrates the various relationships among sensors in the protocol. In that illustration, sensor $S^{(1)}$ is in error. The bidirectional blue dotted arrows show mutual reference sensor relationships between $S^{(1)}$ and $S^{(2)}$, $S^{(3)}$, and $S^{(4)}$. $S^{(1)}$ uses $S^{(5)}$ as a reference sensor, but the reverse relationship does not hold. $S^{(1)}$ and $S^{(7)}$ are not reference sensors for each

other, but $S^{(7)}$ is in $S^{(1)}$'s shortest path to the sink.

Consider $S^{(1)}$, $S^{(2)}$, and $S^{(3)}$ in the example in Fig. 4.5. Let their readings at time t be $S_t^{(1)}$, $S_t^{(2)}$, and $S_t^{(3)}$, respectively. Each sensor receives the readings from the other two sensors at time t. Then, when $S^{(1)}$ exchanges its readings with $S^{(2)}$ and $S^{(3)}$, all three sensors would immediately detect that there is an anomaly (by the two properties in Section 4.2). In that situation, a suboptimal approach (such as the one in [6]) would have $S^{(2)}$ and $S^{(3)}$ report the anomaly to the sink, leaving the sink to count votes and make a decision on the error. That decision would affect not only the battery life of $S^{(2)}$ and $S^{(3)}$, but also that of $S^{(6)}$ and $S^{(8)}$, which are on their respective routing paths to the sink. Another suboptimal alternative would be for $S^{(2)}$ and $S^{(3)}$ to let $S^{(1)}$ know that they believe $S^{(1)}$'s measurement is anomalous, so that $S^{(1)}$ can then report its own error to the sink. While that approach is significantly more energy-efficient than the previous one, it is still suboptimal. In our approach, $S^{(1)}$ implicitly recognizes that $S^{(2)}$ and $S^{(3)}$ must have found it to be in error, and it reports itself as erroneous to the sink.

It is obvious that *at least one message must be necessary* in order for $S^{(1)}$ to implicitly recognize the fact that the majority of its 3 reference sensors found it to be anomalous. The fact that *one message is sufficient* is not obvious, and is crucial in ensuring that the protocol correctly reports the anomaly, while minimizing message transmissions (which is the objective of this thesis). In order to show that one message is sufficient, we use Properties 1 and 2, as stated in Section 4.2.

Lemma 1. *Assume that the similarity between $S^{(1)}$ and $S^{(2)}$ is greater than the similarity between $S^{(1)}$ and $S^{(3)}$. Then the probability that $S^{(1)}$ would mark its own measurement as anomalous with respect to $S^{(2)}$'s measurement is greater than the probability that it would mark its own measurement as anomalous with respect to $S^{(3)}$'s measurement.*

Proof. We know from Property 2 that, if $S_t^{(1)}$ were anomalous, the anomaly would be recognized with greater probability by $S^{(2)}$ than by $S^{(3)}$. From Property 1, we know that if $S^{(2)}$ finds $S_t^{(1)}$ to be anomalous, then $S^{(1)}$ would find $S_t^{(2)}$ to be anomalous with equal probability. The Lemma follows. □

Lemma 1 is phrased from the perspective of $S^{(1)}$ as it is detecting whether its own mea-

surement is anomalous with respect to measurements from $S^{(2)}$ and $S^{(3)}$ at time t. Also, it follows that $S^{(2)}$ is the better sensor to be used by $S^{(1)}$ as a reference for anomaly detection, because its greater similarity with $S^{(1)}$ implies greater sensitivity to anomalies.

Lemma 1 also highlights an important relationship detail. Consider $S^{(1)}$ and $S^{(5)}$ in Fig. 4.5. $S^{(1)}$ uses $S^{(5)}$ as a reference sensor, meaning $S^{(5)}$ sends $S^{(1)}$ its measurements. $S^{(5)}$ may not use $S^{(1)}$ as a reference sensor because it may have found other sensors that are more similar to it. Therefore, $S^{(5)}$ does not consider whether $S_t^{(1)}$ is anomalous at time t, but if it did, and the similarity between $S^{(1)}$ and $S^{(5)}$ were greater than that between $S^{(1)}$ and $S^{(3)}$, then it would have detected $S_t^{(1)}$ as anomalous with greater probability than $S^{(3)}$ would have (by Property 2). However, from Lemma 1, $S^{(5)}$ does not need to consider whether $S_t^{(1)}$ is anomalous at time t for $S^{(1)}$ to know that it did. As long as $S^{(1)}$ found $S_t^{(5)}$ to be anomalous, we know that $S^{(5)}$ would have found $S_t^{(1)}$ to be anomalous with equal probability (by Property 1). Therefore the reference sensor relationship does not need to be a two-way relationship for the protocol to work.

In [6], the authors suggest than any sensor that detects an anomalous measurement must report the anomaly to the sink. However, that leads to unnecessary energy overhead for the various sensors that detect the anomaly, and for the sensors on their multi-hop routing paths. We now show that the erroneous sensor will recognize that other sensors have found it to be anomalous without requiring those sensors to waste messages transmissions communicating their knowledge of the anomaly.

Theorem 1. *In the system model described in Section 2.1, let $S^{(A)}$ be a sensor whose measurement at time t, $S_t^{(A)}$, is deemed anomalous by any neighboring sensor $S^{(V)}$. Then, the P2P error detection protocol, described in Section 4.1, ensures that $S^{(A)}$ will implicitly recognize that $S_t^{(A)}$ is anomalous with respect to that sensor's measurement, $S_t^{(V)}$.*

Proof. If $S^{(V)}$ is one of $S^{(A)}$'s reference sensors, $S^{(A)}$ would evaluate its own measurements with respect to $S^{(V)}$'s measurements and will recognize that $S^{(V)}$ found $S_t^{(A)}$ to be anomalous as soon as it finds that $S_t^{(V)}$ was anomalous (by Property 1).

If $S^{(V)}$ is not one of $S^{(A)}$'s reference sensors, $S^{(A)}$ would not check its measurements against $S^{(V)}$, and will not know that $S_t^{(A)}$ is anomalous with respect to $S_t^{(V)}$. However, based on

how reference sensors are chosen, $S^{(V)}$ not being one of $S^{(A)}$'s reference sensors implies that $S^{(A)}$'s reference sensors are more similar to $S^{(A)}$ than $S^{(V)}$ is to $S^{(A)}$. From Lemma 1, that means that if $S_t^{(A)}$ were anomalous with respect to $S_t^{(V)}$, $S_t^{(A)}$ would also be anomalous with respect to the measurements of *all* of $S^{(A)}$'s reference sensors. In that scenario, although $S^{(A)}$ is not checking its measurements against $S^{(V)}$, $S^{(A)}$ will implicitly recognize that it is anomalous using its reference sensors' measurements. □

Corollary 1. *In the system model described in Section 2.1, consider a sensor that generates a measurement that is deemed anomalous by the majority of that sensor's reference sensors. Exactly one message is sufficient to report the fact that the majority of multiple reference sensors detected the anomaly.*

Corollary 1 follows from Theorem 1, for if a sensor implicitly recognizes itself as erroneous, it is not necessary for any sensor other than the erroneous sensor to report itself as erroneous to the sink. We believe that this result is a major contribution of our work, combining results from anomaly detection and routing theory in the design of an energy-optimal error detection protocol that is easy to implement.

The path of the single message reported by erroneous sensor $S^{(1)}$ is given by the solid red line in Fig. 4.5. That message is sufficient to capture the anomaly detected by the majority of $S^{(1)}$'s reference sensors. No other sensor is required to report the error, unlike in the approach suggested in [6].

4.6 Main Strength and Limitation

The main strength of our approach lies in the fact that we minimize the number of messages required to report an error to the sink. Exactly one message needs to be sent to the sink when the network agrees that a sensor is in error, which happens when the majority of the sensors most sensitive to an anomaly find that the sensor's reading is anomalous.

The P2P protocol scales well to dense sensor networks where each sensor might have several sensors within range to choose from. By controlling the parameter M described in

Section 4.1, the memory requirement for each sensor can be limited to order $O(1)$, for fixed M and T.

The P2P protocol can also be used in the context of mobile sensors, since we periodically refresh the list of M candidate sensors from which R reference sensors are chosen.

The main limitation of our approach is the reliance of each sensor on the existence of at least two similar sensors within its wireless communication range to serve as reference sensors. For simplicity, we assume that reference sensors are always within one hop of the sensor that is using them for reference. Since the one-hop distance implies spatial closeness in a setting where sensors have a limited wireless communication range, it is assumed that a sensor would find sufficient reference sensors to meaningfully vote on an error. However, in a setting with isolated sensors or wireless signal barriers separating nearby sensors, our protocol may not be able to find sufficient reference sensors to vote on an anomaly.

In order to address that limitation, the protocol can be trivially extended to allow sensors to report their own measurements as erroneous, using their own past measurements for reference (without requiring any other sensor). Discussion of that extension is beyond the scope of this thesis, but we provide a solution in [21]. That approach uses the Auto-regressive Integrated Moving Average (ARIMA) model from past measurements to construct a confidence interval to validate future measurements. The choice of confidence interval impacts detection and false positive rates. Those rates can be controlled by setting appropriate thresholds set for classifying measurements as anomalous. An Auto-regressive (AR) model alone may be sufficient to detect anomalies at a computation cost much lower than that of the ARIMA model. The computation cost is important to consider because running complex algorithms on sensor hardware impacts the battery life.

CHAPTER 5

VALIDATION OF SENSOR MEASUREMENTS

In this chapter, we present a detailed description of an anomaly detection approach and an associated similarity metric that satisfy both the properties required by our P2P protocol (stated in Section 4.2). We use isocontours on a bivariate normal distribution to draw an anomaly detection boundary, assuming that T measurements of two sensors have a joint distribution that can be approximated by the normal distribution.

5.1 Summary of Approach

Consider two sensors S_X and S_Y that take T measurements in T time periods. We seek to determine whether a new measurement tuple (x, y) (from the two sensors S_X and S_Y respectively) is statistically consistent with the past T measurements taken by S_X and S_Y. The new measurement would typically arrive at time period $T + 1$.

Consider the simple model where S_Y sends all its measurements to S_X. Let X and Y denote the vector of the past T measurements from S_X and S_Y respectively. Then S_X has both X and Y in its memory. Our assumption is that X and Y are jointly normally distributed. Therefore, S_X can create an isocontour from the jointly normal distribution to define a region of normal and anomalous points.

For illustration (Fig. 5.1), we use two arbitrary sensors from the NZ dataset, and set $T = 300$ to capture measurements during a 5 minute interval. In order to remove the effects of having X and Y at different scales, and to simplify the anomaly detection procedure (to meet low power constraints on sensors), we center the data and divide by the standard deviation. That explains the range of the vertical and horizontal scales in the figure, and why the isocontour is centered at the origin. The red point is an anomalous point (caused

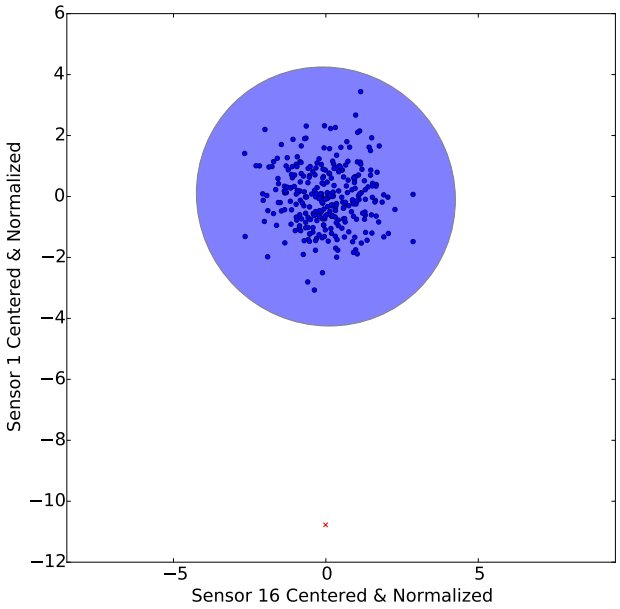

Figure 5.1: Single anomalous measurement (in red) in the NZ dataset is detected by constructing an isocontour (blue shaded elliptical region) as a detection boundary. Normal measurements are inside the isocontour and are jointly Gaussian.

by an earthquake). Note that the measurement was not anomalous as per Sensor 16's measurements, but was anomalous as per Sensor 1's measurements. That is explained in Section 5.7, but for now we just point out that the anomalies are relative to the joint Gaussian model of two sensors.

5.2 Anomaly Detection Approach Assumptions

The main assumptions for this anomaly detection approach are: 1) anomalies can lie anywhere in the two-dimensional vector space spanned by both sensors' normalized measurements, 2) anomalies lie farther away from the cluster centroid than proper measurements, and in a manner that an elliptic isocontour can be used to separate them from proper measurements (as shown in Fig 5.2), while maintaining an acceptable trade-off between true positives and false positives, and 3) that elliptical isocontour must be centered at the centroid of the proper measurements. The choice of the sliding window size, T, is crucial to ensuring that these assumptions hold.

The reasoning behind our anomaly detection procedure applies to two sensors whose mea-

surements are jointly Gaussian. In practice, if they are jointly Gaussian, then detection thresholds can be defined by well-known confidence intervals (or probabilities) for the Gaussian distribution. If they are not strictly Gaussian, we may not be able to associate the threshold with a confidence interval or probability. Even so, as along as the three aforementioned assumptions hold, a valid detection boundary can be drawn using the approach presented in this chapter.

5.3 Isocontours of the Bivariate Normal Distribution

The joint PDF of the Gaussian distribution for two random variables $X \sim N(\mu_X, \sigma_X^2)$ and $Y \sim N(\mu_Y, \sigma_Y^2)$ is given as follows:

$$f_{X,Y}(x,y) = \frac{1}{2\pi\sigma_X\sigma_Y\sqrt{1-\rho^2}} exp\{-\frac{1}{2(1-\rho^2)}[C_{X,Y}(x,y)]\} \tag{5.1}$$

$$C_{X,Y}(x,y) = \frac{(x-\mu_X)^2}{\sigma_X^2} + \frac{(y-\mu_Y)^2}{\sigma_Y^2} - \frac{2\rho((x-\mu_X)(y-\mu_Y)}{\sigma_X\sigma_Y} \tag{5.2}$$

An isocontour is the equation of a hyperplane (in this case, a line) for which the joint distribution has the same value (denoted by U). The equation of the isocontour can be derived as follows:

$$f_{X,Y}(x,y) = U \tag{5.3}$$

$$\Rightarrow \frac{1}{2\pi\sigma_X\sigma_Y\sqrt{1-\rho^2}} exp\{-\frac{1}{2(1-\rho^2)}[C_{X,Y}(x,y)]\} = U \tag{5.4}$$

$$\Rightarrow C_{X,Y}(x,y) = \frac{(x-\mu_X)^2}{\sigma_X^2} + \frac{(y-\mu_Y)^2}{\sigma_Y^2} - \frac{2\rho((x-\mu_X)(y-\mu_Y)}{\sigma_X\sigma_Y} = V \tag{5.5}$$

$$V = -2(1-\rho^2)log(2\pi\sigma_X\sigma_Y\sqrt{1-\rho^2}U) \tag{5.6}$$

Here, V is a constant (a function of U, which is also a constant). Thus, $C_{X,Y}(x,y)$ defines the equation of an ellipse centered at (μ_X, μ_Y) at an angle with respect to the X and Y axes. Clearly, it would be very complicated and computationally expensive to compute $C_{X,Y}(x,y)$

in the above form. This motivates a simplified approach.

5.3.1 Simplified Isocontours of Two Uncorrelated Gaussians

If we were to assume that X and Y were already centered uncorrelated, then $\mu_X = \mu_Y = \rho = 0$, and Eqn. (5.6) simplifies to

$$C_{X,Y}(x,y) = \frac{x^2}{\sigma_X^2} + \frac{y^2}{\sigma_Y^2} = V \tag{5.7}$$

$$V = -2log(2\pi\sigma_X\sigma_Y U) \tag{5.8}$$

In addition, let us find the isocontour with the value U such that U is k standard deviations from the mean. Then,

$$U = f_{X,Y}(k\sigma_X, k\sigma_Y) = \frac{1}{2\pi\sigma_X\sigma_Y} exp\{-\frac{1}{2}[C_{X,Y}(k\sigma_X, k\sigma_Y)]\} \tag{5.9}$$

Substituting into V in Eqn. (5.8), we get

$$C_{X,Y}(x,y) = \frac{x^2}{\sigma_X^2} + \frac{y^2}{\sigma_Y^2} = C_{X,Y}(k\sigma_X, k\sigma_Y) = 2k^2 \tag{5.10}$$

This is a much simpler isocontour of an ellipse that is parallel to the X and Y axes, centered at the origin with major/minor radii given by $\sqrt{2}\sigma_X$ and $\sqrt{2}\sigma_Y$.

5.3.2 Obtaining the Simplified Isocontour

The first step in obtaining the simplified isocontour is to center the data by subtracting the means from both X and Y. The second step is to obtain a transformation matrix such that the transformed data is uncorrelated. That transformation matrix is obtained as follows.

Let $A = \begin{bmatrix} X & Y \end{bmatrix}$ be a $T \times 2$ matrix containing the data. Then the 2×2 covariance matrix for X and Y is given as follows:

$$\frac{A'A}{T-1} = \begin{bmatrix} Var(X) & Cov(X,Y) \\ Cov(Y,X) & Var(Y) \end{bmatrix} \tag{5.11}$$

The covariance matrix is symmetric because $Cov(X,Y) = Cov(Y,X)$. We want to estimate the matrix E that performs the following transformation:

$$AE = A^* \tag{5.12}$$

where $A^* = \begin{bmatrix} X^* & Y^* \end{bmatrix}$ is a $T \times 2$ projection of A, and has uncorrelated columns X^* and Y^*. If $Cov(X,Y) = 0$, there is nothing further to be done because $A = A^*$, and we can directly apply the simplified isocontour Eqn. (5.10).

$Cov(X,Y) \neq 0$, we are effectively interested in rotating the measurements into a new axis where the covariance is zero. That is obtained by Principal Component Analysis (PCA), which states that the orthonormal eigenvectors of the covariance matrix rotate the original data into the principal component space where the data is uncorrelated. After applying PCA, we get the covariance matrix of A^* as

$$\frac{(A^*)'A^*}{T-1} = \begin{bmatrix} L1 & 0 \\ 0 & L2 \end{bmatrix} \tag{5.13}$$

where $L1$ and $L2$ are the eigenvalues of $A'A/(T-1)$, and represent the variance in the direction of the new space spanned by the eigenvectors given by the columns of E in Eqn. (5.12). To show that E is the matrix that produces X^* and Y^* that are uncorrelated, consider the following:

$$\frac{(A^*)'A^*}{T-1} = \frac{(AE)'(AE)}{T-1} = \frac{E'(A'A)E}{T-1} \tag{5.14}$$

From the definition of eigenvectors $E = \begin{bmatrix} E1 & E2 \end{bmatrix}$ and eigenvalues $L = \begin{bmatrix} L1 & 0 \\ 0 & L2 \end{bmatrix}$, of the matrix $C_A = \frac{A'A}{T-1}$,

$$C_A E = EL \tag{5.15}$$

$$\Rightarrow E^{-1} C_A E = L \tag{5.16}$$

That is a simple proof of one of the basic principles from Linear Algebra, called the *diagonalization* of C_A. Noting that by orthonormality, $E' = E^{-1}$, we can substitute into Eqn. (5.14)

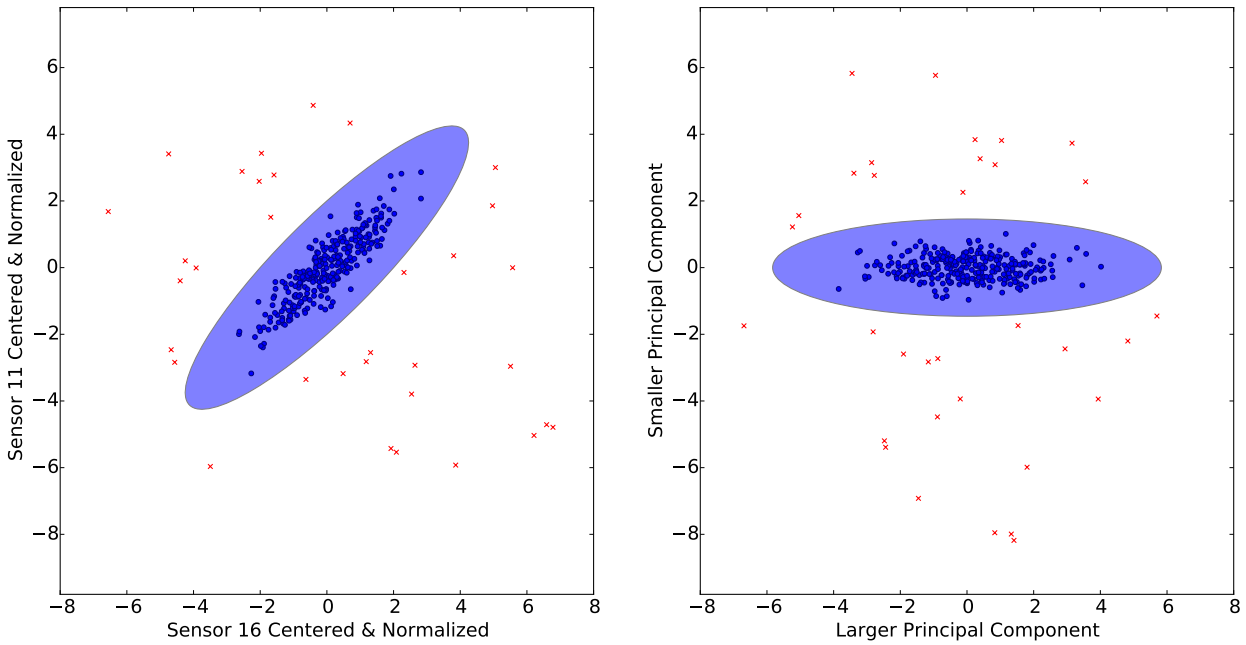

Figure 5.2: Anomalies (red crosses) in the NZ dataset due to earthquake observed in normalized measurement space (left) and the space spanned by the two principal components (right).

to get the following:

$$\frac{(A^*)'A^*}{T-1} = \frac{E'(A'A)E}{T-1} = \frac{E^{-1}(A'A)E}{T-1} = L \tag{5.17}$$

where L is a diagonal matrix containing the eigenvalues of $A'A$. Therefore $\frac{(A^*)'A^*}{T-1}$ is diagonal, and the columns of A^*, which are X^* and Y^*, are thus uncorrelated. X^* and Y^* represent the principal components in the orthogonal subspace Fig. 5.2 (right plot), while X and Y represent the points in the original space of sensor measurements (left plot).

With these new uncorrelated vectors in the new principal component space, we can apply Eqn. (5.10). Note that we cannot apply that equation directly on X and Y when they are correlated.

$$C_{X^*,Y^*}(x^*, y^*) = \frac{(x^*)^2}{\sigma^2_{(X^*)}} + \frac{(y^*)^2}{\sigma^2_{(Y^*)}} = 2k^2 \tag{5.18}$$

Note that in order for this to work, we had to rotate not only X and Y, but also the test data point (x, y) to get (x^*, y^*). The rotation was obtained from the transformation E,

resulting in the points being aligned in a way that the direction of maximum variance is in line with the horizontal axis. This is illustrated for two sensors in the NZ dataset in Fig. 5.2.

5.3.3 Calculating the Angle of Rotation

The data X and Y was rotated in the 2-D space to produce X^* and Y^* which were uncorrelated. Note that X and Y are to some extent blended together in X^* and Y^*. So in the new principal component space (Fig. 5.2 (right)), X^* and Y^* do not directly correspond to the original sensor measurements, but to some blend of the measurements. This rotation was performed purely for mathematical simplification, which in turn leads to efficient computation.

The ellipse C_{X^*,Y^*} is essentially the rotation of the ellipse $C_{X,Y}$. The angle of rotation describes the angle of the rotated ellipse with respect to the axes of the original ellipse. Calculating the angle of rotation is not useful for anomaly detection, but we present it here for completeness of the mathematical intuition. We used this approach in plotting the ellipse in the figures because the plotting tools required the angle to be specified as a parameter.

Let us give names to the elements of E. Let $E = \left[\begin{smallmatrix} e_{00} & e_{01} \\ e_{10} & e_{11} \end{smallmatrix}\right]$. And let θ be the angle of rotation. Then there is a one-to-one correspondence between the elements of E and the rotation matrix.

$$E = \begin{bmatrix} e_{00} & e_{01} \\ e_{10} & e_{11} \end{bmatrix} = \begin{bmatrix} \cos\theta & -\sin\theta \\ \sin\theta & \cos\theta \end{bmatrix} \tag{5.19}$$

$$\Rightarrow \theta = \arctan(e_{10}/e_{00}) \tag{5.20}$$

In implementing the function in code, one must note that it is possible (though in our applications highly unlikely) that $e_{00} = 0$, leading to a divide by zero error. That simply means that $\theta = 90°$ (if $e_{10} > 0$) or $\theta = 270°$ (if $e_{10} < 0$). The Numpy library in Python has a function called *arctan*2 which is an alternative to *arctan*, and takes care of those special cases.

5.4 Anomaly Detection Procedure

In this section, we explain the algorithm that goes into *is_anomalous*(), the function used in Stage 2 of the P2P protocol in line 5 of Fig. 4.3. If Sensor S_X receives all measurements from sensor S_Y, then S_X can determine whether a particular reading of S_Y was anomalous. Let the test reading be y and have a corresponding reading x measured by S_X at the same time period. S_X builds a model of S_Y's measurements using T measurements from the past. If y was found to be anomalous as per that model, then S_X declares y to be in error. The model we use is the bivariate normal distribution described in Section 5.3.

Let X be the past T measurements of S_X and Y be the past T measurements of S_Y. Let $\leftarrow$ denote the assignment operator. In summary, the anomaly detection approach is composed of the following steps:

1. Center the data for numerical simplicity so that the scatter plot is centered at the origin. Here data refers to both the historic measurements X and Y as well as the test point (x, y)

$$X \leftarrow X - \mu_X \qquad Y \leftarrow Y - \mu_Y \tag{5.21}$$

$$x \leftarrow x - \mu_X \qquad y \leftarrow y - \mu_Y \tag{5.22}$$

2. Normalize the data by dividing by standard deviation. This ensures that the difference in scale of magnitudes does not matter. For example, a sensor that is located closer to a region of large seismic activity (a volcano, for example) may have an amplitude much greater than that of a farther away sensor. We want to remove that amplitude disparity because that allows us to give equal weight to anomalies in the direction of both sensors. If we had not done that, a deviation in the direction of the sensor that measures a larger amplitude would automatically be weighted more than a deviation in the direction of the smaller amplitude. Normalization also takes care of the fact that some sensors may not be calibrated to have a standard unit (like the cast of all

our NZ data).

$$X \leftarrow X/\sigma_X \qquad Y \leftarrow Y/\sigma_Y \tag{5.23}$$

$$x \leftarrow x/\sigma_X \qquad y \leftarrow y/\sigma_Y \tag{5.24}$$

As a consequence of this step, $\sigma_X = \sigma_Y = 1$.

3. Compute the covariance matrix C_A of X and Y, as explained in Eqn. (5.3).

$$A \leftarrow \begin{bmatrix} X & Y \end{bmatrix} \tag{5.25}$$

$$C_A \leftarrow \frac{A'A}{T-1} \tag{5.26}$$

4. Compute the orthonormal eigenvectors E and eigenvalues L of C_A. A computationally simple way of doing this is presented in Section 5.4.1.

$$E, L \leftarrow eig(C_A) \tag{5.27}$$

The diagonal elements of L give the variance in the rotated space. $L = \left[\begin{smallmatrix} \sigma^2_{(X^*)} & 0 \\ 0 & \sigma^2_{(Y^*)} \end{smallmatrix}\right]$

5. Transform the test point into the principal component space given by E.

$$\begin{bmatrix} x^* & y^* \end{bmatrix} \leftarrow \begin{bmatrix} x & y \end{bmatrix} E \tag{5.28}$$

6. For a given detection threshold k, the point test point (x, y) is anomalous if the following condition holds, as explained in Eqn. (5.18):

$$\frac{(x^*)^2}{\sigma^2_{(X^*)}} + \frac{(y^*)^2}{\sigma^2_{(Y^*)}} > 2k^2 \tag{5.29}$$

5.4.1 Cost-efficient Computation of Orthonormal Eigenvectors and Eigenvalues

While designing the validation approach for a peer-to-peer validation mechanism, it is important to consider the computation cost of validation. In this subsection we show that the above detection scheme can be computed with very simple addition and multiplication operations.

For a 2x2 covariance matrix, the eigenvectors and eigenvalues can be computed using the following simple Python code. Note that no library functions were called other than the sqrt (square root function).

```
import numpy as np
def eig(X):
    D = X[0,0]*X[1,1]-X[0,1]*X[1,0]
    Tr = X[0,0]+X[1,1]
    L1 = Tr/2.0 + np.sqrt(Tr**2/4.0 -D)
    L2 = Tr/2.0 - np.sqrt(Tr**2/4.0 -D)
    if X[1,0] != 0:
        E1 = np.matrix([L1-X[1,1], X[1,0]]).reshape(2,1)
        E2 = np.matrix([L2-X[1,1], X[1,0]]).reshape(2,1)
        E1 = E1/np.linalg.norm(E1)
        E2 = E2/np.linalg.norm(E2)
    else:
        E1 = [1, 0]
        E2 = [0, 1]
    return np.array([L1, L2]),np.hstack([E1,E2])
```

Listing 5.1: A simplified implementation of the eig function

Note that the matrix X in the above example must be symmetric (a property inherent to covariance matrices). Therefore $X[0,1] = X[1,0]$, and the first condition checks to see if the matrix is a diagonal matrix. If it is a diagonal matrix, it means that the two sensors were uncorrelated to begin with. Hence there is no need to transform them onto a space where they are uncorrelated, and the transformation matrix is the identity matrix.

We now explain the mathematics of the code. Let $X = \left[\begin{smallmatrix} a & b \\ c & d \end{smallmatrix}\right]$. By definition of eigenvectors

(E) and eigenvalues (L),

$$Xv = \lambda v \Leftrightarrow (X - \lambda I)v = 0 \tag{5.30}$$

where v is a 2×1 eigenvector, λ is a scalar eigenvalue, and I is the 2×2 identity matrix. In order for Eqn. (5.30) to have a non-trivial solution, we require

$$det(X - \lambda I) = 0 \Rightarrow det(\left[\begin{smallmatrix} a-\lambda & b \\ c & d-\lambda \end{smallmatrix}\right]) = 0 \tag{5.31}$$

$$\Rightarrow \lambda^2 - (a+d)\lambda + (ad - bc) = 0 \tag{5.32}$$

where *det* is the determinant function. Let the $D = det(X) = ad - bc$ and $Tr = tr(X) = a + d$ (these are defined in lines 3 and 4 of Code 5.1). The two eigenvalues can be obtained by solving the quadratic Eqn. (5.32), and the solutions are given in lines 5 and 6 of Code 5.1. Let the first eigenvector $E1 = \left[\begin{smallmatrix} e_{00} \\ e_{10} \end{smallmatrix}\right]$ have the corresponding eigenvalue $L1$. Then, from Eqn. (5.30),

$$ce_{00} + (d - L1)e_{10} = 0 \Rightarrow \frac{e_{00}}{e_{10}} = \frac{(L1 - d)}{c} \tag{5.33}$$

Since we require orthonormal vectors, E1 is the normalized (by $L-2$ norm) form of the vector $\left[\begin{smallmatrix} (L1-d) \\ c \end{smallmatrix}\right]$. This is given for $E1$ (and similarly for $E2$) in lines 8 to 11 of Code 5.1. Note that this solution is only valid in the case where $X[1,0] = c \neq 0$ because of the division by c in Eqn. (5.33). The eigenvectors are combined into a transformation matrix $E = [E1, E2] = \left[\begin{smallmatrix} e_{00} & e_{01} \\ e_{10} & e_{11} \end{smallmatrix}\right]$

Note that lines 8 to 11 of Code 5.1 can be collapsed into a single line of Python code, but we have separated them here for better readability. Our separation of code explains how the eigenvectors are related to their eigenvalues.

5.4.2 Algorithm Complexity

Since the anomaly detection approach is executed on low-cost sensor hardware, it is essential that the implementation be simple and memory requirements be minimal. The computations in Steps 1–3 of the procedure in Section 5.4 are all $O(T)$, and Steps 4–6 are $O(1)$. Since the procedure is repeated for R reference sensors, the total algorithm complexity is $O(RT) = O(1)$ since R and T are fixed for a given WSN.

5.4.3 Robustness of Implementation

When we say that X and Y contain the past T measurements taken by sensors S_X and S_Y, we mean the past T normal measurements. Therefore, if a test measurement (x, y) is found to be anomalous, it is discarded from the model. This ensures that the model is robust and cannot easily become biased due to outliers. If the anomalies were included in the model, the area of the isocontour would effectively increase, and measurements that were earlier flagged as anomalous may no longer be flagged as anomalous as they may now fall within the isocontour.

5.5 Similarity Metric

We say that the measurements of two sensors are similar if they are tightly clustered in the 2-dimensional space. That tight clustering may be defined in many ways, but we use the area of the $k\sigma$ isocontour to determine how similar two sensors are. Mathematically, the degree of similarity is expressed as the area of the ellipse in Eqn. (5.18). That is given as follows:

$$Similarity(S_X, S_Y) = [2\pi k^2 \sigma_{(X^*)} \sigma_{(Y^*)}]^{-1} \tag{5.34}$$

5.5.1 Computation of Similarity Metric

The formula given in Eqn. (5.34) is the correct formula to calculate the area of the ellipse, and is a perfectly valid similarity metric. The purpose of the similarity metric, however,

is for a sensor to compare its similarity to other sensors and obtain an ordering of similar sensors from which it can obtain its reference sensors. Consider three sensors S_X, S_Y, S_Z. If S_Y is more similar to S_X than S_Z is to S_X,

$$[2\pi k^2 \sigma_{(X^*)}\sigma_{(Y^*)}]^{-1} < [2\pi k^2 \sigma_{(X^*)}\sigma_{(Z^*)}]^{-1} \Rightarrow [\sigma^2_{(X^*)}\sigma^2_{(Y^*)}]^{-1} < [\sigma^2_{(X^*)}\sigma^2_{(Z^*)}]^{-1} \tag{5.35}$$

The above relationship is valid because we use the same value for k across all sensors to define a threshold. Therefore, we can define an equivalent similarity metric (for ranking purposes) as follows:

$$Similarity(S_X, S_Y) = [\sigma^2_{(X^*)}\sigma^2_{(Y^*)}]^{-1} \tag{5.36}$$

Computing the formula in Eqn. (5.36) is more efficient than computing the formula in Eqn. (5.34) because we already had $L1 = \sigma^2_{(X^*)}$ and $L2 = \sigma^2_{(Y^*)}$ from the two eigenvalues of the covariance matrix of $\begin{bmatrix} X & Y \end{bmatrix}$. So we simply take their product, and skip taking the square root and other operations. Also note that this version of the similarity metric is independent of the anomaly detection threshold k.

5.6 Demonstrating Required Properties of Approach

This approach has two properties that are critical to our design of the P2P validation protocol. The two properties were assumed in the analysis of the protocol in Section 4.5 when proving that our approach can achieve the minimum number of messages that need to be sent in order to report the error. We now show that our approach satisfies those two properties, and is thereby suitable for the protocol.

5.6.1 Symmetry

In this subsection, we show that our anomaly detection approach satisfies Property 1, as stated in Section 4.2.

In Section 5.4, we assumed that Sensor S_X receives all measurements from sensor S_Y and

performs anomaly detection. If we also assumed that Sensor S_Y receives all measurements from sensor S_X, then the question is whether or not the same pair (x, y) would be determined as anomalous by S_Y.

Symmetry is not always guaranteed by anomaly detection approaches (see Appendix A.1 for an example of an approach that fails to provide symmetry). Let X and Y be centered and normalized measurements of two sensors S_X and S_Y. When S_X performs anomaly detection, it constructs the matrix in Step 3 of Section 5.4 as $A \leftarrow \begin{bmatrix} X & Y \end{bmatrix}$. S_Y would similarly construct the matrix as $\hat{A} \leftarrow \begin{bmatrix} Y & X \end{bmatrix}$. In order to show symmetry, we now show that this construction leads to the same condition for anomaly detection in Eqn. (5.29). We use the 'hat' notation to distinguish the results of the $\hat{A}$ construction.

Notice that the following column swap elementary transformation can be used to relate A and $\hat{A}$

$$\hat{A} = A \begin{bmatrix} 0 & 1 \\ 1 & 0 \end{bmatrix}, A = \hat{A} \begin{bmatrix} 0 & 1 \\ 1 & 0 \end{bmatrix} \tag{5.37}$$

The corresponding covariance matrix is given as follows:

$$\hat{C_A} \leftarrow \frac{\hat{A}'\hat{A}}{T-1} \tag{5.38}$$

$$\tag{5.39}$$

Substituting from Eqn. (5.37),

$$\hat{C_A} = \frac{\begin{bmatrix} 0 & 1 \\ 1 & 0 \end{bmatrix} A'A \begin{bmatrix} 0 & 1 \\ 1 & 0 \end{bmatrix}}{T-1} = \begin{bmatrix} 0 & 1 \\ 1 & 0 \end{bmatrix} C_A \begin{bmatrix} 0 & 1 \\ 1 & 0 \end{bmatrix} \tag{5.40}$$

$$C_A = \begin{bmatrix} a & b \\ c & d \end{bmatrix} \Rightarrow \hat{C_A} = \begin{bmatrix} d & c \\ b & a \end{bmatrix} \tag{5.41}$$

Note that the characteristic equation for $\hat{C_A}$ is identical to the equation for C_A given in Eqn. (5.32). Therefore, the eigenvalues are exactly the same, except that we must name the

larger of the eigenvalues as $\hat{\sigma_Y^*}$.

$$\hat{\sigma_Y^*} = \sigma_X^* \tag{5.42}$$

$$\hat{\sigma_X^*} = \sigma_Y^* \tag{5.43}$$

The equation for computing eigenvectors and eigenvalues of $\hat{C_A}$ is given as follows:

$$\hat{C_A}\hat{E} = \hat{E}\hat{L} \tag{5.44}$$

where $\hat{C_A}$, $\hat{E}$ and $\hat{L}$ are all 2×2 matrices. L is a 2×2 diagonal matrix of eigenvalues. We showed that $L = \hat{L}$. Similarly we can apply Eqn. (5.33) to show that $\hat{E} = \begin{bmatrix} 0 & 1 \\ 1 & 0 \end{bmatrix} E$.

In Step 4. of Section 5.4, S_X rotated the test point $\begin{bmatrix} x & y \end{bmatrix}$ as follows:

$$\begin{bmatrix} x^* & y^* \end{bmatrix} \leftarrow \begin{bmatrix} x & y \end{bmatrix} E \tag{5.45}$$

Similarly, S_Y would rotate the test point $\begin{bmatrix} y & x \end{bmatrix}$ as follows:

$$\begin{bmatrix} \hat{y}^* & \hat{x}^* \end{bmatrix} \leftarrow \begin{bmatrix} y & x \end{bmatrix} \hat{E} = \begin{bmatrix} y & x \end{bmatrix} \begin{bmatrix} 0 & 1 \\ 1 & 0 \end{bmatrix} E = \begin{bmatrix} x^* & y^* \end{bmatrix} \tag{5.46}$$

Combining the above equation with Eqn. (5.43), we obtain the anomaly detection equation for S_Y, which is the same as it is for S_X in Eqn. (5.29).

5.6.2 Greater Similarity Implies Greater Sensitivity to Anomalies

In this subsection, we show that our similarity metric (described in Section 5.5) satisfies Property 2, as stated in Section 4.2.

Let $Similarity(S_X, S_Y) > Similarity(S_X, S_Z)$ for some sensors S_X, S_Y, and S_Z. From the definition of the similarity metric in Eqn. (5.34), the area of the isocontour spanned by the normalized measurements of S_X and S_Y is smaller than the corresponding area spanned by

the normalized measurements of S_X and S_Z. With the assumption that anomalies are spread out farther away from the centroid than are proper measurements, S_X is more likely to detect anomalies if it were to choose S_Y instead of S_Z as a reference sensor because anomalies are more likely to fall outside the smaller isocontour formed by S_X and S_Y. Hence Property 2 is satisfied.

Note that if the area of the isocontour is smaller, more anomalies will be detected, but also more false positives may result. If the area is larger, fewer anomalies will be detected, but there would also be fewer false positives. Therefore, an appropriate threshold k must be set to a good trade-off between true and false positives. In all our experiments, we set $k = 3$ and found that it achieves a perfect detection rate for all sensors and a zero false-positive rate.

5.7 Illustration of Approach on Datasets

In this section, we demonstrate anomaly detection approach and also demonstrate important features of the similarity metric on our three datasets. For the Berkeley dataset we use $T = 30$, grouping 30 hours of data in one cluster. For the TAO dataset we use $T = 30$, grouping 5 hours of data in one cluster. For the NZ dataset we use $T = 300$, grouping 5 minutes of data in one cluster.

5.7.1 Detecting Anomalies in the Datasets

In this subsection, we demonstrate our anomaly detection approach on all three datasets.

Consider the two sensors Sensor 1 and Sensor 16 in the NZ dataset. In Fig. 5.1, it can be seen that the anomalous point is only anomalous with respect to Sensor 1 and not with respect to Sensor 16. That is because Sensor 16 measured the earthquake later than Sensor 1 did. The waveforms along with anomalies flagged by the approach are illustrated in Fig. 5.3, and the lag between Sensor 1 and Sensor 16 detecting the quake is clear in Fig. 5.3.

We also experimentally verified that our anomaly detection approach does indeed have the symmetric property. From Sensor 1's perspective, 67 anomalies were discovered in 86400

measurements during the 24 hr period with respect to Sensor 16's measurements. Conversely, from Sensor 16's perspective, 67 anomalies were discovered during that period with respect to Sensor 1's measurements and those anomalies were reported at the exact same time indices as those reported by Sensor 1. Note that each of the two sensors are performing anomaly detection independent of the other. That is, the fact that one sensor finds the other sensor to be anomalous is in no way communicated to the other sensor. Therefore the probability of the two sensors having the exact same match in this case is 6×10^{-7}. That highly precise match was expected because we know that symmetry is mathematically supported.

The 67 anomalies detected from the 86400 measurements were a result of the robust anomaly detection approach discussed in Section 5.4.3. If the robust approach were not used, we found from experiments that 33 anomalies would have been detected in the same time period. That is because the initial anomalies would bias the model in a way that makes future anomalies seem normal. That is, the isocontour would be expanded to accommodate the initial anomalies in the model, leading to a wider range of what is normal.

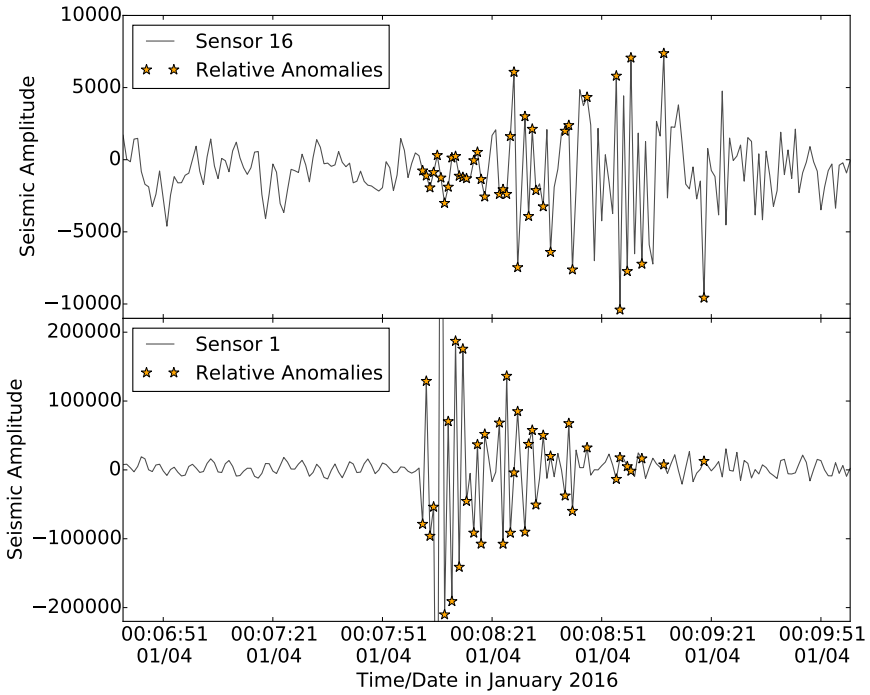

Figure 5.3: Anomalies (yellow stars) due to the earthquake presented in the seismic waveform in the NZ Dataset (200 sec view).

Figure 5.3 highlights that it is not necessary for both sensors to produce anomalous mea-

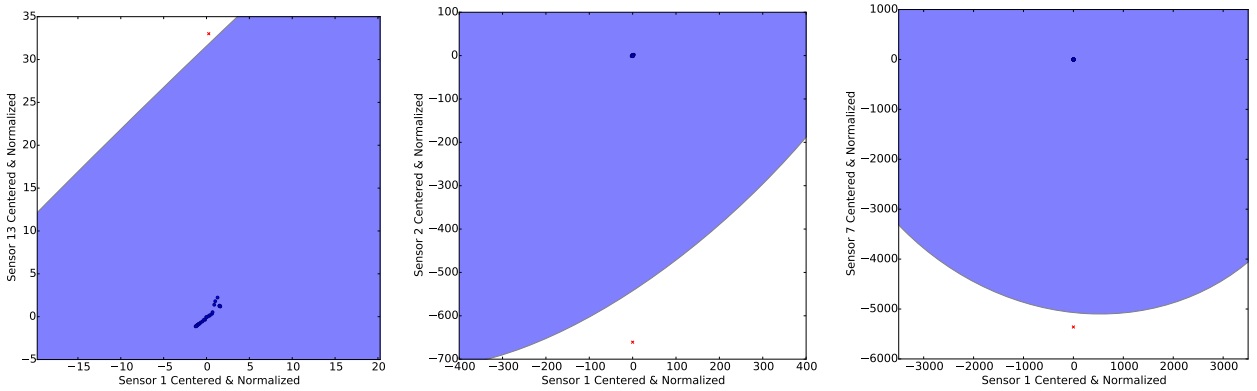

(a) Berkeley- Isocontour drawn at $k = 75$

(b) TAO- Isocontour drawn at $k = 500$

(c) NZ- Isocontour drawn at $k = 75$

Figure 5.4: Anomalies (red crosses) in the three datasets are egregious. They would be detected even if the isocontour were drawn 75, 500 and 3600 standard deviations from the mean in the Berkeley, TAO and NZ datasets, respectively.

surements at the same time for the anomaly to be detected. Since anomalies are detected in pairs of sensor measurements, it can be seen in Fig. 5.3 that at times anomalies are due to Sensor 1's measurements and at other times anomalies are due to Sensor 16's measurements. In order to ascertain which sensor is actually in error, we invoke the majority voting procedure described in the protocol in Chapter 4. If a sensor believes its own reading is anomalous based on the measurements taken at the same time by the majority of its reference sensors, it will report itself as being in error to the sink.

An important point to notice in Fig. 5.2 is that there are points that are not anomalous with respect to either Sensor 11 or Sensor 16. They are anomalous with respect to the joint distribution of both sensors' measurements. In other words, if the region capturing normal consumption were rectangular, those anomalies would not be detected. They are only detected because the region is elliptical. Since we did want to capture those anomalies, the elliptical isocontour captured the detection boundary better than a rectangular region would have.

In all three datasets, the anomalies due to errors were so egregious that our approach easily detected them. Centering the data in the TAO dataset caused the anomalous points at -9.99 °C to go further negative (to approximately -35 °C), where the correct measurements were around the origin. Dividing that by a fractional standard deviation further exaggerated

the anomaly to the extent that it would be detected even if the isocontour were drawn 500 standard deviations from the mean. Similarly, the errors in the Berkeley and NZ dataset could be detected by isocontours drawn at 75 and 3600 standard deviations from the mean, respectively. As shown in Fig. 5.4 for all three datasets, the anomalies due to errors were so egregious that they could be easily distinguished from legitimate rare events. For example, in the NZ dataset, a $k = 3600$ isocontour could detect an anomaly caused by a fault, but it would have been too large to detect an earthquake. A $k = 3$ isocontour would detect errors due to faults and earthquakes. Using both isocontours, the two errors types can be differentiated.

5.7.2 Similarity Metric and Physical Distance

In this section we illustrate the relationship between the similarity metric and physical distance in our dataset. Recall that we had analyzed the properties of the similarity metric in relation to the protocol in Section 4.1.

Consider the 4 location markers in the largest circle in the top left of Fig. 5.5. Those sensors are located around a volcano. We picked one of those sensors, and ranked the similarity of all 40 other sensors in the dataset with that sensor (let us refer to it as S_X). The 41 sensors were located all around the country of New Zealand including small islands (like Chatham Island). Of those 41 sensors, 5 are marked with smaller circles in the figure, to avoid confusion with the other highway symbols shown by Google Maps.

Our first observation is important to show that our choice of similarity metric (explained in Section 4.2) works for our protocol. That observation is that the top 3 sensors on the ranked list of sensors were the nearest three at that same volcano as S_X. Therefore, our similarity metric picked the sensors that were physically closest to the one being considered. We believe that it is because the sensor readings are from an almost identical distribution.

Our second observation is that the normalizing constant used in normalizing the sensor data before deriving the similarity metric cannot be arbitrarily chosen (Step 3 of the anomaly detection approach in Section 5.4). To test the effect, we normalized the data by the $L - 2$ norm of the T measurement values, instead of the standard deviation. We found that the

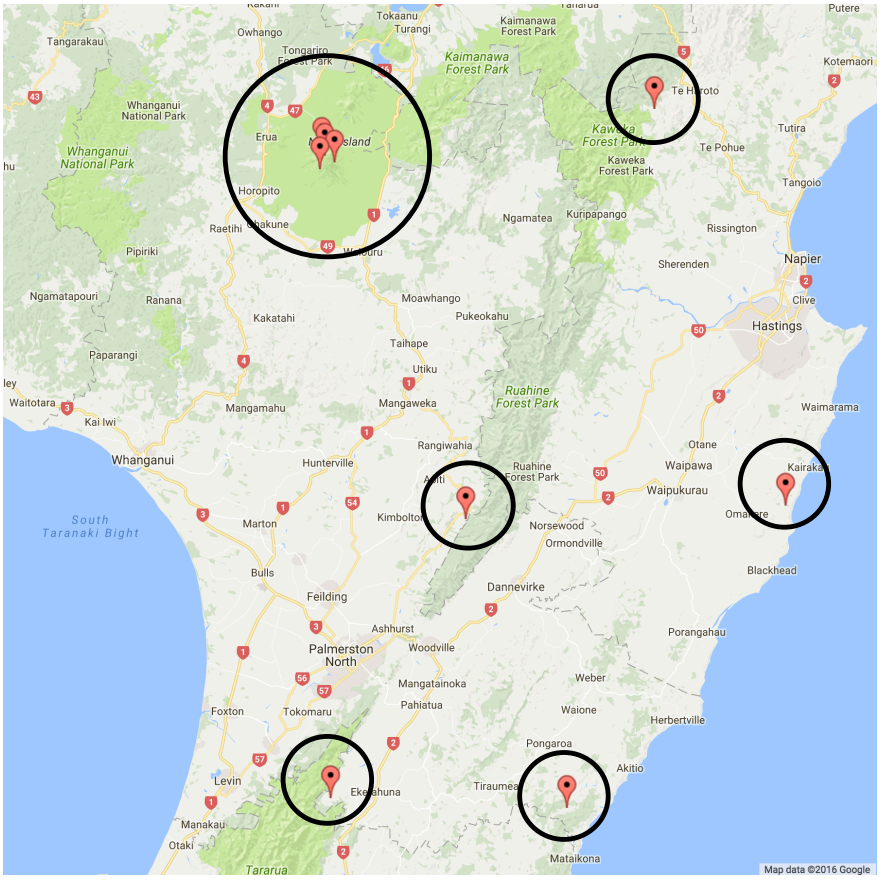

Figure 5.5: Map of physical location of select seismic wave sensors in the NZ dataset. The four sensors grouped in the largest circle are located around a volcano.

resultant similarity metric produced a ranking that had arbitrary sensors in the top 3 for S_X, none of which were at the volcano. That is because the standard deviation preserves properties of the original distribution that the $L-2$ norm does not.

Our third observation is that the ranking (using the standard deviation) outside of the top 3 is not really indicative of physical distance. For instance, S_X's similarity with the sensor at the top right of Fig. 5.5 is less than the similarity with the sensor at the bottom right of the figure. despite the fact that the sensor at the top right is clearly closer to S_X. We believe that this is because of two reasons. First, the sensors farther away from the volcano belonged to a different seismic network maintained by a different organization, and therefore the data collection and calibration methods might have been different. The sensors at the volcano all belonged to the same network. Second, the location of the sensor, with respect to the surface terrain might have affected the readings. Those effects might be due

to the way winds blow or other geological factors. The sensors at the volcano, on the other hand, were all on the same hill so similar to each other. Third, external disturbances due to moving vehicles, animals, machinery, etc., may create different amounts of noise at different locations.

The conclusion is that the similarity metric captures physical distance only within a local area. Outside of that area, no guarantees can be made on the relationship between similarity and physical distance. That does not necessarily hurt our approach because each sensor is only identifying reference sensors within its wireless range which is inherently restricted to a local area.

CHAPTER 6

PROTOCOL EVALUATION

We evaluated the centralized and P2P validation protocols using our own implementation of the protocols in a trace-driven simulator. In this section, we present the simulator and our simulation results. The simulator allows us to quantify the longevity and reachability of the network, when using the centralized and P2P protocols. Longevity and reachability are the two metrics we care about, and were defined in Chapter 2. Our results show that the P2P protocol described in Chapter 4 increases longevity and reachability, highlighting its usefulness. The simulations are performed on the three datasets described in Chapter 3.

6.1 Sensor Network Protocol Simulator

Several simulators exist for modeling WSNs, as described in [22]. However, those simulators either fail to conveniently support the implementation of P2P validation on top of existing functionality, or fail to capture the impact of various sensor actions on battery consumption. NS-2 [23] is a general-purpose network simulator that is targeted towards IP networks, but it does not consider power consumption or cost metrics for energy-efficient routing as adjustable parameters. TOSSIM [24] is an emulator specifically for TinyOS sensors developed by the TinyOS project team, but it suffers from many of the same limitations [22]. To focus on the application and routing layers of the network stack in developing an energy-efficient P2P validation protocol, we developed a trace-driven simulator of a WSN in Python. The simulator performs shortest-path routing and implements the application-layer protocols for both centralized and P2P validation.

6.1.1 Simulator Design

The simulator is logically divided into three components: 1) the simulation engine that bootstraps the simulation, 2) the sensor class that contains the code that would run on sensor motes, and 3) the sink class that contains the code that would be executed at the sink (on a server at the base station). The components are illustrated in Fig. 6.1.

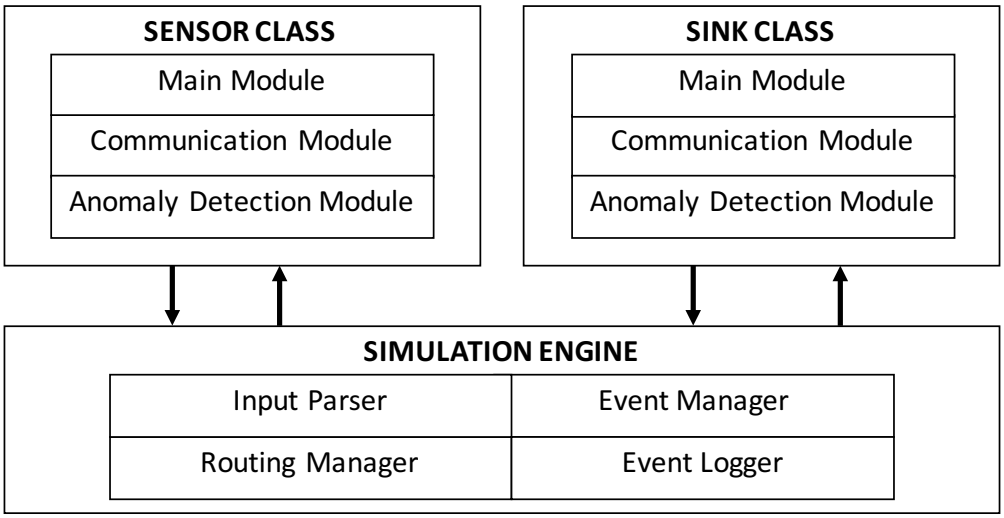

Figure 6.1: Components of the custom-built discrete event simulator.

In the P2P protocol implementation, the sensor class implements all three stages of the protocol, described in Section 4.1. In the centralized implementation, the sensor class simply sends all measurements to the sink at every time period, so that the sink may perform anomaly detection in real-time. In both the centralized and P2P protocol implementations, the sink class implements Stage 3 of the protocol, as described in Fig. 4.4.

Both the sensor and the sink classes contain a communication module that handles the application and routing layer protocol messages, an anomaly detection module that implements the mechanism described in Chapter 5, and a main module that coordinates the other two modules as per the protocol. On the sink, anomaly detection is performed with respect to reference sensors that may be chosen from any sensor in the network (not limited to the wireless range of each sensor). We obtain the top 5 reference sensors for each sensor when performing anomaly detection at the sink.

The simulation engine contains an input parser, event manager, routing manager and

event logger. The input manager parses datasets and sensor layout description files (containing spatial coordinates of sensors). The event manager stores and runs synchronous and asynchronous events performed by the sensor and sink. Synchronous events include measurement reading and reporting. Asynchronous events are communication events relating to error reports. The sensor and sink class communicate with each other through the routing manager in the simulation engine, which reads and writes to message buffers in the sensor and sink classes. The routing manager implements static and time-varying routing protocols to route messages between sensors and the sink. The event logger is used by the sensor and sink classes to records statistics that allow us to trace the trajectory of the simulation and evaluate performance metrics for different experiments.

6.1.2 Simulation Parameters

The simulator contains several configurable parameters that describe WSN settings. Location coordinates are one such parameter, and they describe the physical locations of the sensors and the sink. We place sensors in a 2-dimensional coordinate space for illustrative simplicity, although we note that the implementation can be trivially extended to support a 3-dimensional space. The second set of parameters describes the energy consumption of the sensor motes in the network. We categorized CPU processes into long and short processes. Long processes occur only in the P2P validation protocol (where the processing onus is on the sensors), causing more battery drain due to CPU than in the centralized validation protocol.

For the evaluation in this thesis, we assumed the use of the Mica2Dot sensors with weather boards deployed at the Intel Berkeley Research Lab [2]. We obtained values for the energy consumption of the CPU, radio transmission and radio receive from the third-generation Mica2Dot sensor datasheet [25], and note that the choice of those values can have a major effect on the evaluation results. The values for the Berkeley dataset deployment are presented in Table 6.1.

In order to complete the simulation in reasonable time, we scaled down the battery capacity of the sensors. For simplicity, we assume that the time at which sensors die will scale

linearly with increased battery capacity. We believe that is a reasonable assumption given homogeneous sensor hardware. We leave a simulation time scaling analysis for future work. We assume the same time scaling factor given in Table 6.1 for all three datasets deployments. That assumption is reasonable if we also assume the following: if the sensor transmitter hardware consumes more power in one deployment, then that deployment is equipped with proportionately greater battery capacity.

The sensor battery capacity in the simulation (0.2 mAh) corresponds to 4 button cells of 200 mAh each[1]. We include a correction factor to account for battery capacity degradation (due to imperfect battery quality or environmental effects), and to account for sensor activities that we did not carefully model (such as the idle state when asleep). Therefore, we say the effective battery life of four button cells is reduced from 800 mAh to 666 mAh (a reduction of nearly 18%. In each time step, all alive sensors broadcast their readings to neighbors within their wireless transmission range. By diving all times shown in the results and plots by the time scaling factor given in Table 6.1, one can obtain the number of simulation time steps that were run.

6.2 Protocol Implementation

In the centralized validation protocol, the sensors report their measurements to the sink at every time epoch. These messages are forwarded by sensors that lie between the sender and the sink. Upon receiving each measurement, the sink performs anomaly detection, as described in Chapter 5.

In the P2P validation protocol, the sensors broadcast their measurements to their one-hop neighbors at every time epoch. Each sensor determines whether its own measurement is in error with regard to measurements from its reference sensors. If a measurement is in error, the sensor reports the error to the sink through the shortest path, and falls back to a forwarding mode. In this forwarding mode, the sensor does not report its own measurements, but acts as a routing intermediary between other sensors and the sink. All sensors periodically send a single message containing a batch of B measurements every B time periods to the

[1]Button cell capacity obtained from http://www.ti.com/lit/ug/tidu797c/tidu797c.pdf

Table 6.1: Simulation Parameters for Berkeley Dataset

Parameter	**Value**	**Description**
Sensor batter capacity	0.2 mAh	This is a time scaling choice so we can observe the death of the system. We use the realistic value of 666 mAh in performing time scaling.
Energy for transmit	2e-4 mAh	Transmitter current is 25 mA as per Mica2 datasheet. We assume the time to transmit is 0.3 seconds. Value is $25mA \times 0.3$ ms/3600
Energy for receive	6.7e-5 mAh	Transmitter current is 8 mA as per Mica2 datasheet. We assume the time to transmit is 0.3 seconds. Value is $8mA \times 0.3$ ms/3600
Energy for CPU	6.7e-5 mAh	Same as energy for receive. Applicable only to the P2P protocol for anomaly detection.
Batch Period	3600	We assume the data is packaged and sent to the sink in the P2P approach after 3600 packets have been collected.
Reporting Frequency	1 min	1 simulation step is 1 min in the original simulation time (before scaling).
Time scaling factor	2.31 $\times$	1 simulation step is 2.31 days after time scaling. 1440 min are in 1 day. Scale by 666/0.2 to adjust for battery life. Value is $666/(0.2 \times 1440)$

sink. Those raw measurements may be used by the WSN operator to estimate the state of the environment being monitored. B is configurable, and in our evaluation, we chose $B = 10$ time periods.

Both the P2P and centralized validation protocols can run on top of a dynamic, battery-aware routing protocol, such as those described in [15], to further improve survivability. For this thesis, we implement the Minimum Battery Cost Routing (MBCR) presented in [15] for its advantage in extending the overall network reachability.

For illustration, we simulate the 54-sensor network from the Intel Berkeley dataset, assuming a 9×6 grid layout with the sink near the center (see Fig. 6.6). The sensors were spaced apart from each other such that each sensor's range could allow for communication with only its immediate neighbor (no diagonal interactions). That grid layout is envisioned for multiple rooms in a single floor of a building, and there could be walls anywhere between the sensors as long as they do not interfere with the wireless range. That layout could also potentially be used for monitoring soil moisture in a rectangular field. We chose the layout for its simplicity in illustrating the impact of different routing and validation protocols.

6.2.1 Protocol Implementation in Simulator

In the centralized error detection protocol, the sensors report their measurements to the sink at every time epoch. These messages are forwarded by sensors that lie between the sender and the sink. Upon receiving each measurement, the sink performs anomaly detection, as described in Chapter 5.

In the P2P error detection protocol, the sensors broadcast their measurements to their one-hop neighbors at every time epoch. Each sensor determines whether its own measurement is in error with regard to measurements from its reference sensors. If a measurement is in error, the sensor reports the error to the sink through the shortest path, and falls back to a routing-only mode. In this routing-only mode, the sensor does not report its own measurements, but acts as a routing intermediary between other sensors and the sink.

6.2.2 Routing Implementation in Simulator

Both the P2P and centralized error detection protocols can run on top of a variety of routing protocols, including battery-aware routing protocols described in [15] and [26], to further improve reachability. For this thesis, we implemented static rounding and the Minimum Battery Cost Routing (MBCR) approach presented in [15]. MBCR was chosen for its advantage in extending the overall network reachability.

Static Routing

In static routing, we used Dijkstra's algorithm to calculate the shortest path between each sensor and the sink, using a homogeneous edge cost of 1. These routes were never updated (hence the name "static").

Minimum Battery Cost Routing

In MBCR, we used Dijkstra's algorithm to calculate the shortest path between each sensor and the sink, using a time-varying edge cost.

Let R be the set of all root sensors (the sensors located within wireless range of the sink), and $N(S_X)$ be the set of neighbors of sensors S_X. The *cost to sink*, C, for a sensor S_X at time t can be given as follows:

$$C(S_X, t) = \begin{cases} 0 \text{ if } S_X \in R \\ \min_{S_i \in N(S_X)}[\frac{1}{Battery(S_i,t)} + C(S_i, t)] \text{ else} \end{cases} \tag{6.1}$$

The edge cost for the root sensors is always zero. At each time t, each root sensor sends its own measurements to its neighboring sensors for anomaly detection. When it sends the measurements, it piggybacks a *cost to sink* value that is the inverse of its battery life. Each neighbor of that root sensor in turn sends its measurements to its own neighboring sensors along with a *cost to sink* that is the inverse of that sensor's battery life added to the root sensor's *cost to sink*. The process continues recursively until all sensors have a *cost to sink* defined at time t. The piggybacking ensures that the protocol does not generate any extra

messages.

There are scenarios where piggybacking is insufficient and extra messages need to be generated. Consider a sensor $S_X \notin R$ that is connected to a root sensor through two different paths. At time t, S_X receives its first *cost to sink*. Since this is the first *cost to sink* at time t, S_X must set its own *cost to sink* to the value it receives. It then propagates that cost to its own neighbors by piggybacking it onto its own measurements. If S_X receives another *cost to sink* message from a different path at time t after the first message, then it compares this new cost with its existing *cost to sink*. If the new cost is greater, nothing needs to be done and the message is ignored. If the new cost is lower, then S_X must update its *cost to sink* and propagate that update to its neighbors by means of a dedicated *cost to sink* message. As a result, additional messages are generated.

6.2.3 Illustration of Simulation Results

Berkeley: Actual Layout

We illustrate the 54-sensor network from the Intel Berkeley dataset, simulating the Mica2Dot sensors used in that dataset [2], and assuming the sink is at the center of the lab. All sensors were configured to use wireless transmission power that provided a range of 10 meters indoors. In agreement with the authors of [14], we did not set the wireless range too large because increasing it requires an exponential increase in transmission power. Decreasing the range, however, forces multi-hop routing, which increases the reliance of sensors farther away from the sink on routing sensors to maintain connectivity with the sink.

Figures 6.2- 6.5 are drawn to scale with the sensor layouts obtained from the real deployment in the Intel Berkeley lab. The figures include snapshots at four different days since the start of the simulation. The first snapshot shows the start of the simulation, when all sensors were alive, and the last snapshot was taken when all sensors except the root sensors had lost connectivity with the sink.

Figures 6.4 and 6.5 illustrate the MBCR protocol. As seen for Day 185 and Day 245 in Figs. 6.4 and 6.5, the sensors that were closest to the sink in the centralized protocol tended

to exhaust their battery the fastest because they had to frequently forward messages on behalf of more distant sensors.

In the P2P protocol, all sensors compute whether their measurements are anomalous with respect to the measurements that they receive from reference sensors, and that adds to computation costs. Therefore, it can be seen that on Day 185, the energy depleted is more uniform across the sensor network in the P2P protocol than in the centralized protocol. Even so, it takes 200 more days for 53 sensors to become unreachable in the P2P approach than in the centralized approach, as seen in Figs 6.4(c) and 6.5(d). *Hence, our P2P protocol obtains a good trade-off between computation and communication costs, improving reachability by over 80%.*

6.2.4 Berkeley: Grid Layout

In this experimental layout, the 54 sensors are arranged in a 9×6 grid with the sink near the center. Figures 6.6 and 6.7 illustrate battery drain in the centralized and P2P protocols for static routing, respectively. 30 sensors lose reachability after 115 days, and they all lose reachability after 145 days in the centralized protocol. It takes 638 days (over $5\times$ as long) for the P2P approach to disconnect those 30 sensors, and 645 days (over $4\times$ as long) to disconnect all sensors.

It is clear from the illustrations in Fig. 6.8 and Fig. 6.9 that the routing paths change over time. Those paths represent the paths between the sensors and sink that are optimal on the MBCR cost function. All observations for the static routing (such as the uniformly P2P load on sensors in the P2P approach) apply to the MBCR protocol. In the centralized protocol, MBCR routing disconnects only 2 sensors after 115 days, while it disconnected 30 sensors at that same time with static routing (in Fig. 6.6). However, ultimately static routing takes more time to disconnect all sensors because MBCR re-routes sensors to maintain connectivity, while increasing the load on sensors near the sink. The P2P approach has a greater gain over the centralized approach in MBCR than it did in static routing, extending overall reachability by nearly 5 times.

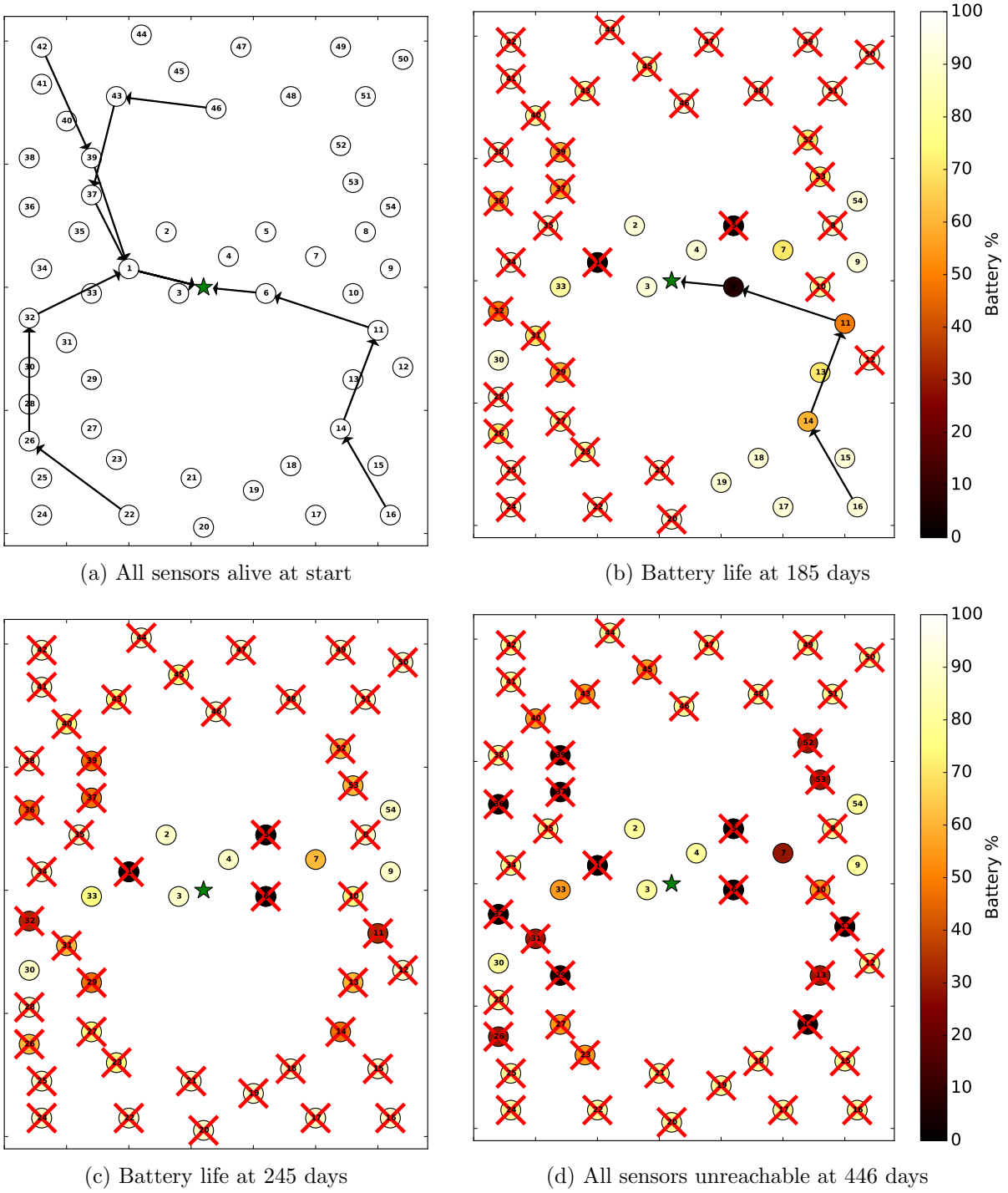

(a) All sensors alive at start

(b) Battery life at 185 days

(c) Battery life at 245 days

(d) All sensors unreachable at 446 days

Figure 6.2: Centralized validation protocol (Berkeley: Actual Layout): Battery life illustration for static routing with routing paths shown for 4 arbitrary sensors. Sink is the star in the center. Crossed-out sensors are unreachable.

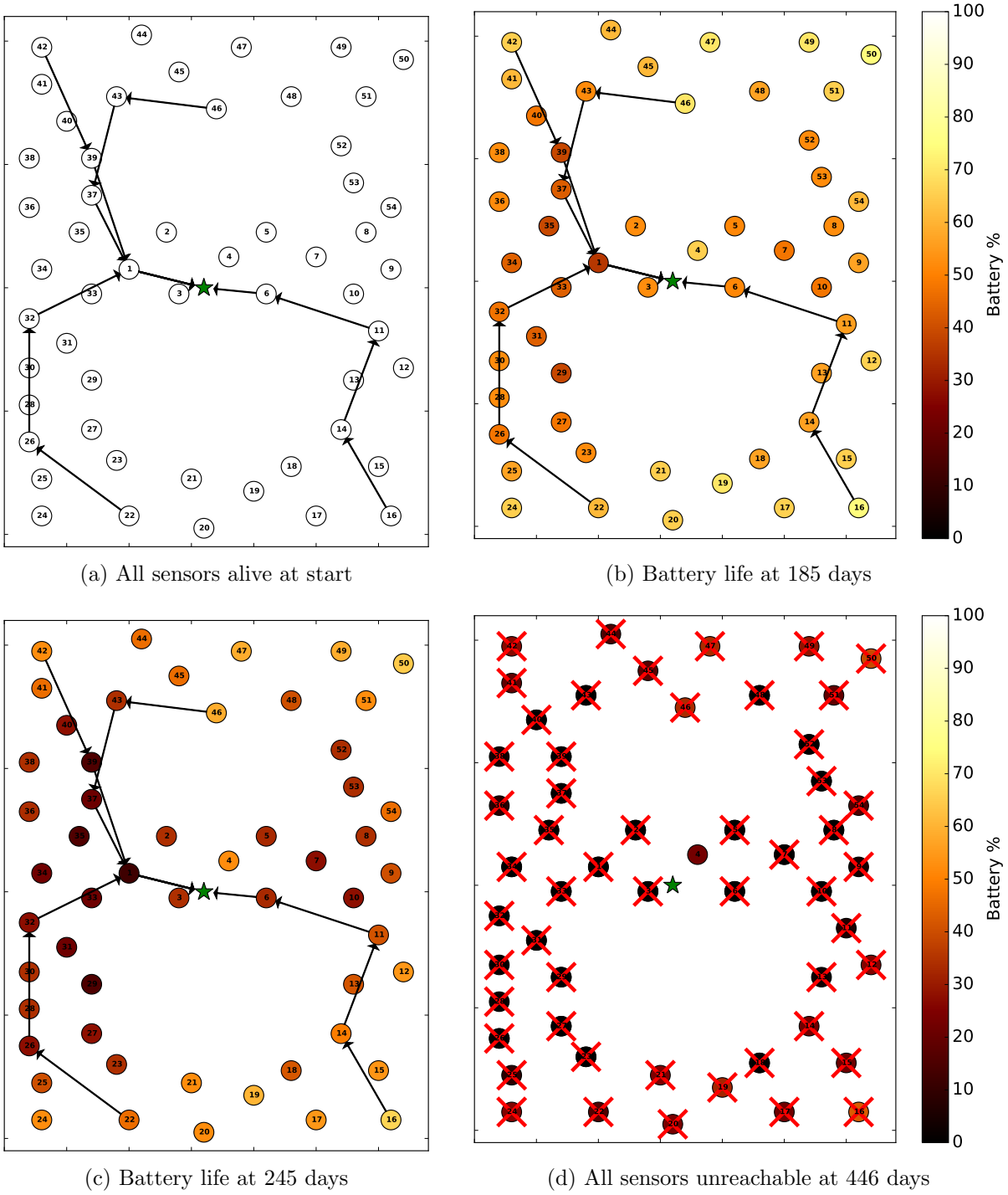

(a) All sensors alive at start

(b) Battery life at 185 days

(c) Battery life at 245 days

(d) All sensors unreachable at 446 days

Figure 6.3: P2P validation protocol (Berkeley: Actual Layout): Battery life illustration for static routing with routing paths shown for 4 arbitrary sensors. Sink is the star in the center. Crossed-out sensors are unreachable.

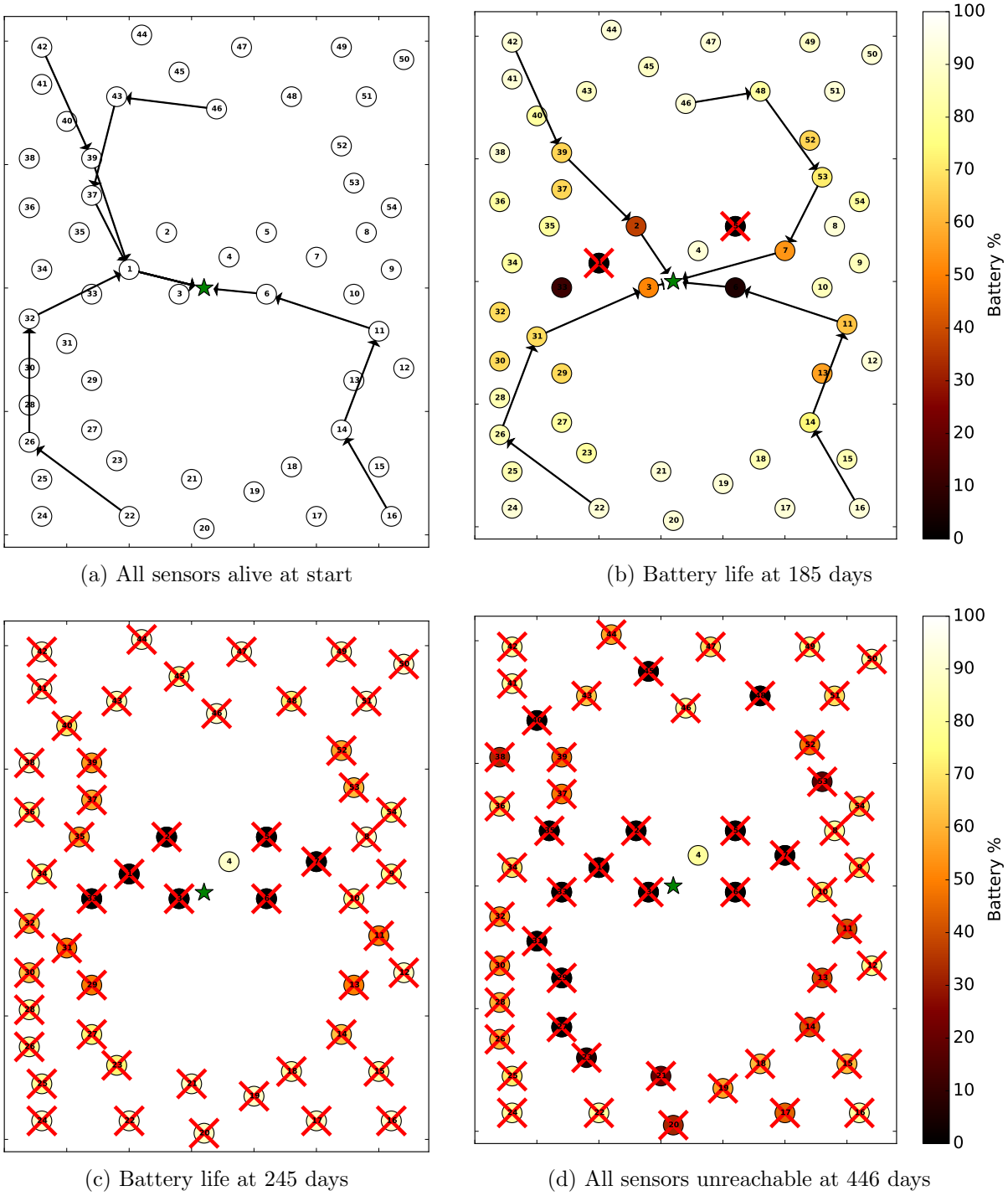

(a) All sensors alive at start

(b) Battery life at 185 days

(c) Battery life at 245 days

(d) All sensors unreachable at 446 days

Figure 6.4: Centralized validation protocol (Berkeley: Actual Layout): Battery life illustration for MBCR routing with routing paths shown for 4 arbitrary sensors. Sink is the star in the center. Crossed-out sensors are unreachable.

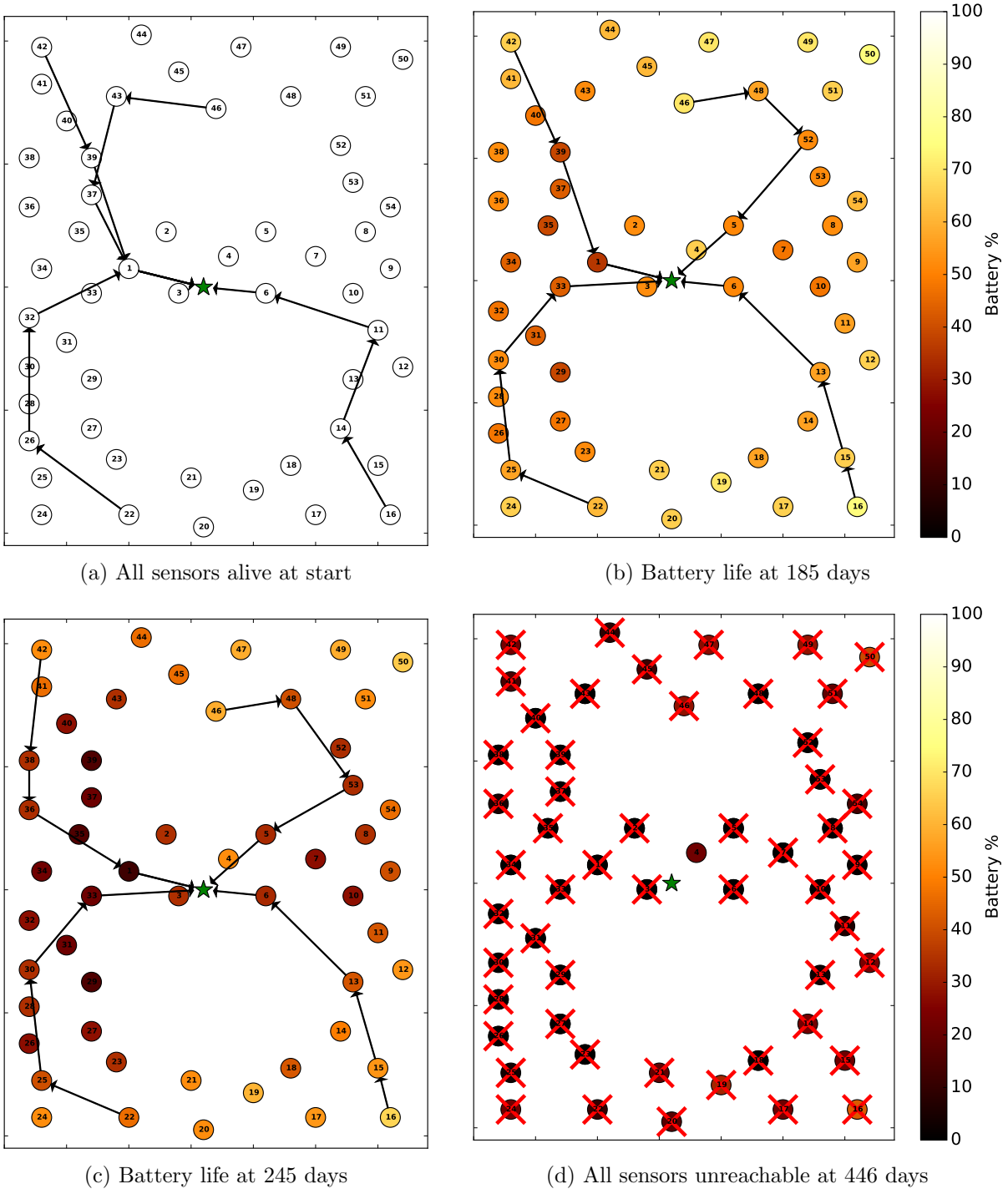

(a) All sensors alive at start

(b) Battery life at 185 days

(c) Battery life at 245 days

(d) All sensors unreachable at 446 days

Figure 6.5: P2P validation protocol (Berkeley: Actual Layout): Battery life illustration for MBCR routing with routing paths shown for 4 arbitrary sensors. Sink is the star in the center. Crossed-out sensors are unreachable.

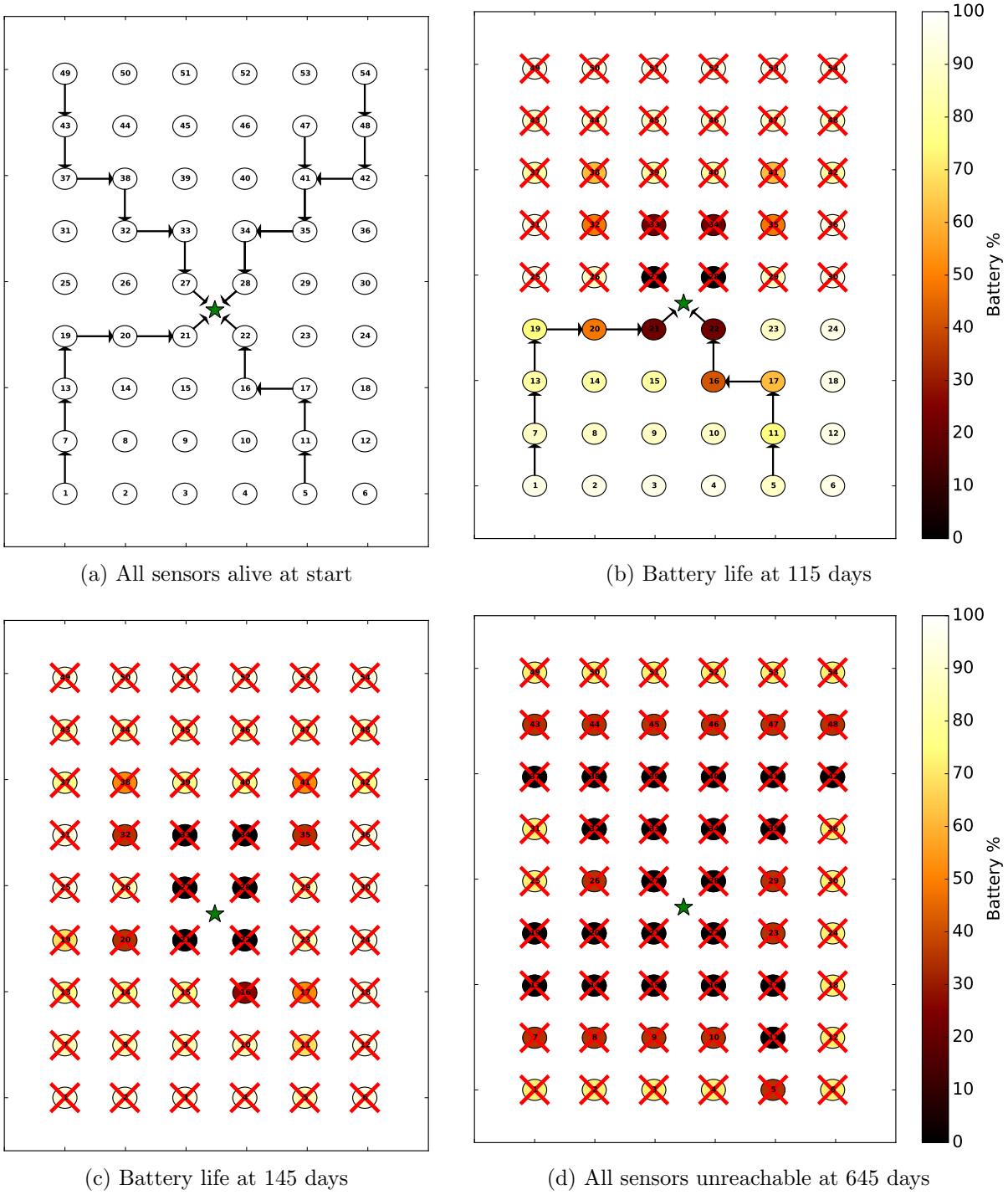

(a) All sensors alive at start

(b) Battery life at 115 days

(c) Battery life at 145 days

(d) All sensors unreachable at 645 days

Figure 6.6: Centralized validation protocol (Berkeley: Grid Layout): Battery life illustration for static routing with routing paths shown for 4 arbitrary sensors. Sink is near the center. Crossed-out sensors are unreachable.

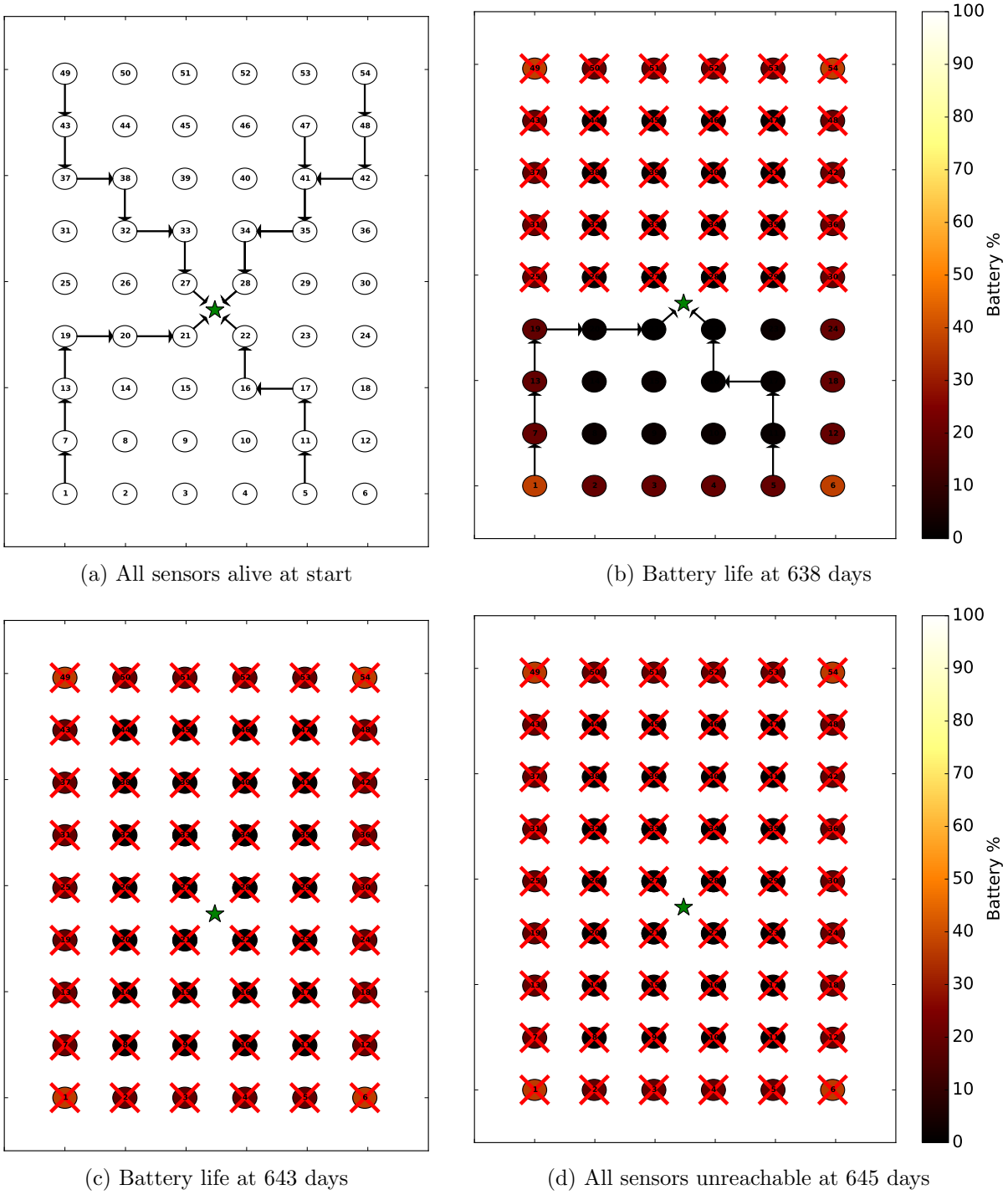

(a) All sensors alive at start

(b) Battery life at 638 days

(c) Battery life at 643 days

(d) All sensors unreachable at 645 days

Figure 6.7: P2P validation protocol (Berkeley: Grid Layout): Battery life illustration for static routing with routing paths shown for 4 arbitrary sensors. Sink is near the center. Crossed-out sensors are unreachable.

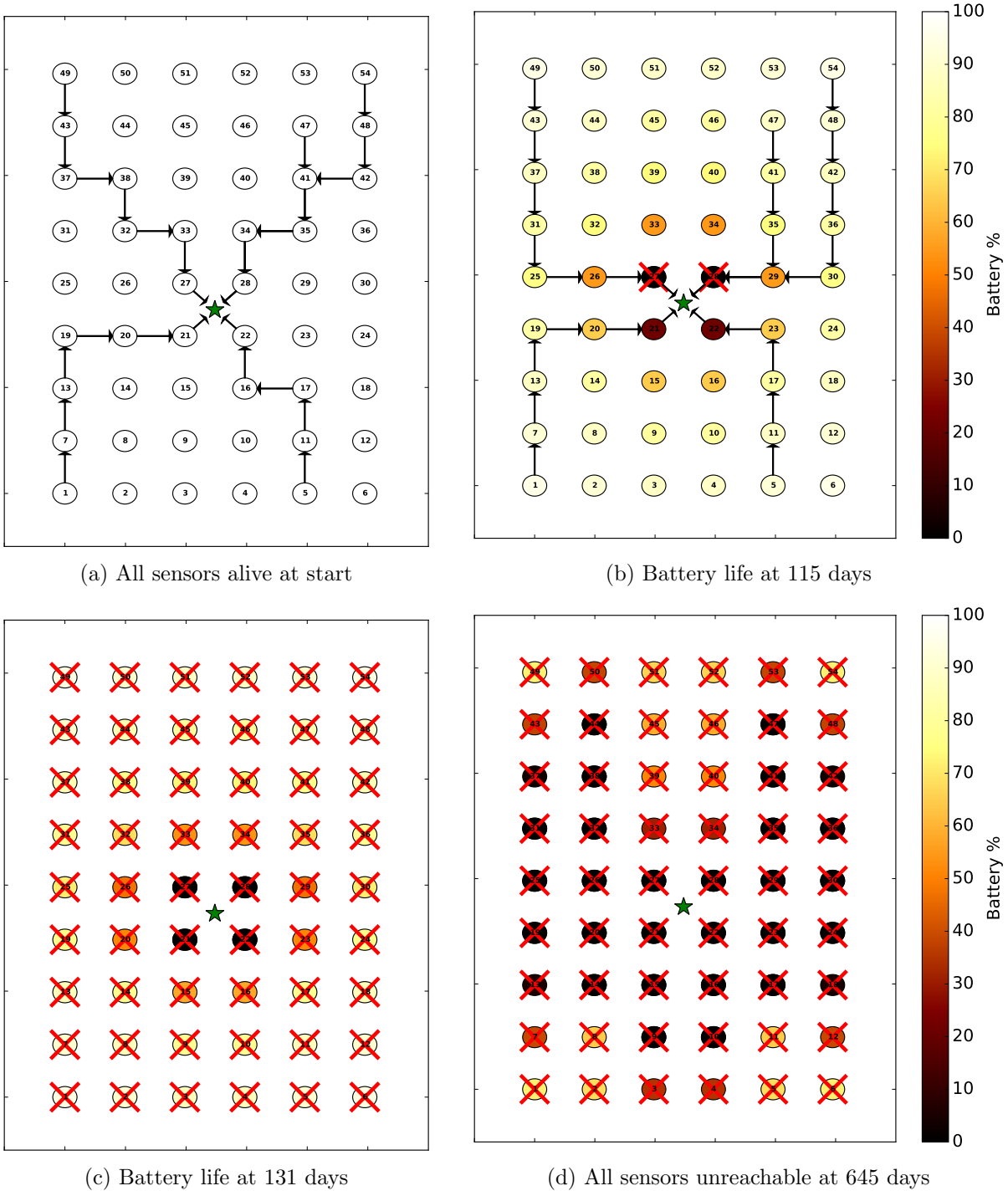

(a) All sensors alive at start

(b) Battery life at 115 days

(c) Battery life at 131 days

(d) All sensors unreachable at 645 days

Figure 6.8: Centralized validation protocol (Berkeley: Grid Layout): Battery life illustration for MBCR routing with routing paths shown for 4 arbitrary sensors. Sink is near the center. Crossed-out sensors are unreachable.

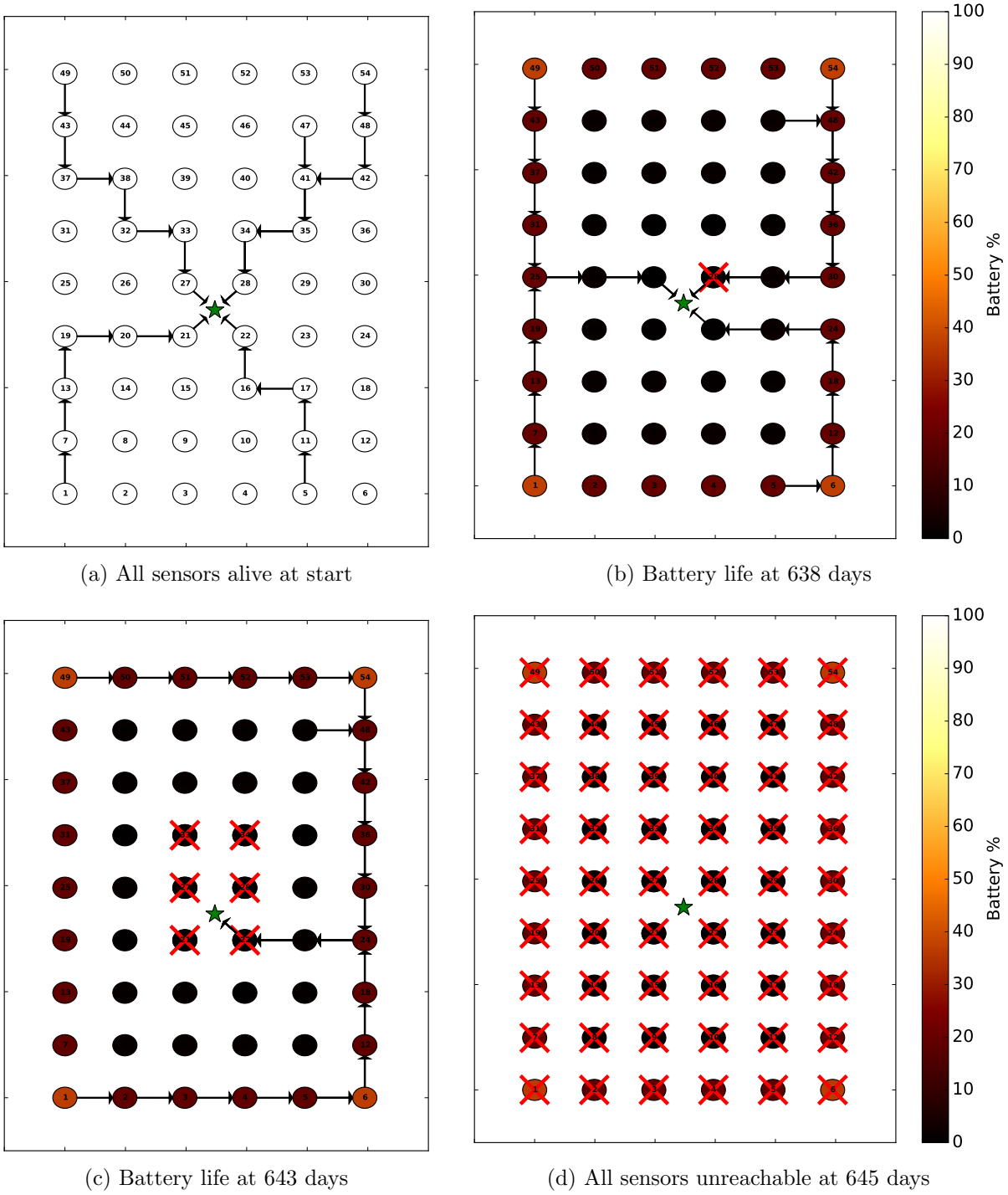

(a) All sensors alive at start

(b) Battery life at 638 days

(c) Battery life at 643 days

(d) All sensors unreachable at 645 days

Figure 6.9: P2P validation protocol (Berkeley: Grid Layout): Battery life illustration for MBCR routing with routing paths shown for 4 arbitrary sensors. Sink is near the center. Crossed-out sensors are unreachable.

6.2.5 NZ: Actual Layout

For the NZ dataset, we consider five sensors spaced around Mount Ruapehu (which is an active volcano in New Zealand) in a ring topology. We do not consider the remaining sensors in the dataset because they are spread out hundreds of miles apart, and located in different regional networks. The sink could not be placed in the center of the ring (inside the volcano), so it was placed in the ring, within range of two of the sensors (which achieves better reachability than having it within range of only one sensor, which would be a routing bottleneck). Snapshots for static routing in both protocols are illustrated in Fig. 6.10 and Fig. 6.11. On Day 629, 3 sensors had just lost reachability with the centralized protocol. That day is also clearly marked by the solid red line in Fig. 6.17.

Snapshots for MBCR routing in both protocols are illustrated in Fig. 6.12 and Fig. 6.13. It is clear from both static and MBCR illustrations that the P2P approach dramatically improves reachability.

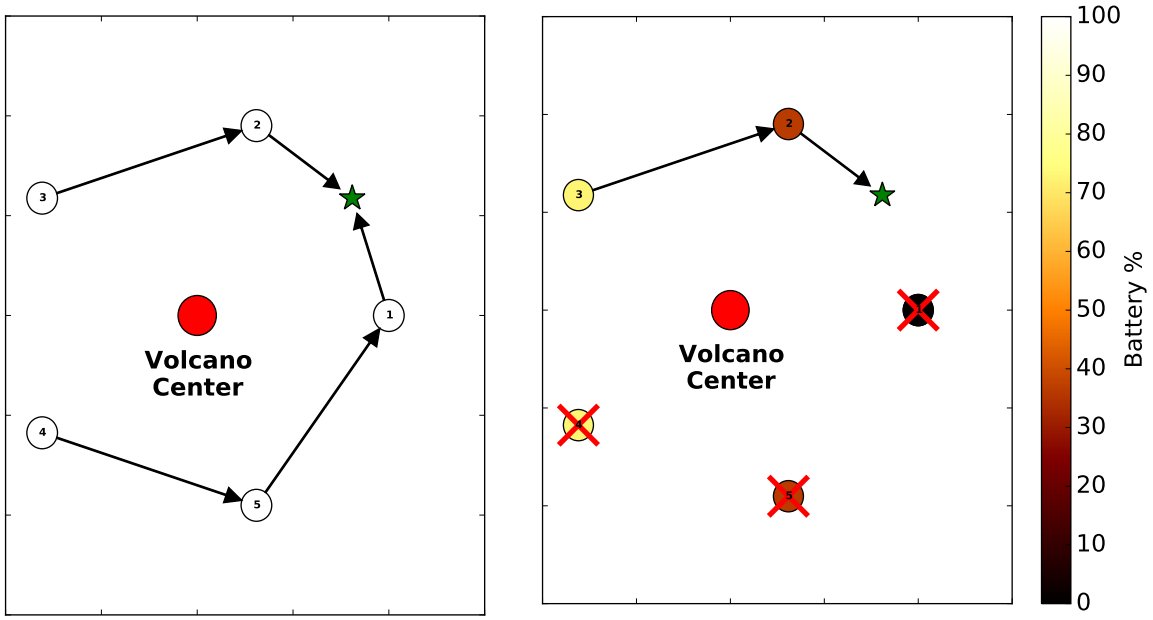

(a) All sensors alive at start

(b) Battery life at 629 days

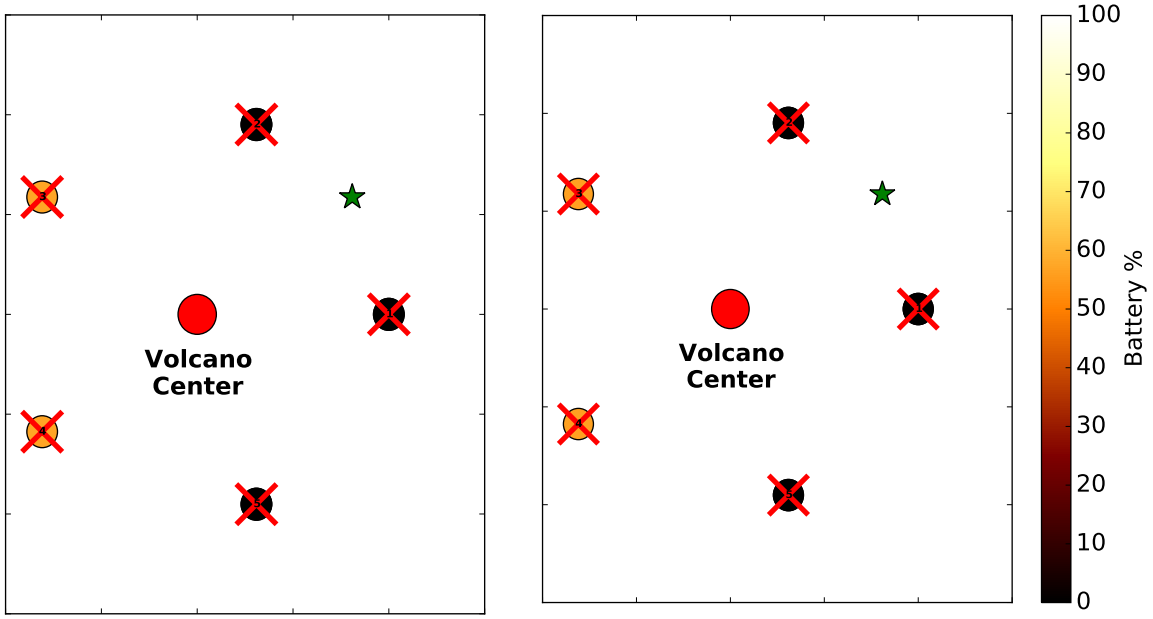

(c) Battery life at 990 days

(d) All sensors unreachable at 1004 days

Figure 6.10: Centralized validation protocol (NZ: Actual Layout): Battery life illustration for static routing with routing paths shown for 2 arbitrary sensors. Sink is the star in the ring topology. Crossed-out sensors are unreachable.

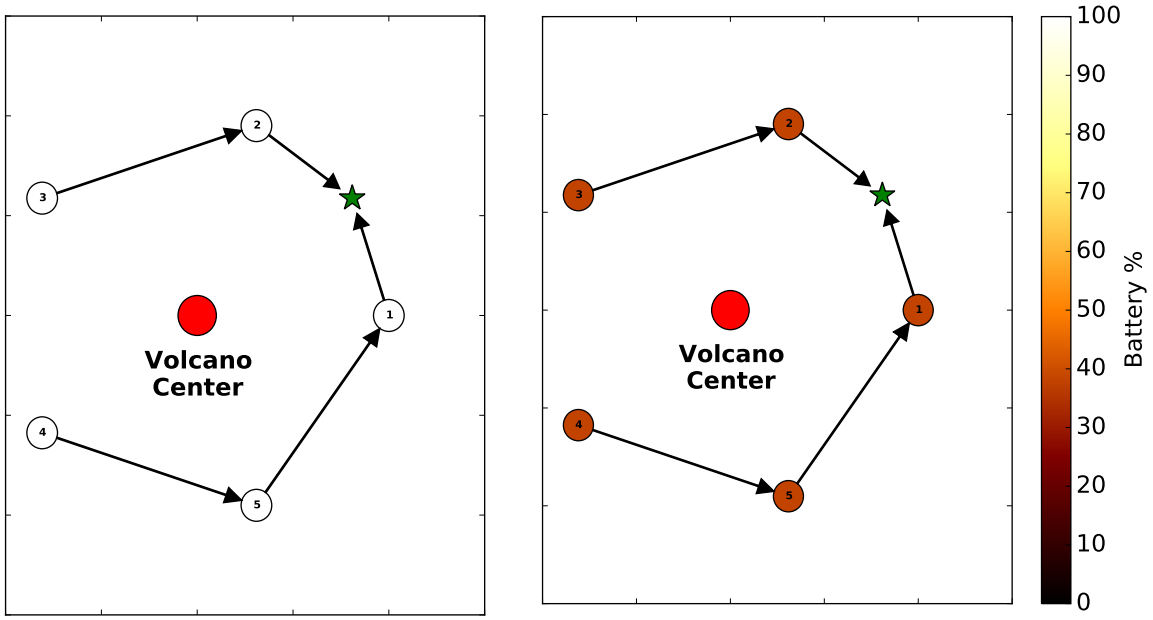

(a) All sensors alive at start

(b) Battery life at 629 days

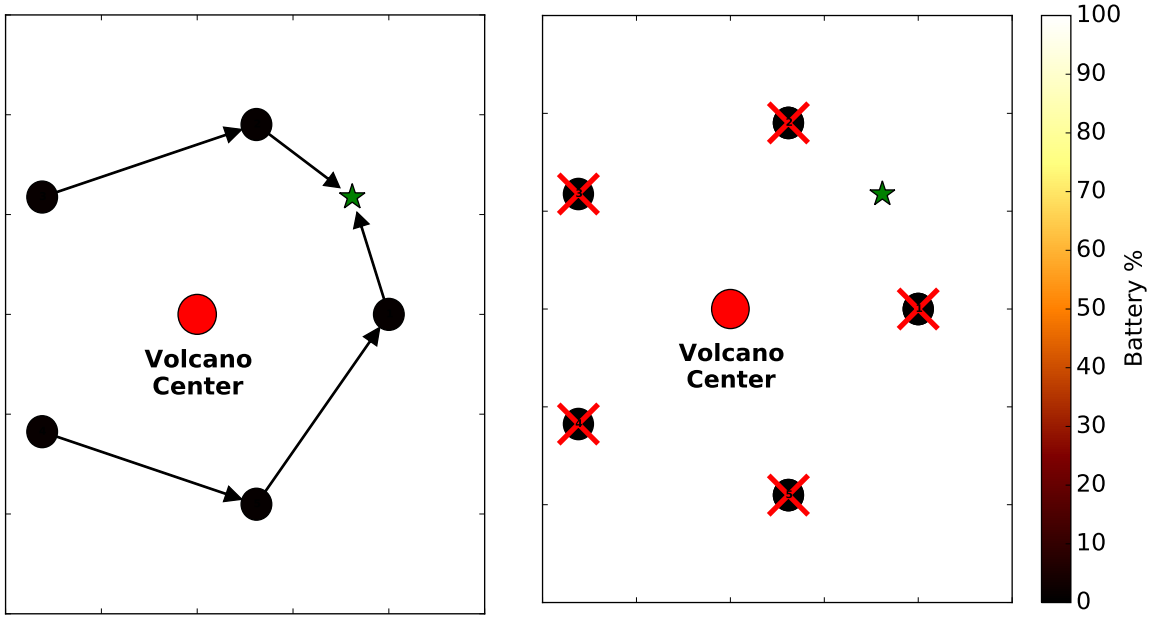

(c) Battery life at 990 days

(d) All sensors unreachable at 1004 days

Figure 6.11: P2P validation protocol (NZ: Actual Layout): Battery life illustration for static routing with routing paths shown for 2 arbitrary sensors. Sink is the star in the ring topology

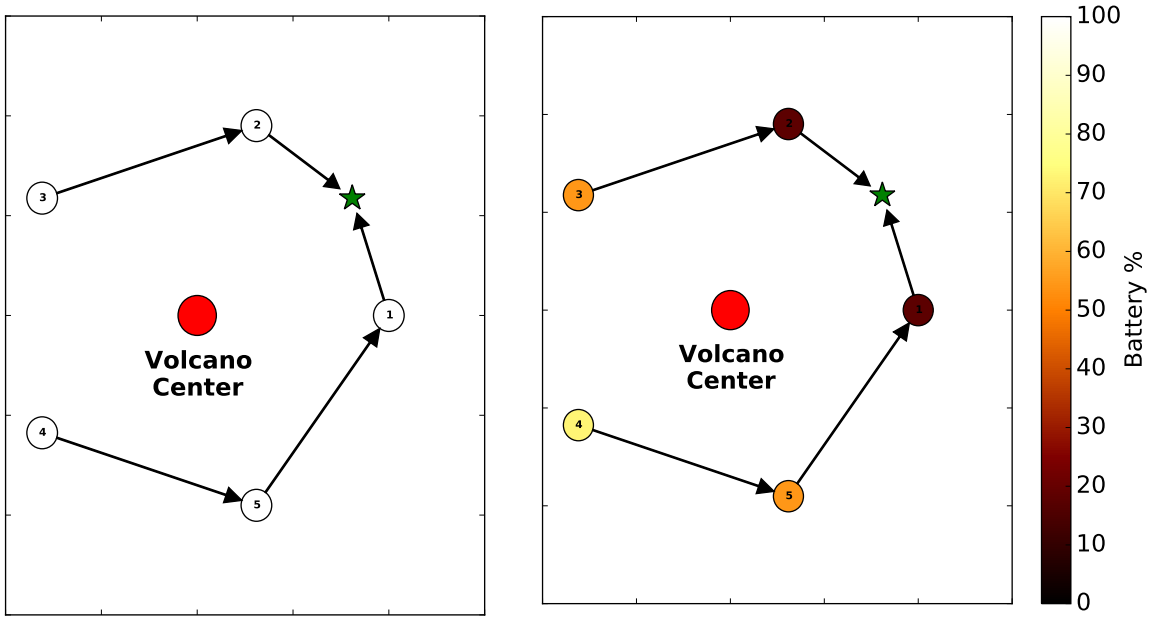

(a) All sensors alive at start

(b) Battery life at 629 days

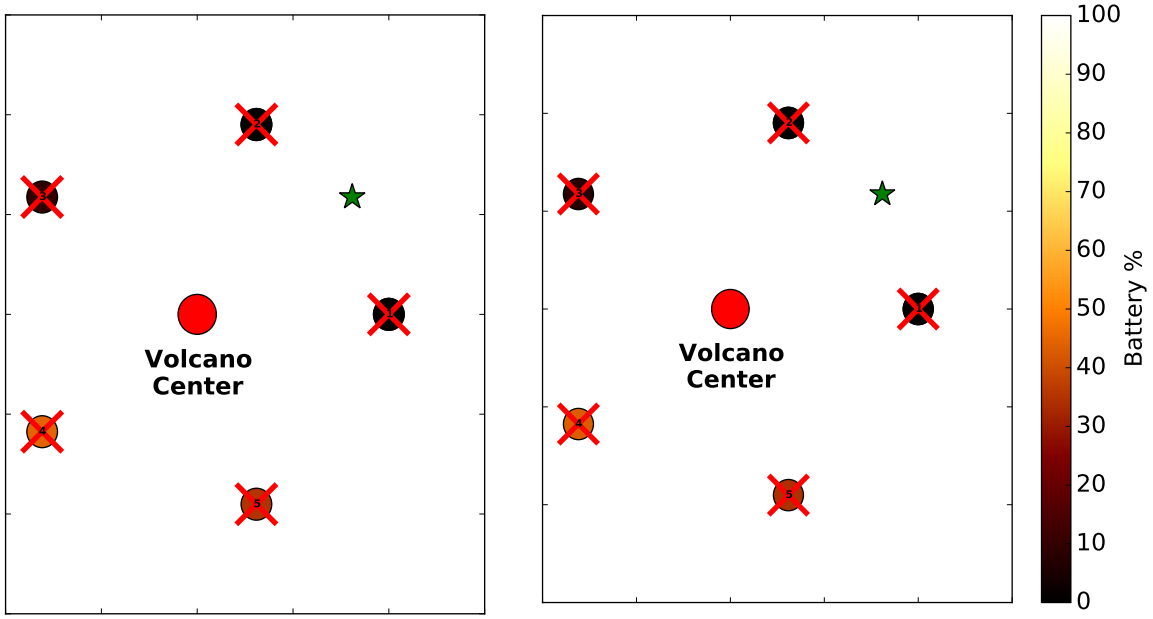

(c) Battery life at 990 days

(d) All sensors unreachable at 1004 days

Figure 6.12: Centralized validation protocol (NZ: Actual Layout): Battery life illustration for MBCR routing with routing paths shown for 2 arbitrary sensors. Sink is the star in the ring topology

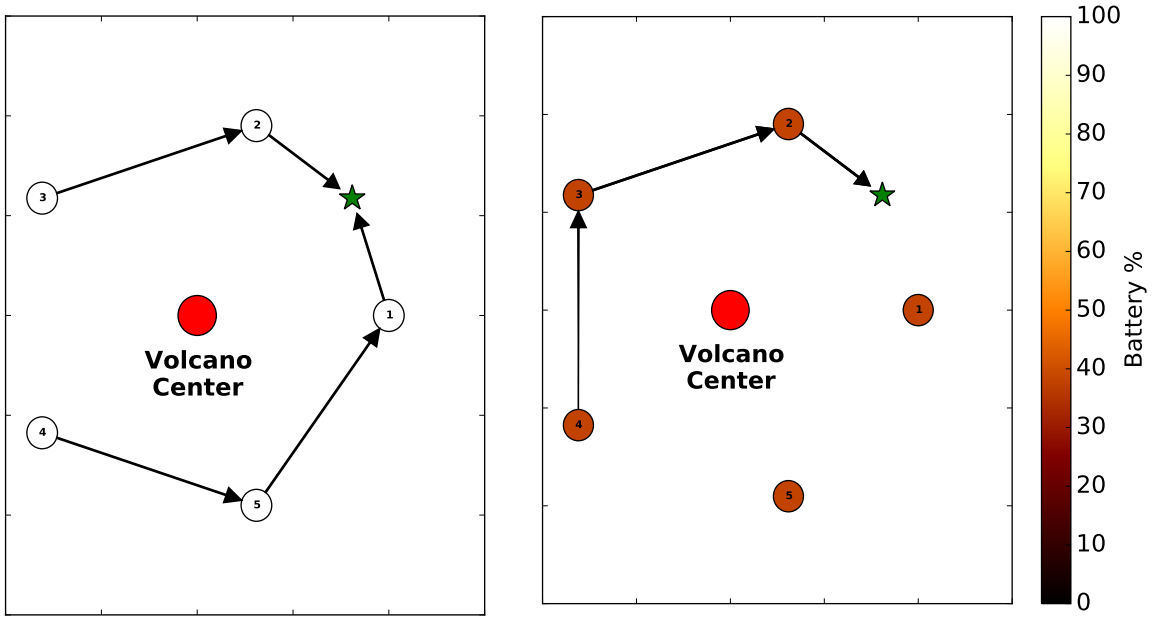

(a) All sensors alive at start

(b) Battery life at 629 days

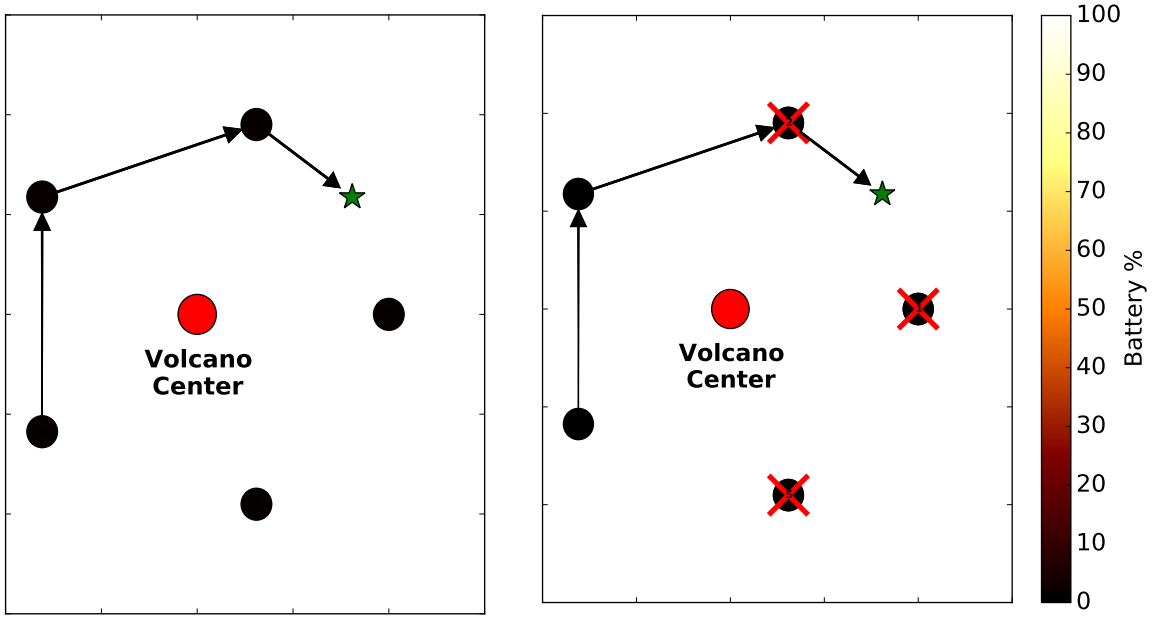

(c) Battery life at 990 days

(d) All sensors unreachable at 1004 days

Figure 6.13: P2P validation protocol (NZ: Actual Layout): Battery life illustration for MBCR routing with routing paths shown for 2 arbitrary sensors. Sink is the star in the ring topology

6.3 Detection Accuracy Results

In terms of error detection accuracy, both the centralized and P2P algorithms performed equally well on all datasets, consistently identifying the faulty sensors and reporting zero false positives at an isocontour threshold of $k = 3$. For the NZ dataset, that threshold successfully reported anomalies due to faults as well as abnormal seismic activity. We manually inspected potential false positives and noticed that there were indeed deviations in the data when errors were reported.

6.4 Reachability Results

We designed experiments on our simulator that illustrate the impact of the P2P and centralized validation protocols on sensor network longevity and reachability. We evaluated both protocols on three different datasets having different sensor layouts. In general, the results show that reachability is maximized with our P2P protocol using MBCR routing. The P2P protocol also improves longevity up until sensors get disconnected. Once sensors are disconnected, the centralized protocol provides better longevity due to less CPU drain. However that advantage of the centralized protocol is irrelevant because the sensors are effectively dead from the sink's perspective once they are disconnected.

6.4.1 Notation for Metrics

We describe our evaluation metrics, stated in Section 2, formally in this subsection.

Let $\Lambda(t) = \lambda$ be the number of sensors that are dead (due to battery depletion) at time t.

Then $\mathit{Longevity}(\lambda) = \min\{t : \Lambda(t) = \lambda\}$. In other words, longevity can be described as the inverse function of $\Lambda(t)$. However, illustrating $\Lambda(t)$ is more intuitive because functions of time are more commonly illustrated. Therefore, we illustrate $\Lambda(t)$ instead.

Let $\Omega(t) = \omega$ be the number of sensors that have lost end-to-end connectivity with the sink (in other words, become unreachable) at time t.

Then $\mathit{Reachability}(\omega) = \min\{t : \Omega(t) = \omega\}$. In other words, reachability can be described

as the inverse function of $\Omega(t)$. However, illustrating $\Omega(t)$ is more intuitive for the same reasons as it was for $\Lambda(t)$.

The system should ideally have both high *Longevity* and high *Reachability*. That is because we want the sensors to last longer and be reachable for longer periods of time.

6.4.2 Berkeley Dataset (Actual Layout)

Figure 6.14(a) is in agreement with Figs. 6.4 and 6.5. As shown in Fig. 6.14(a), the P2P approach improves reachability for all of the sensors in MBCR and 85% of the sensors in static routing. The remaining few sensors that survived in static routing were on few or zero multi-hop routes to begin with because of their location in the lab. Thus, their communication overhead was the same in both protocols, and the computation overhead high in P2P.

For 50% of the sensors in static routing, the P2P protocol improved reachability by over 4× that of the centralized protocol. Those sensors became unreachable when the root nodes they forwarded through died. MBCR improved their reachability because it dynamically found a new route to maintain connectivity with the sink. Therefore, our P2P protocol had lesser of an advantage over the centralized protocol with MBCR routing.

6.4.3 Berkeley Dataset (Grid Layout)

It is clear from Fig. 6.15 that the P2P approach improves reachability by three to four times. The MBCR routing protocol provides negligible improvement over static routing in reachability of the network as a whole, not favoring any specific sensors for greater reachability.

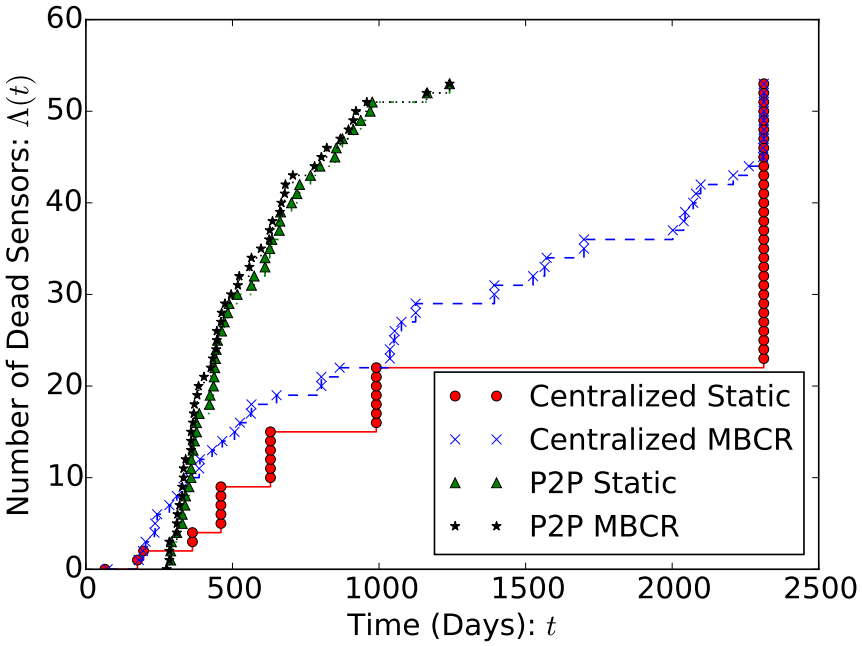

(a) Longevity

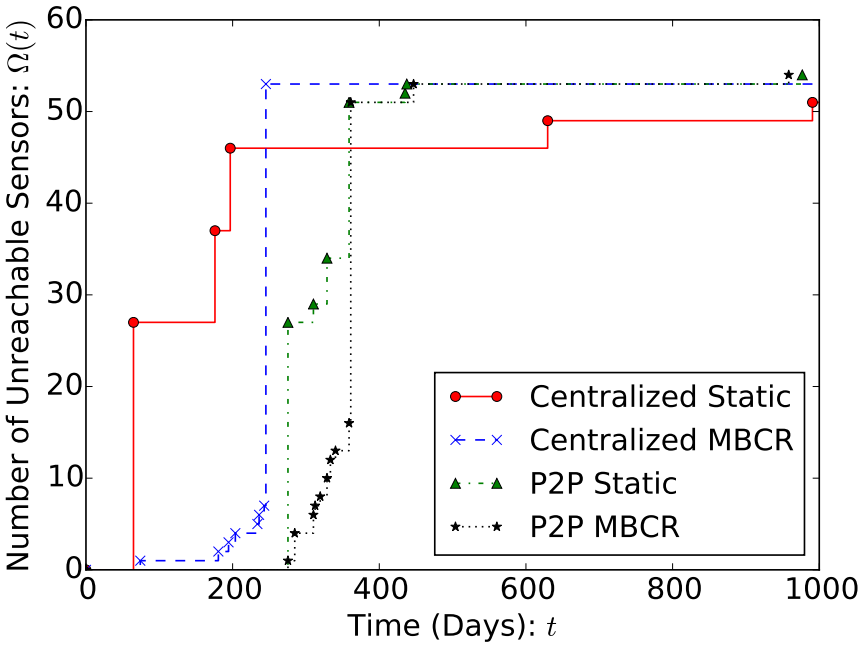

(b) Reachability

Figure 6.14: Results for Intel Berkeley Dataset (Actual Layout). The inverse functions of Longevity and Reachability, which are the number of sensors dead and unreachable, respectively, are plotted.

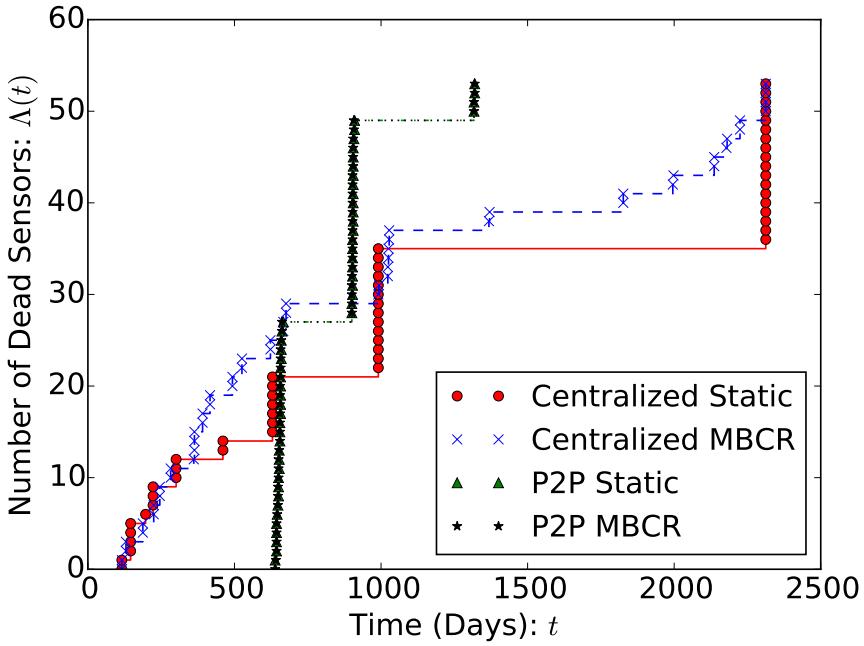

(a) Longevity

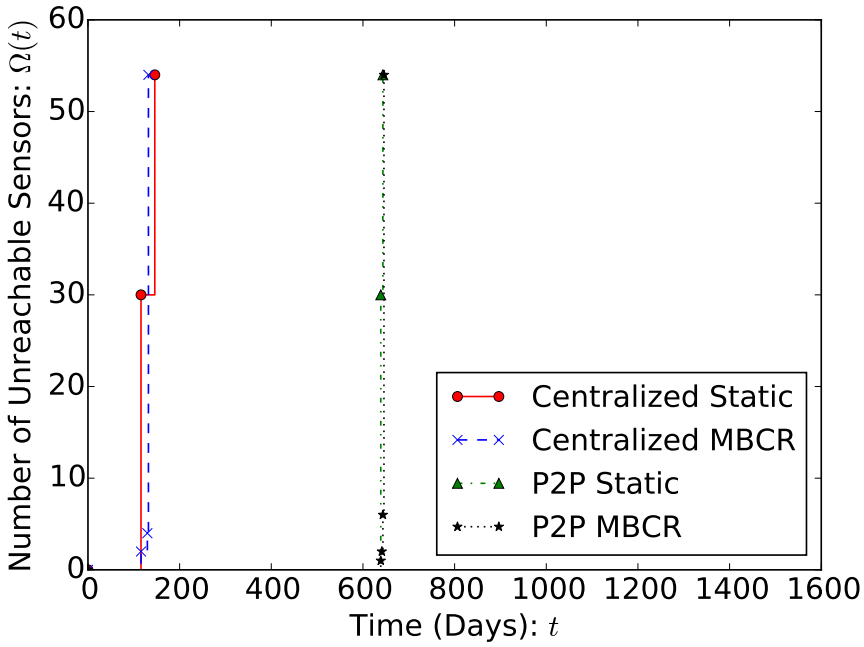

(b) Reachability

Figure 6.15: Results for Intel Berkeley Dataset (Grid Layout). The inverse functions of Longevity and Reachability, which are the number of sensors dead and unreachable, respectively, are plotted.

6.4.4 TAO Dataset Experiments

In this layout, all 8 sensors were placed in a linear physical topology to resemble their actual placement on the equator. The sink was placed at one end. The P2P protocol improved reachability by 4.5× over the centralized protocol for both static and MBCR routing, as shown in Fig. 6.16.

6.4.5 NZ Dataset Experiments

The P2P protocol improved reachability by 60% and 30% over the centralized protocol for static and MBCR routing, respectively for 60% of sensors, as illustrated in Fig. 6.17. The P2P protocol performed equally well with static and MBCR routing because of a lack of routing options in the limited topology (reachability was extended by MBCR by only two days, and the overlapping curves are not shown separately in the figure to improve readability).

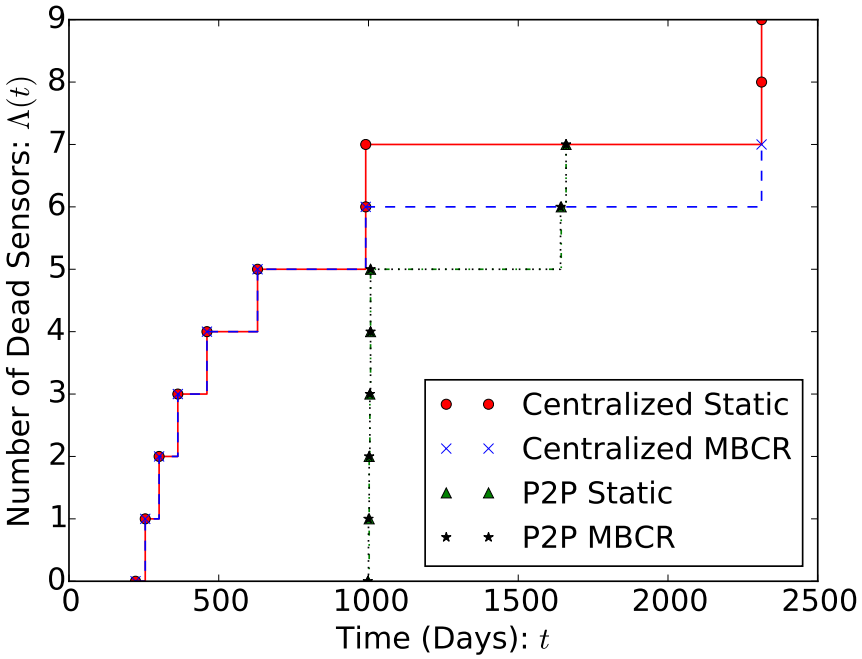

(a) Longevity

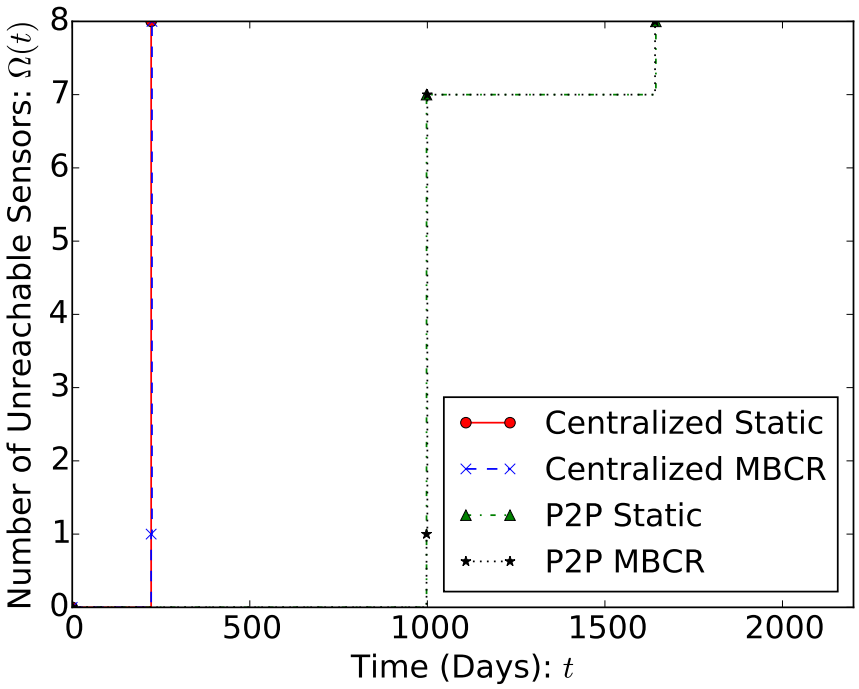

(b) Reachability

Figure 6.16: Results for TAO Dataset. The inverse functions of Longevity and Reachability, which are the number of sensors dead and unreachable, respectively, are plotted.

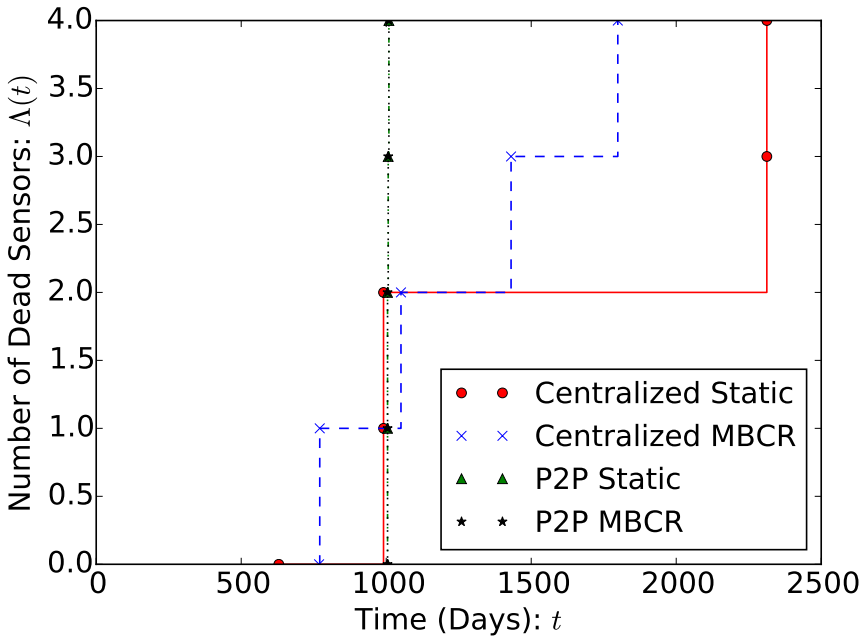

(a) Longevity

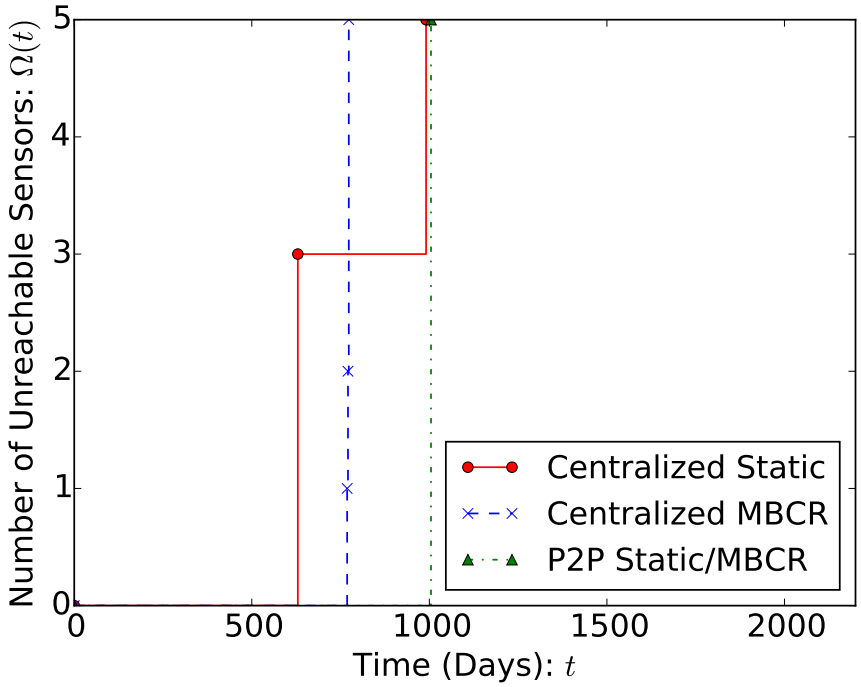

(b) Reachability

Figure 6.17: Results for NZ Dataset. The inverse functions of Longevity and Reachability, which are the number of sensors dead and unreachable, respectively, are plotted.

CHAPTER 7

RELATED WORK

There is an extensive literature on the design of anomaly detection protocols (surveyed in [27]), and on energy-efficient protocols for WSNs (surveyed in [9]). The literatures on those two topics are largely separate, despite the need for an integrated solution. The topics have separately received attention from the dependable systems and networks community [7, 13, 14, 17, 19], as cited throughout the thesis.

Elnahrawy and Nath [28] leverage contextual information in the form of spatial correlations to detect anomalies, similar to our approach. However, they fail to address the impact of adding validation features on sensor battery and WSN survivability.

Paola et al. [29], propose an adaptive distributed outlier detector algorithm to detect faults in WSNs. The algorithm overlays a Bayesian network on the network topology that propagates belief in the sensor's correctness. The limitation of that approach is that conditional probabilities on the hidden variables in the Bayesian network need to be computed for each sensor offline using supervised learning. In contrast, our approach is completely unsupervised, significantly simplifying its installation and set-up.

Dua et al. [30] rely on a hardware-based trusted platform module (TPM) on each sensor to enable trust by attesting to the integrity of the data. We do not require an expensive TPM approach because we assume that a sensor may report false data, but not maliciously or in collusion with others.

Meng et al. [11] present two techniques to ascertain the true value reported by multiple, possibly unreliable sensors by leveraging the correlation among different sensors. In their system, the sensors act as clients and submit their information to a centralized server. The server solves an optimization problem to detect anomalies. Our method takes a different approach and allows each sensor to act locally as a measurement validator to minimize the

overhead of routing packets through the WSN to a centralized server.

Rajasegarar et al. [31] propose an in-network anomaly detector that uses a cluster-based approach for energy efficiency. However, the way the authors measure dissimilarity and form clusters differs from our approach. The authors use Euclidean distances as a way to measure dissimilarity and use a fixed-width clustering algorithm, while we use regression based techniques to measure dissimilarity.

Branch et al. [32] also demonstrate an in-network anomaly detection approach, but they make the assumption that every sensor in the network has to be made aware of the anomaly. We relax that assumption in our model and require that a quorum of validating sensors in a group be aware of the anomalous sensor in that group. This results in reduced message transmission in the power-constrained network, yet it effectively and efficiently serves the purpose of identifying the faulty sensor.

A patent by Samsung [33] proposes a scheme in which an aggregator collects information from a number of sensors and informs the base station (sink). A base station selects one or more verifiers and commands the aggregator to submit the information to the verifiers for verification. The verifiers choose a random subset of the sensors and query them to determine whether the aggregator's result is truthful. This differs from our approach, in which every sensor could in theory act as a validator with no explicit coordination or command from an aggregator or base station.

Sundaram and Eugster [17] provide a lightweight tracing mechanism for debugging sensor networks when messages are lost, dropped or received out of order. We do not consider such errors, and instead focus on measurement errors.

Zhang and Liu [34] present DataGuard, a software-based approach to protect the integrity of the memory and software running on the sensors from attacks. Unlike our work, that approach is not concerned with detecting non-malicious measurement errors.

Khalil et al. [13] present SLAM, a method to monitor neighboring sensors for suspicious behavior using a Sleep-Wake protocol that extends battery life. While our approach can use similar sleep-wake methods, we monitor sensors for erroneous measurements, and not suspicious behavior.

Basile et al. [19] provide a method that uses Hidden Markov Models to characterize anoma-

lies as caused by malicious or non-malicious faults. That method can be used in conjunction with our work, if a network administrator desired to make that differentiation.

Liu et al. [7] describe the detection of erroneous measurements in structural health monitoring applications. They do no consider the impact of their methods on sensor battery life, and their approaches may dramatically benefit from our work.

CHAPTER 8

CONCLUSION

In this thesis, we developed a P2P protocol that detects erroneous measurements in a WSN while simultaneously minimizing the impact of the detection overhead on its reachability. Using a simulation tool built to evaluate the protocol, we confirmed our hypothesis that sensor networks that employ the naive centralized error detection approach will drain sensors near the sink, disconnecting sensors farther away from it. In contrast, the P2P approach is less harsh on the sensors near the sink. The P2P protocol trades off computation savings for communication savings; it moves the onus of error detection from the sink onto the sensors themselves, and in doing so, it minimizes the number of messages required to report an error. Since communication consumes more energy on a sensor than computation, that trade-off effectively allows sensors to remain connected to the sink for a significantly longer period of time.

In our distributed protocol, anomalous data from erroneous sensors were flagged by the sensors themselves and reported to the sink. In future work, we may explore a self-healing approach in which sensors report anomalies to a validators in the network that are nearer to them than the sink. A validator would command an erroneous sensor to stop measuring and reporting data. That would obviate the need to report to the sink, saving even more energy. However, the sink would lose some knowledge of what is happening in the network and therein lies a trade-off.

APPENDIX A

UNSUITABLE ANOMALY DETECTION APPROACHES

In this appendix we describe anomaly detection approaches that were considered, but not adopted because of their unsuitability for the purpose of validating sensor measurements.

A.1 OLS Linear Regression

Our first thought was to use *ordinary least squares* (OLS) linear regression because we observed that sensor values tended to be linearly related, as seen in Fig. 3.3, in all our datasets.

Consider two sensors $S^{(1)}$ and $S^{(19)}$ whose measurements at time t, $S_t^{(1)}$ and $S_t^{(19)}$, are linearly related as follows:

$$S_t^{(19)} = mS_t^{(1)} + c + \epsilon \tag{A.1}$$

The variables m and c are scalars representing the slope and intercept of the linear relationship, and the residual $\epsilon \sim N(0, \sigma^2)$ represents Gaussian white noise in the relative measurements. Given this Gaussian assumption, which is also made in [10], OLS linear regression is solved by minimizing the $L2$-norm of the residuals (which is itself a vector of ϵ values obtained from T latest sensor measurements). Since T is not large, the closed-form solution for linear regression can be computed without having to resort to CPU-intensive gradient descent methods.

Consider the scenario in which sensor $S^{(19)}$ validates its measurements with respect to another sensor $S^{(1)}$ with which it is linearly related. $S^{(19)}$ does so by building a model of $S^{(1)}$'s measurements using linear regression and storing the model parameters m, c, and σ. Those model parameters are estimated using the latest T measurements of $S^{(1)}$, which were

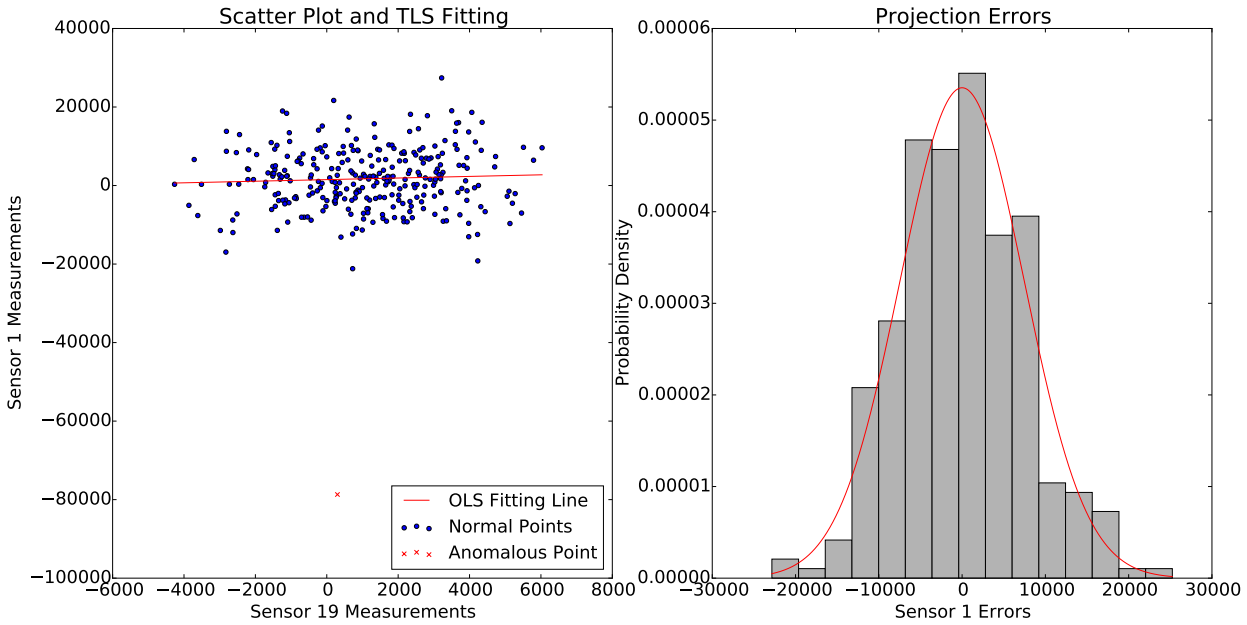

Figure A.1: NZ dataset: OLS regression used in anomaly detection.

stored in $S^{(19)}$'s memory. At time t, $S^{(19)}$ computes the residual $\epsilon_t = S_t^{(2)} - (mS^{(1)} + c)$ and compares this to a threshold. This is illustrated in Fig. A.1, where the past residuals (or fitting errors) of $S^{(1)}$ clearly form a Gaussian distribution.

There are many ways to choose a threshold for anomaly detection, and the choice determines the detection (true positive) and false positive rate. We adopt the common 3σ threshold, where $\epsilon \sim N(0, \sigma^2)$. If the observed residual $|\epsilon_t| > 3\sigma$, then the probability that $S_t^{(2)}$ is valid given $S_t^{(1)}$ is $P(|\epsilon_t| > 3\sigma) = 0.3\%$, so $S_t^{(2)}$ will be flagged as anomalous.

The similarity metric is used by each sensor in our protocol to decide which other sensors should be its reference sensors for the purposes of anomaly detection. If $S^{(1)}$ and $S^{(2)}$ are perfectly collinear, then $\epsilon_t = S_t^{(2)} - (mS_t^{(1)} + c) = 0$. If they are highly collinear, then $|\epsilon_t| = |S_t^{(2)} - (mS_t^{(1)} + c)|$ approaches zero. This implies that σ must also approach zero, since $\epsilon \sim N(0, \sigma^2)$ can be written as $\epsilon = \sigma z$, where $z \sim N(0, 1)$. As a result, high collinearity implies a smaller σ (sensor measurements are very similar), and low collinearity implies a larger σ (sensor measurements are dissimilar). Therefore, collinearity is a suitable similarity metric.

The failure of this method lies in its asymmetry. Symmetry was an essential property of the algorithm for our protocol, as described in Section 4.5. Figure A.2 shows that even

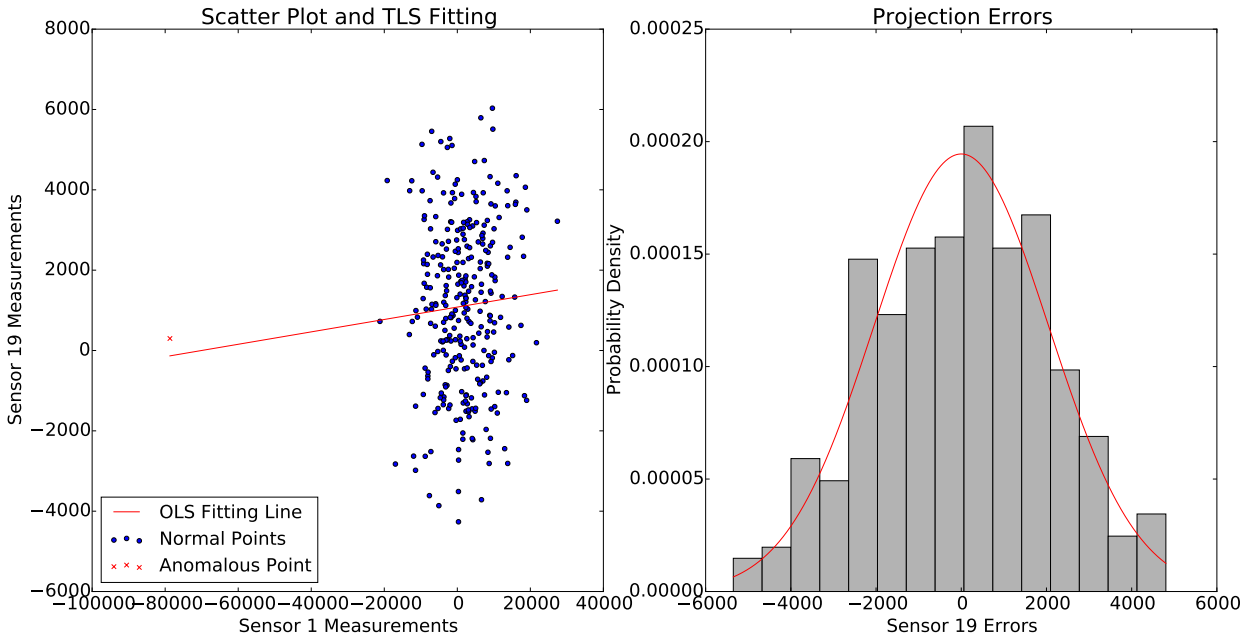

Figure A.2: NZ dataset: Failure of OLS regression used in anomaly detection.

though the measurement taken by Sensor 1 appears anomalous with respect to Sensor 19, the reverse does not hold. The measurement taken by Sensor 19 is not anomalous with respect to Sensor 1 because of the manner in which the fitting line is drawn by OLS regression. The line is drawn to minimize the vertical distance (parallel to the vertical axis) between points and the line.

A.2 TLS Linear Regression

Total least squares (TLS) linear regression or *orthogonal regression* provides a symmetric approach to finding a fitting line by finding a line that minimizes the orthogonal distance between the points and the line.

In order to estimate the line, we can use the Eckart-Young theorem to relate the minimization of the Frobenius norm of the projection errors with the principal components of the measurement data. We omit the details here, but it can be proven that this method is symmetric in the fitting line it produces. The projection errors of the original data points on the fitting line are Gaussian, as shown in Fig. A.3.

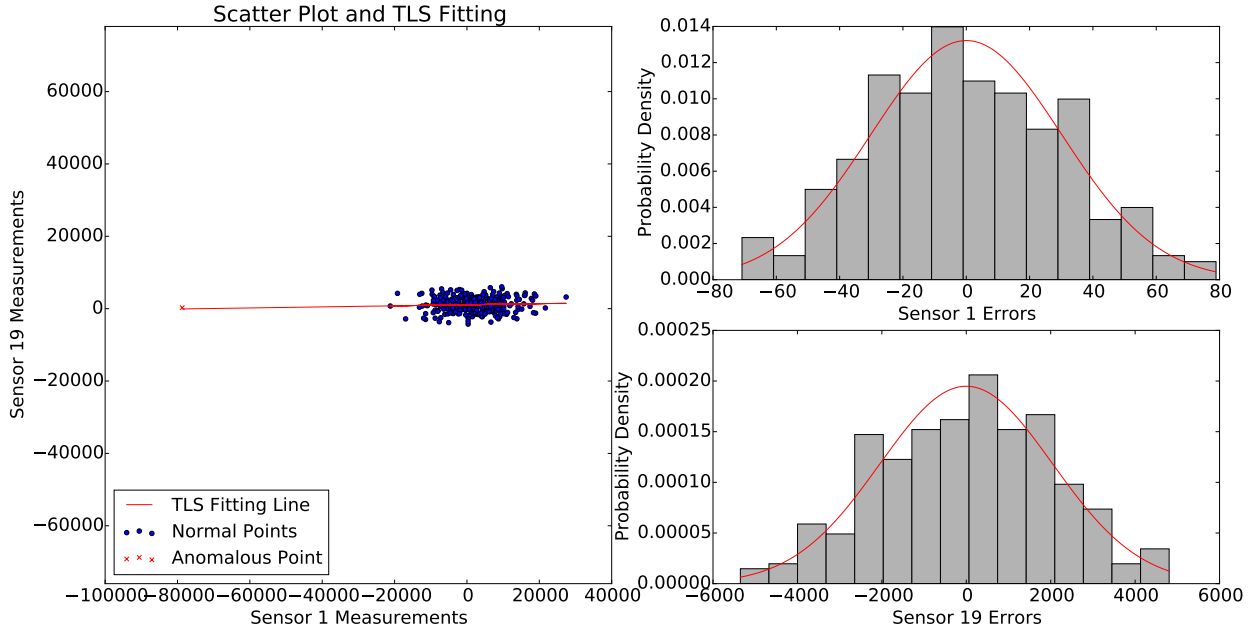

(a) Sensor 19 with respect to Sensor 1

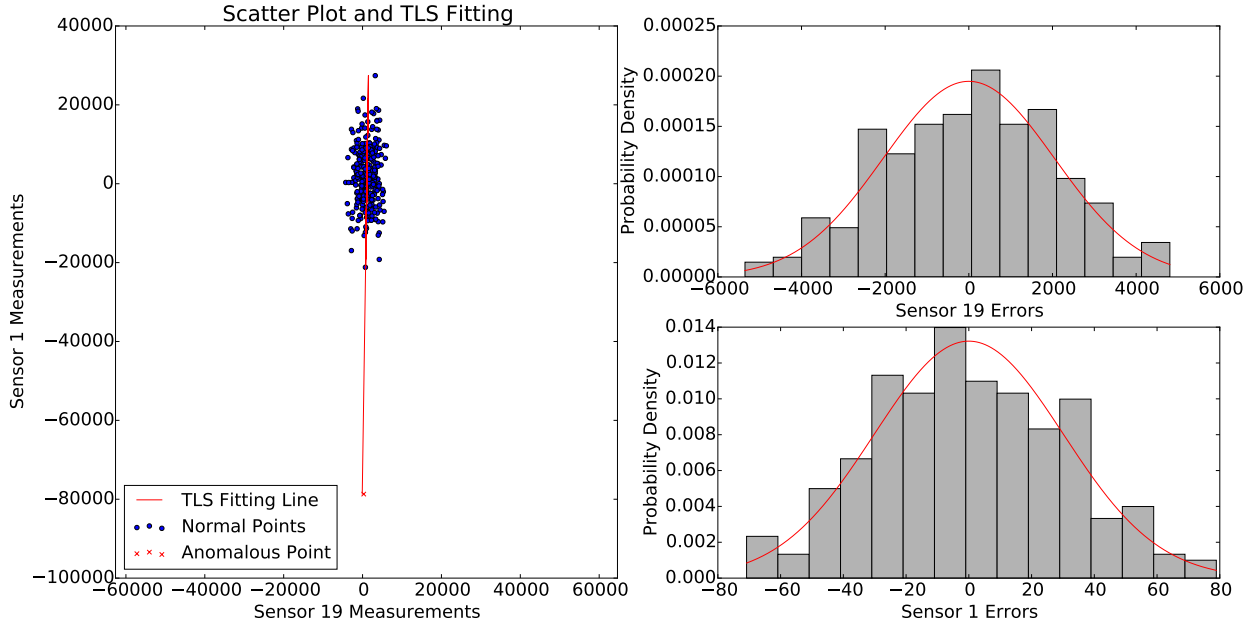

(b) Sensor 1 with respect to Sensor 19

Figure A.3: NZ dataset: TLS regression used in anomaly detection.

Although this approach provides symmetry, unlike OLS regression, it is not suitable for anomaly detection. As can be seen in Fig. A.3, the anomalous point lies almost on the best fit line. Therefore, the approach does not detect the anomaly.

A good approach would not look for anomalies in only one dimension because that could miss the anomaly in the orthogonal dimension. Therefore we choose to use a two-dimensional approach leveraging bivariate Gaussian isocontours.

A.3 Correlation and Dot Products

Correlation and dot products have been suggested in related work [27] for anomaly detection. We believe that these are reasonable similarity metrics, but impractical for anomaly detection. Both correlation and dot products apply to vectors. Assume that we have T points of historic data from two sensors. That can produce one value for the correlation or the dot product. With that one value it is difficult to tell whether a new pair of points from the two sensors is anomalous or not. One would need to calculate the change that the new value causes to the correlation or dot product, assuming that those values do not tend to change much (to the best of our knowledge, there is no well-known underlying probabilistic behavior associated with that change). In our approach, however, there is a clear decision boundary constructed from a bivariate normal distribution, which captures the tendency of the data to cluster together.

APPENDIX B

SENSOR ID AND NAME MAPPING

B.1 Berkeley Dataset

The sensors were numbered as given in the layout in [2].

B.2 TAO Dataset

0 - sst0n110w

1 - sst0n125w

2 - sst0n140w

3 - sst0n155w

4 - sst0n165e

5 - sst0n170w

6 - sst0n180w

7 - sst0n95w

B.3 NZ Dataset

0 - APZ.HHZ.10.NZ

1 - BFZ.HHZ.10.NZ

2 - BKZ.HHZ.10.NZ

3 - COVZ.HHZ.10.NZ

4 - CTZ.HHZ.10.NZ

5 - CVZ.HHZ.10.NZ

6 - DCZ.HHZ.10.NZ

7 - DSZ.HHZ.10.NZ

8 - EAZ.HHZ.10.NZ

9 - ETVZ.HHZ.10.NZ

10 - FOZ.HHZ.10.NZ

11 - FWVZ.HHZ.10.NZ

12 - GLKZ.HHZ.10.NZ

13 - GRZ.HHZ.10.NZ

14 - GVZ.HHZ.10.NZ

15 - HAZ.HHZ.10.NZ

16 - MAVZ.HHZ.10.NZ

17 - MLZ.HHZ.10.NZ

18 - MQZ.HHZ.10.NZ

19 - MRZ.HHZ.10.NZ

20 - MSZ.HHZ.10.NZ

21 - MWZ.HHZ.10.NZ

22 - MXZ.HHZ.10.NZ

23 - PUZ.HHZ.10.NZ

24 - PXZ.HHZ.10.NZ

25 - PYZ.HHZ.10.NZ

26 - THZ.HHZ.10.NZ

27 - TLZ.HHZ.10.NZ

28 - TMVZ.HHZ.10.NZ

29 - TOZ.HHZ.10.NZ

30 - TRVZ.HHZ.10.NZ

31 - TSZ.HHZ.10.NZ

32 - TUZ.HHZ.10.NZ

33 - WCZ.HHZ.10.NZ

34 - WEL.HHZ.10.NZ

35 - WHVZ.HHZ.10.NZ

36 - WHZ.HHZ.10.NZ

37 - WIZ.HHZ.10.NZ

38 - WKZ.HHZ.10.NZ

39 - WSRZ.HHZ.10.NZ

40 - WVZ.HHZ.10.NZ

REFERENCES

[1] GeoNet Project, "GeoNet National Seismograph Network dataset," Date Last Accessed: 6 Nov 2016. [Online]. Available: http://doi.org/10.21420/G2WC7M

[2] S. Madden, "Intel lab data," 2004, Date Last Accessed: 6 Nov 2016. [Online]. Available: http://db.csail.mit.edu/labdata/labdata.html

[3] G. Tolle, J. Polastre, R. Szewczyk, D. Culler, N. Turner, K. Tu, S. Burgess, T. Dawson, P. Buonadonna, D. Gay, and W. Hong, "A macroscope in the redwoods," in *In Proceedings SenSys '05*. New York, NY, USA: ACM, 2005, pp. 51–63.

[4] R. Szewczyk, A. Mainwaring, J. Polastre, J. Anderson, and D. Culler, "An analysis of a large scale habitat monitoring application," in *Proceedings of SenSys '04*. New York, NY, USA: ACM, 2004, pp. 214–226.

[5] J. Burrell, T. Brooke, and R. Beckwith, "Vineyard computing: sensor networks in agricultural production," *IEEE Pervasive Computing*, vol. 3, no. 1, pp. 38–45, Jan 2004.

[6] G. Werner-Allen, K. Lorincz, J. Johnson, J. Lees, and M. Welsh, "Fidelity and yield in a volcano monitoring sensor network," in *Proceedings of OSDI '06*. USENIX Association, 2006, pp. 381–396.

[7] X. Liu, J. Cao, M. Bhuiyan, S. Lai, H. Wu, and G. Wang, "Fault tolerant wsn-based structural health monitoring," in *2011 IEEE/IFIP 41st International Conference on Dependable Systems Networks (DSN)*, June 2011, pp. 37–48.

[8] S. Kim, S. Pakzad, D. Culler, J. Demmel, G. Fenves, S. Glaser, and M. Turon, "Health monitoring of civil infrastructures using wireless sensor networks," in *Proceedings of IPSN '07*, April 2007, pp. 254–263.

[9] G. M. Shafiullah, A. Gyasi-Agyei, and P. J. Wolfs, "A survey of energy-efficient and qos-aware routing protocols for wireless sensor networks," in *Novel Algorithms and Techniques In Telecommunications, Automation and Industrial Electronics*, T. Sobh, K. Elleithy, A. Mahmood, and M. A. Karim, Eds. Dordrecht: Springer Netherlands, 2008, pp. 352–357.

[10] S. Alag, A. M. Agogino, and M. Morjaria, "A methodology for intelligent sensor measurement, validation, fusion, and fault detection for equipment monitoring and diagnostics," *Artificial Intelligence for Engineering Design, Analysis and Manufacturing*, vol. 15, no. 4, pp. 307–320, Sep. 2001.

[11] C. Meng, W. Jiang, Y. Li, J. Gao, L. Su, H. Ding, and Y. Cheng, "Truth discovery on crowd sensing of correlated entities," in *Proceedings of SenSys '15*. New York, NY, USA: ACM, 2015, pp. 169–182.

[12] S. Madden, M. J. Franklin, J. M. Hellerstein, and W. Hong, "TAG: A Tiny AGgregation Service for ad-hoc sensor networks," *SIGOPS Oper. Syst. Rev.*, vol. 36, no. SI, pp. 131–146, Dec. 2002.

[13] I. Khalil, S. Bagchi, and N. B. Shroff, "Slam: Sleep-wake aware local monitoring in sensor networks," in *37th Annual IEEE/IFIP International Conference on Dependable Systems and Networks (DSN'07)*, June 2007, pp. 565–574.

[14] G. Khanna, S. Bagchi, and Y.-S. Wu, "Fault tolerant energy aware data dissemination protocol in sensor networks," in *Proc. of DSN*, June 2004.

[15] C. K. Toh, H. Cobb, and D. A. Scott, "Performance evaluation of battery-life-aware routing schemes for wireless ad hoc networks," in *Proceedings of ICC '01*, vol. 9, 2001, pp. 2824–2829 vol.9.

[16] A. Das, I. Gupta, and A. Motivala, "Swim: scalable weakly-consistent infection-style process group membership protocol," in *Proceedings of DSN*, 2002, pp. 303–312.

[17] V. Sundaram and P. Eugster, "Lightweight message tracing for debugging wireless sensor networks," in *2013 43rd Annual IEEE/IFIP International Conference on Dependable Systems and Networks (DSN)*, June 2013, pp. 1–12.

[18] L. Paradis and Q. Han, "Tigra: Timely sensor data collection using distributed graph coloring," in *Proceedings of PerCom '08*, March 2008, pp. 264–268.

[19] C. Basile, M. Gupta, Z. Kalbarczyk, and R. K. Iyer, "An approach for detecting and distinguishing errors versus attacks in sensor networks," in *International Conference on Dependable Systems and Networks (DSN'06)*, June 2006, pp. 473–484.

[20] Pacific Marine Environmental Laboratory, "Tropical Atmosphere Ocean Project," Date Last Accessed: 6 Nov 2016. [Online]. Available: http://www.pmel.noaa.gov/tao/proj_over/mooring.shtml

[21] V. Badrinath Krishna, R. K. Iyer, and W. H. Sanders, "ARIMA-Based Modeling and Validation of Consumption Readings in Power Grids," in *Proceedings of Critical Information Infrastructure Security (CRITIS)*. Springer Verlag, 2015.

[22] F. Yu, "A survey of wireless sensor network simulation tools," April 2011. [Online]. Available: http://www.cse.wustl.edu/~jain/cse567-11/ftp/sensor/index.html

[23] Information Sciences Institute, "The network simulator - NS-2," January 2016. [Online]. Available: http://www.isi.edu/nsnam/ns/

[24] P. Levis and N. Lee, "TOSSIM: A simulator for TinyOS networks," June 2003. [Online]. Available: http://www.tinyos.net/tinyos-1.x/doc/nido.pdf

[25] "Mica2dot wireless microsensor mote," Date Last Accessed: 6 Dec 2016. [Online]. Available: https://www.eol.ucar.edu/isf/facilities/isa/internal/CrossBow/DataSheets/mica2dot.pdf

[26] F. Ferrari, M. Zimmerling, L. Mottola, and L. Thiele, "Low-power wireless bus," in *Proceedings of SenSys*. New York, NY, USA: ACM, 2012, pp. 1–14.

[27] Y. Zhang, N. Meratnia, and P. Havinga, "Outlier detection techniques for wireless sensor networks: A survey," *Commun. Surveys Tuts.*, vol. 12, no. 2, pp. 159–170, Apr. 2010.

[28] E. Elnahrawy and B. Nath, "Context-aware sensors," in *Proceedings of EWSN '04*. Berlin, Heidelberg: Springer Berlin Heidelberg, 2004, pp. 77–93.

[29] A. De Paola, S. Gaglio, G. Re, F. Milazzo, and M. Ortolani, "Adaptive Distributed Outlier Detection for WSNs," *Cybernetics, IEEE Transactions on*, vol. 45, no. 5, pp. 902–913, May 2015.

[30] A. Dua, N. Bulusu, W.-C. Feng, and W. Hu, "Towards trustworthy participatory sensing," in *Proceedings of HotSec'09*. Berkeley, CA, USA: USENIX Association, 2009, pp. 8–8.

[31] S. Rajasegarar, C. Leckie, M. Palaniswami, and J. Bezdek, "Distributed anomaly detection in wireless sensor networks," in *Proceedings of ICCS '06*, Oct 2006, pp. 1–5.

[32] J. Branch, B. Szymanski, C. Giannella, R. Wolff, and H. Kargupta, "In-network outlier detection in wireless sensor networks," in *Proceedings of ICDCS '06*, 2006, pp. 51–51.

[33] E. Kim, J. Yi, A. Fomin, A. Afanasyeva, and S. Bezzateev, "Method and system for performing distributed verification with respect to measurement data in sensor network," Aug. 2012, US Patent 8,255,689.

[34] D. Zhang and D. Liu, "Dataguard: Dynamic data attestation in wireless sensor networks," in *2010 IEEE/IFIP International Conference on Dependable Systems Networks (DSN)*, June 2010, pp. 261–270.